# Design of a Li-ion Battery Pack Emulator

by

David Novák

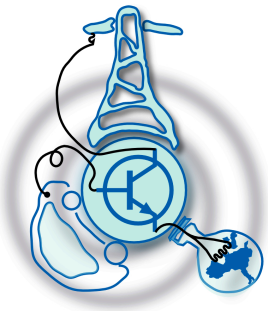

Submitted to the Department of Electrical Engineering, Electronics, Computers and Systems
in partial fulfillment of the requirements for the degree of
Erasmus Mundus Master Course in Sustainable Transportation and Electrical Power Systems
at the
UNIVERSIDAD DE OVIEDO
September 2015

© Universidad de Oviedo 2015. All rights reserved.

Author .....

Certified by .....
Pablo García Fernández
Associate Professor
Thesis Supervisor

Certified by .....
Mireia Barenys Espadaler
Industry Co-advisor
Thesis Supervisor

**Design of a Li-ion Battery Pack Emulator**

by

David Novák

Submitted to the Department of Electrical Engineering, Electronics, Computers and Systems
on September 1, 2015, in partial fulfillment of the
requirements for the degree of
Erasmus Mundus Master Course in Sustainable Transportation and Electrical Power Systems

## Abstract

Due to the continuously increasing portion of renewable energy sources that are being connected to the grid, grid energy storage systems are now calling for attention more than ever before, to improve the grid's power quality and stability. For this purpose, Li-ion Batteries (LIBs) are currently considered as the most promising technology, because of its relative maturity and premise that the cost for LIBs shall decrease significantly in the forthcoming years.

Hence, recognizing the potential of LIBs and their still relatively high cost, this study aims to develop a Li-ion Battery Emulator (BE). This BE shall therefore substitute a real LIB in any desired power system, microgrid or smartgrid laboratory setup, allowing to proceed further in both research and industry related applications.

In this work, firstly the motivation for the choice of LIBs is presented, following with background of the Li-ion technology and a thorough description of LIB characteristics. Next, a literature review of the state of the art of LIB models is provided. Based on the literature review, three data sheet based LIB models are developed in Matlab-Simulink and compared (i.e. Shepherd's original model, Shepherd's modified model and Curve fitting model). The most suitable model: the Curve fitting model, is further optimized for direct C-code generation through Embedded-Coder platform in Matlab-Simulink, upon which the generated C-code is successfully implemented inside a fixed-point Digital Signal Processor (DSP).

Thesis Supervisor: Pablo García Fernández
Title: Associate Professor

Thesis Supervisor: Mireia Barenys Espadaler
Title: Industry Co-advisor

# Acknowledgments

To my closest family for its endless support throughout the entire period of my studies, which has lead me all the way up to the accomplishment of this Master thesis.

Also, I would like to devote this Master thesis to my grandparents who have always stayed behind me, though could not stay for long enough to see this particular piece of work finished.

My thanks also belong to the collective of professors at the Electrical Engineering Department at the University of Oviedo for their friendly but demanding approach to teaching. Particularly thanks to Prof. Pablo García Fernández for his support throughout the whole Erasmus Mundus Master course.

Last but not least, my thanks to Mireia Barenys Espadaler, my Thesis Co-advisor for her professional and well-rounded guidance.

# Contents

# List of Figures

# List of Tables

# Chapter 1

# Introduction

## 1.1 Introduction

Constantly increasing penetration of Renewable Energy Sources (RESs) that have emerged in pursue of cleaner energy generation, have placed a certain burden on the local electrical grids due to their generally intermittent behavior. It is then rather common situation that in locations where the grid is weak and the penetration of RESs is high, the grid bounces on the edge of stability at risk of a blackout. Grid Energy Storage Systems (GESSs) can provide certain release of this tension on the grid by smoothing (firming) the generated power, as one application of many, and so help to maintain the grid's power quality and reliability [53].

Among all the GESSs today, it is a Li-ion Battery (LIB), which is seen as the most perspective grid energy storage technology in the near future [8], [30]. At the current situation however, it is still a very expensive technology that makes its large scale deployment difficult with only several real projects implemented up to date.

Moreover, the cost of this technology also represents certain barrier for research institutions and research groups at universities, which are keen to implement this technology as part of their power system/microgrid/smartgrid setups. Additionally, a similar problem arises in the industry, that wish to be prepared for the well anticipated large scale LIB deployment and need to test their Power Conditioning Systems (PCSs) prior to real LIB deployment.

This study therefore concentrates on this issue, through development of a LIB model, or the so-called Battery Emulator (BE); which can be implemented instead of a real LIB for the purpose of a complete system analysis, serving both the researcher and the industry.

## 1.2 Thesis Objectives

The main objectives of the thesis are:

1. Depict the main characteristics and properties of LIBs,
2. Provide a review of the current battery-modeling techniques with emphasis on LIBs,
3. Develop a LIB model in Matlab-Simulink based on a real LIB data sheet information, and
4. Implement the model developed in a fixed-point Digital Signal Processor (DSP).

## 1.3 Thesis Outline

This study is further structured as follows: In Chapter 2, the motivation for LIBs and its comparison to other GESSs is presented. In Chapter 3, various LIB chemistries are reviewed in context of their GESS potential. Chapter 4 describes the main characteristics and phenomenons of LIBs, serving as a background for the following chapters devoted to LIB model development. In Chapter 5 the state of the art of LIB modeling techniques is introduced, with the first LIB model (i.e. Curve fitting model) presented in Chapter6, including its data sheet based building procedure, C-code optimization and complete analysis. Next, another two well-known data sheet based models (i.e. Shepherd's original model and Shepherd's modified model) are modeled and compared to the previous Curve fitting model, all in Chapter 7. The whole study is concluded with some recommendations for future work development in Chapter 8.

# Chapter 2

# Motivation for LIBs

## 2.1 LIBs vs other GESSs

From the large number of GESSs that have been developed up to date, the Battery Energy Storage Systems (BESSs) and the LIB in particular is currently considered as the best choice.

One of the main advantages that place LIB on the front in terms of technology, in comparison to other GESSs can be seen in Fig. 2-1. As shown, Li-ion (as a reference to all Li-ion technologies) provides a good reaction time, ranging from ms to several hours, and that at relatively high power, allowing the technology to be implemented in both high power and high energy applications.

Another advantage of LIB or any BESS in general in comparison to Pumped Storage Hydro (PSH) and Compressed Air Energy Storage (CAES) is the possibility to deploy it theoretically at any place or at any point of the grid, respectively. This is practically not possible with PSH and CAES that are restricted by their topological and geographical requirements, which in most cases put them far from the grid. Furthermore, both: PSH and CAES are very capital intense and require a long planning procedure prior to their implementation [26].

In comparison to Super capacitors (EDLC - Electric double-layer capacitor) and Flywheel (FW) technologies that represent devices with very fast reaction times, their location within the grid is generally not restricted, although their disadvantage lies in

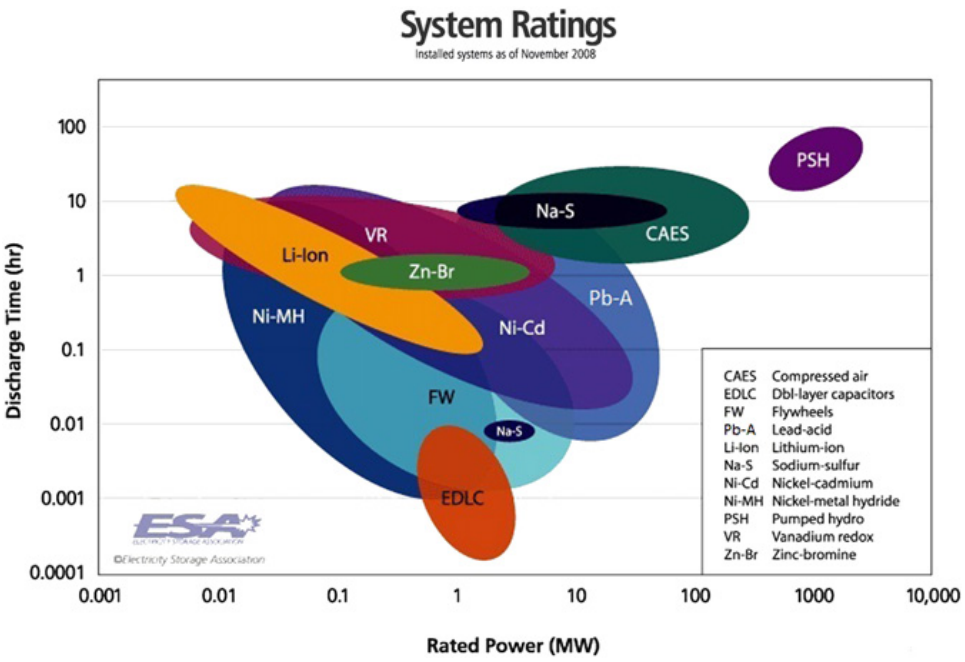


Figure 2-1: Comparison of energy storage technologies - Discharge time vs Rated power [26]

high self-discharge that does not make them suitable for high energy applications [26].

The beneficial "distributed feature" of BESSs, including LIBs, can be seen in Fig. 2-2, in which several applications are always listed in regards to a particular place in the grid, ranging all the way from power generation up to power consumption.

## 2.2 LIBs vs other BESSs

Although there are several types of Li-ion batteries within the general term LIB, which will be further elaborated on in Chapter 3, it can be generally said that LIB stands out over the other battery technologies in the following aspects [47], [46], [8]:

- High energy density (low weight),

- Long cycle-life,

- Low self-discharge,

- Relatively high charge/discharge capability.

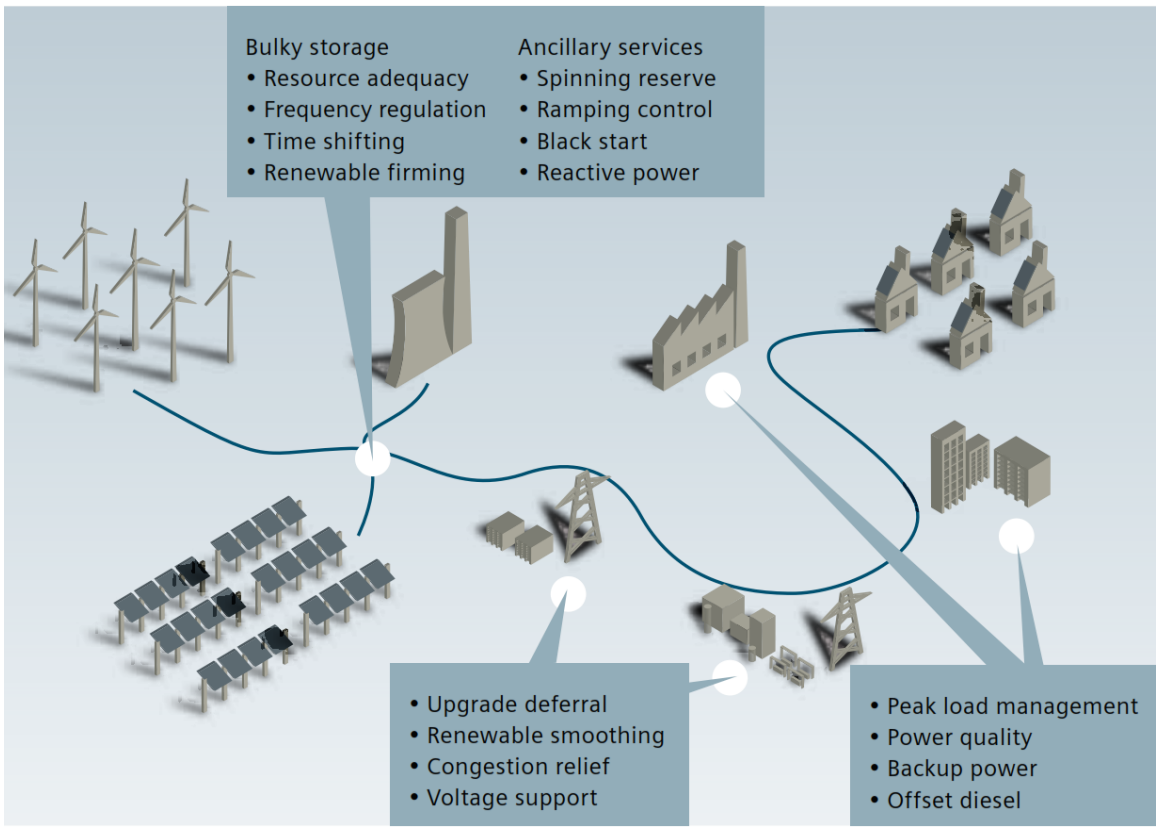


Figure 2-2: Distributed GESS applications [2]

This dominance can be also seen in Fig. 2-3, where, specific power vs specific energy is depicted for various energy storage technologies at the cell level, as they are considered for the automotive industry. It should be noted that although the application is different, the battery cells are in most cases the same. Hence, more similar examples in which the automotive industry crosses with the grid energy storage industry will be seen throughout the report. From another perspective, the advantages of LIBs can be seen in Fig. 2-4.

Hence, it can be seen that Li-ion provides many benefits over other battery counterparts from the technological point of view. Moreover, to give a better understanding of the particular differences, a brief description of the main BESS technologies are presented in the next section.

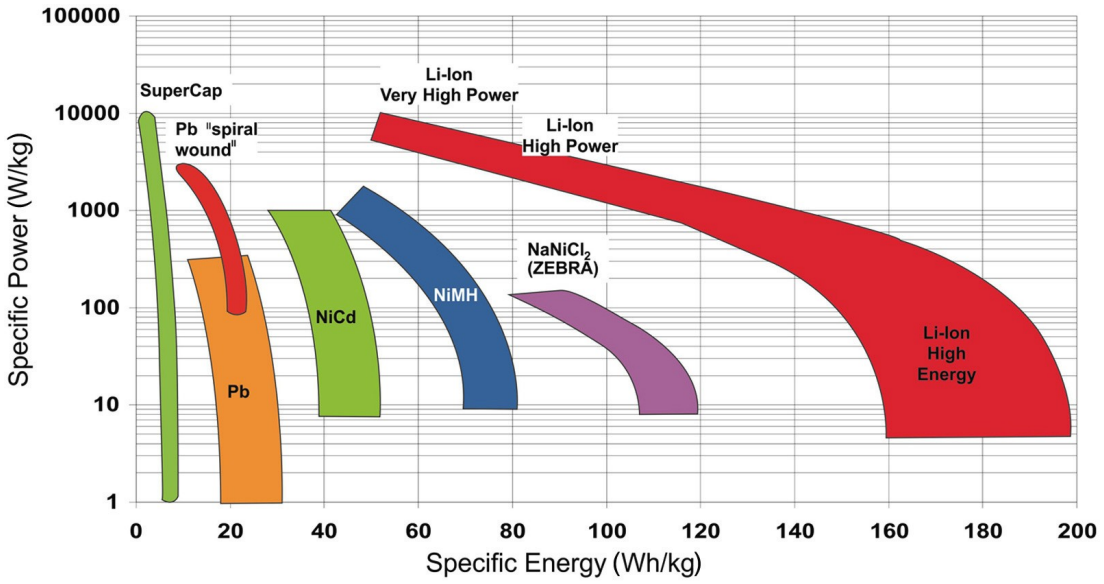


Figure 2-3: Comparison of various energy storage technologies in regards to automotive industry (Specific Power vs Specific Energy), SuperCap: supercapacitor; Pb: lead; Li-ion: lithium-ion; NiCd: nickel–cadmium; NiMH: nickel–metal hydride; NaNiCl : sodium–nickel chloride; ZEBRA: Zero Emission Battery Research Activities [8]

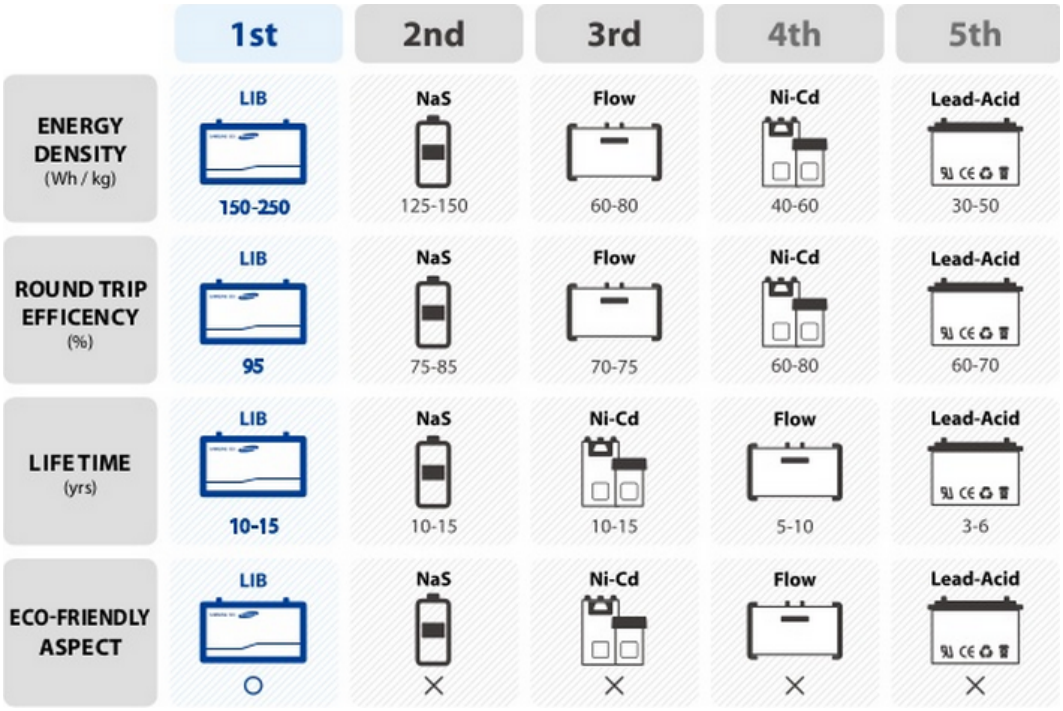


Figure 2-4: General comparison of BESSs [41]

## 2.3 Ni-MH, Pb-A, VR and other BESSs

As shown earlier in Fig. 2-1, there are several BESSs to consider in competition with LIBs, including: Ni-MH, Pb-A, Na-S, Zn-Br, and VR battery. In this section, some of these are elaborated to provide the reader with a broader knowledge of BESSs in context of the large scale grid integration.

### Nickel-Metal Hydride (Ni-MH)

In case of Ni-MH, with reference to Fig. 2-1, this technology has certain potential due to its large operating span. Furthermore, it is inherently safer than a LIB, can operate within a large temperature range of -30 to +75°C, and so far have proved to be very reliable in the automotive industry. This technology however is not quite considered for its implementation as a large scale GESS, due to the following disadvantages: relatively high self-discharge, memory effect and lower energy density (60% of a LIB), plus high cost for nickel [26], [52].

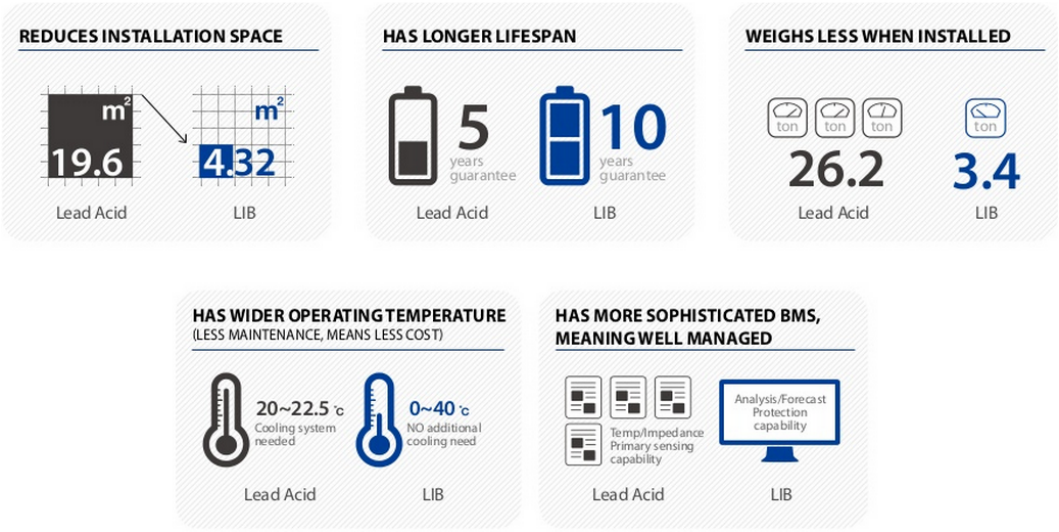


Figure 2-5: A general comparison between a Lead-Acid battery vs LIB [41]

### Lead-Acid (Pb-A)

Pb-A batteries have a very long history through which they have evolved into two main types: flooded and valve regulated lead-acid batteries. Today this technology

is considered as one of the most mature, providing stable performance in many applications, including several large scale GESSs. The biggest project up to date was built in California with capacity of 10MW/40MWh. On the other hand, Pb-A in comparison to a LIB has lower energy density and low cycle-life. Furthermore, Pb-A is not environmentally friendly due to the toxic lead [26]. A comparison between Pb-A and a LIB, as given by Samsung in [41], can be seen in Fig. 2-5.

### Sodium-Sulphur (Na-S)

Na-S is a relatively new technology reaching back to 1960s. Its use was initially considered for automotive industry but was left and continued only in the direction of GESSs. The main reason for this decision was the fact that the Na-S optimally operates at very high temperatures between 300 and 350 °C that would cause serious problems in a vehicle. In terms of GESSs, this technology however developed into certain maturity and is being considered as one of the cheapest among GESSs today. There are many projects around the world, with the largest Na-S plant of 34MW/245MWh of capacity. Na-S batteries have high cycle life, high energy density and high peak power capability.

The main concerns about this technology arise from the high operating temperature and high reactivity of sodium with atmosphere in case the containment should break. During a regular battery operation, the high operating temperature is maintained by internal chemistry processes, however, in case of an outage, self-discharge of as much as 20% per day can occur just because of the temperature loss [26]. A great study solving the issue of a Power Conditioning System (PCS) in a real PV plant with 4.1MW Na-S battery can be found in [49].

### Vanadium Redox (VR)

Even newer than Na-S battery is a Vanadium Redox battery, which was firstly introduced in the early 1980's. Unlike the other types of BESSs, a VR battery is different as it is a flow battery. This means that a VR battery typically composes of two liquid electrolytes that are stored separately in two tanks, one for each electrolyte, creating

two half-cells of a single battery. An example of a typical VR battery structure can be seen in Fig. 2-6. The key of the operation consists of pumping the electrolyte from one tank to the other through a membrane at which a chemical (redox) reaction produces electrical potential between 1.4 - 1.6V. Interestingly, the separation of electrolytes and the reaction membrane allows to have a battery with decoupled energy and power characteristics. This means that by increasing the volume of the two tanks, the battery adds up on energy but do not gain any power. Similarly, when only the size of the reaction membrane is increased, the battery's power rises but the battery's energy stays the same [26].

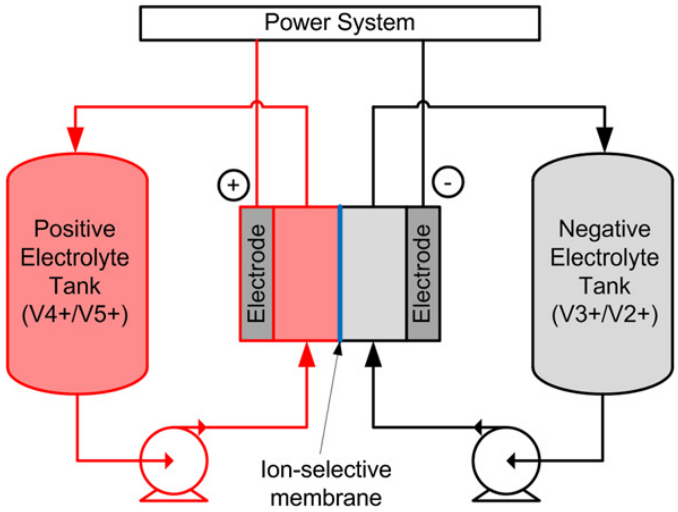


Figure 2-6: A typical structure of Vanadium Redox flow battery [26]

The main issue of a VR battery is related to its limited operational temperature range that is in between +10 and +35°C. This technology is however considered as a very young technology that still has not reached its maturity. An extensive research is under development in various areas, including: extension of the operating temperature range, increase of the specific power/energy characteristics, and development of new reaction membranes. Even at this point however, VR batteries are already known as batteries with: extremely large cycle life, moderate cost, moderate efficiency, but more importantly, no self-discharge. Their real implementation can be already seen in several projects, mainly low scale, with some large scale (units of MW/MWh) projects at the horizon [26].

## 2.4 Cost Outlook for LIBs

As already stated at the very beginning, the main issue with LIBs up to the date has been its high cost, arising from the scarcity of lithium itself and still relatively small scale production of LIBs. For this reason, Li-ion was essentially kept only in customer electronics, where it still greatly dominates the market, with limited use in automotive and energy sectors. Nonetheless, also this situation has been changing over the past several years with more projects seen in both energy and automotive industry [47], [46].

The future cost projections then suggest a dramatic decrease in costs with anticipated approach of LIBs to their mass production [8]. In some cases it is estimated for the cost to fall down from around $500/kWh in 2015 to $200/kWh in 2020 (estimation [38]). Moreover, further reductions in cost are also claimed by battery manufacturers, such as A123 Systems, promising cost drop to $100/kWh also by 2020 [13]. An estimation of a possible cost decrease by Kromer et al (2007), & RMI Analysis is shown in Fig. 2-7.

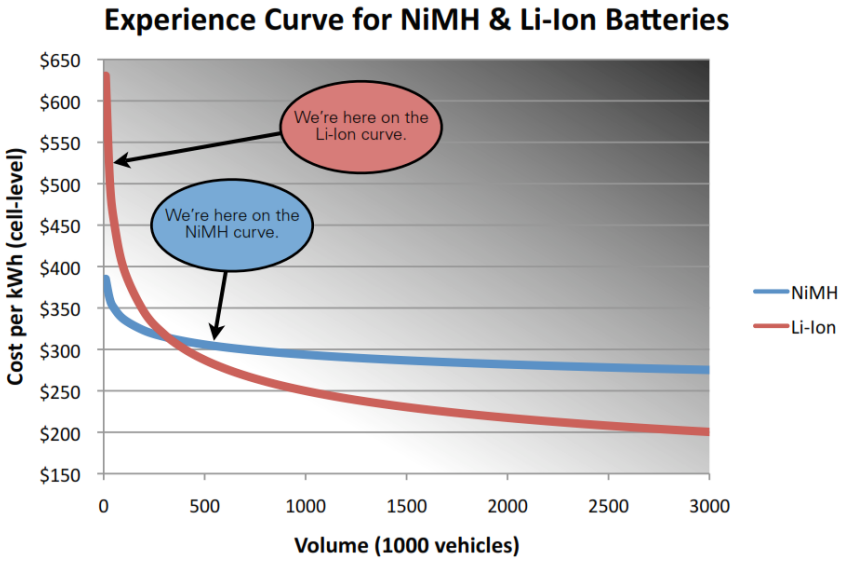


Figure 2-7: Estimation of LIB and Ni-MH cost based on experience curve prediction (i.e. cost development based on the quantity of EV manufactured) [3]

# Chapter 3

# Background for LIBs

Based on the high interest in LIBs and its future potential, this chapter puts more light on various chemistries that are hidden behind the general term *Li-ion battery* or LIB as it has been referred to in this study.

One of the ways, in which the LIBs are classified is based on their anode material that divides the LIB family into two major groups. The first group, which is also most known is *Li-ion* based battery and the other is *Li-metal* based battery. In the following sections, the Li-ion group is introduced first with the Li-metal next. At the end of this chapter, several emerging LIB chemistries that are currently under development are also presented.

## 3.1 Li-ion Batteries

This type of battery is the most common as of now. The internal composition consists from a graphite anode (graphitic carbon), which in most cases has layered structure; a cathode formed by a certain type of a lithium metal oxide, and an electrolyte. The electrolyte generally composes of a lithium salt solution ($LiPF_6$) with an organic solvent that is part of a separator.

The principle of operation lies in the following: when charging the battery, the lithium atoms in the cathode transform into lithium ions and travel through the electrolyte towards the carbon anode. At anode the lithium ions recombine with

carbon, again forming lithium atoms. The same in a reverse order applies during battery discharge [47]. In Fig. 3-1, a general structure of a Li-ion battery can be seen.

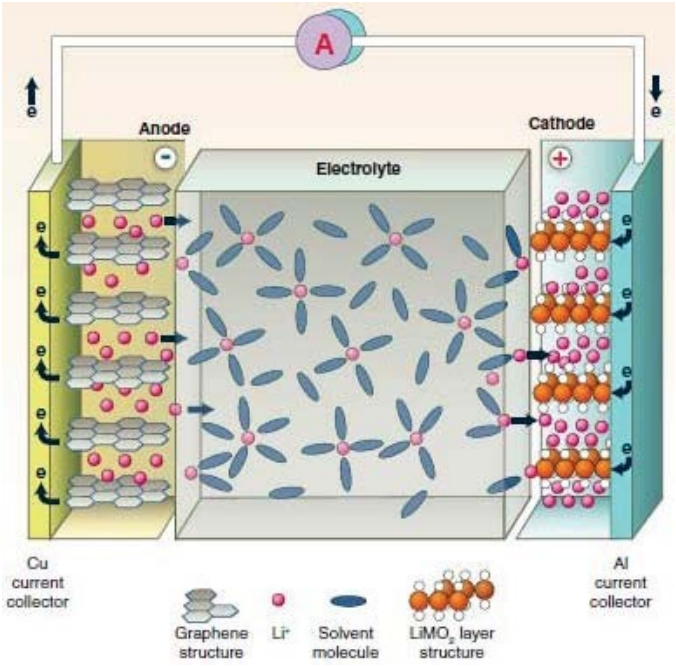


Figure 3-1: General Li-ion battery structure [47]

Since the first commercialization of a Li-ion battery in 1991 many various types have been developed along the way, pursuing the goal of lower cost and better physical properties. An overview of the most known in the Li-ion family are presented in the following paragraphs.

### Lithium Cobalt Oxide - LCO ($LiCoO_2$)

Lithium cobalt oxide ($LiCoO_2$) or LCO was developed as the first commercial LIB, introduced by Goodenough, and commercialized by Sony in 1991. It is a mature technology, which is still very popular in portable consumer electronics, mainly in cell-phones and laptops. This technology is known for its relatively high energy density, high cycle-life and high discharge voltage as compared to other battery types, such as Ni-MH, Ni-Cd and Pb-A [47], [6], [32].

Comparing this technology to other LIBs, the disadvantages are: short lifetime, and limited specific power. That is; to charge or discharge this type of a battery,

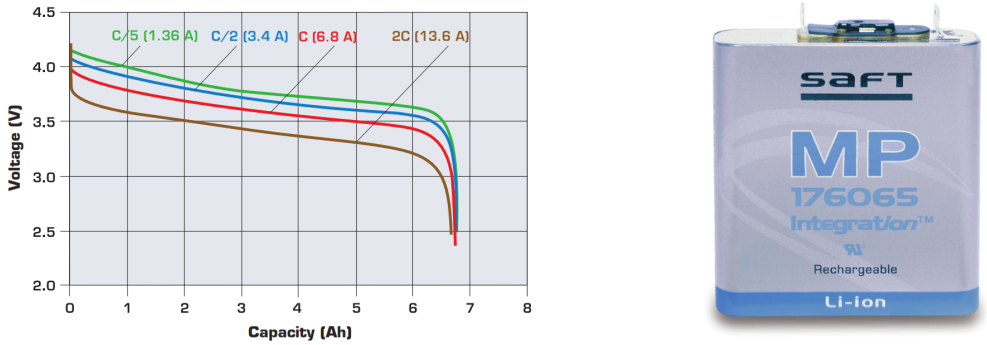


(a) Discharge characteristics at 20°C (b) Prismatic battery cell

Figure 3-2: Saft MP 176065 LCO Prismatic Cell

the charging/discharging current should not exceed the nominal battery rating (i.e. 1C rate, explained further in Chapter 4). If exceeded, an overheating and additional stresses are caused. LCO batteries have also the lowest thermal stability of all commercial cathode materials [32]. An example of a LIB from a well-known French battery manufacturer SAFT can be seen in Fig. 3-2, with a complete data sheet in Appendix B. Another LCO cell data sheet example from Boston Power can be also seen in Appendix C.

The battery is typically rated at 3.7V, with specific energy density between 110 - 190 Wh/kg and life-cycle between 500 - 1000 cycles. The battery's internal structure consists of a graphite carbon anode as it is the case of all the batteries in this section and a cobalt oxide cathode with layered structure as shown in Fig. 3-3a.

The high price of cobalt and poor thermal stability however make this type of battery not very suitable for high volume (large-scale) applications.

Manufacturers: Sony, Kokam, Boston Power, Saft

### Lithium Nickel Oxide - LNO ($LiNiO_2$)

With intent to eliminate cobalt for its high cost, an LNO topology has been analyzed. It has the same crystal structure as LCO, provides higher specific energy (around 15-20%) and has lower cost. On the down side however, this type has even lower stability than LCO. To improve this technology, other elements, including Al, Co, Cu and Mn are added, resulting in new battery types, such as: NCA and NMC as shown below.

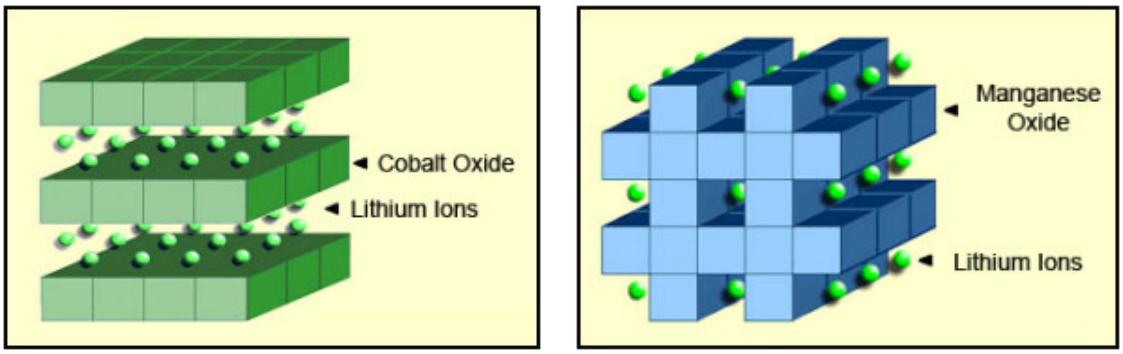


(a) LCO and LNO cathode structure (b) LMO cathode structure

Figure 3-3: Layered vs spinel cathode structure [6]


(a) Panasonic NCR18650B cell (NCA) (b) Keeppower NCA battery cells

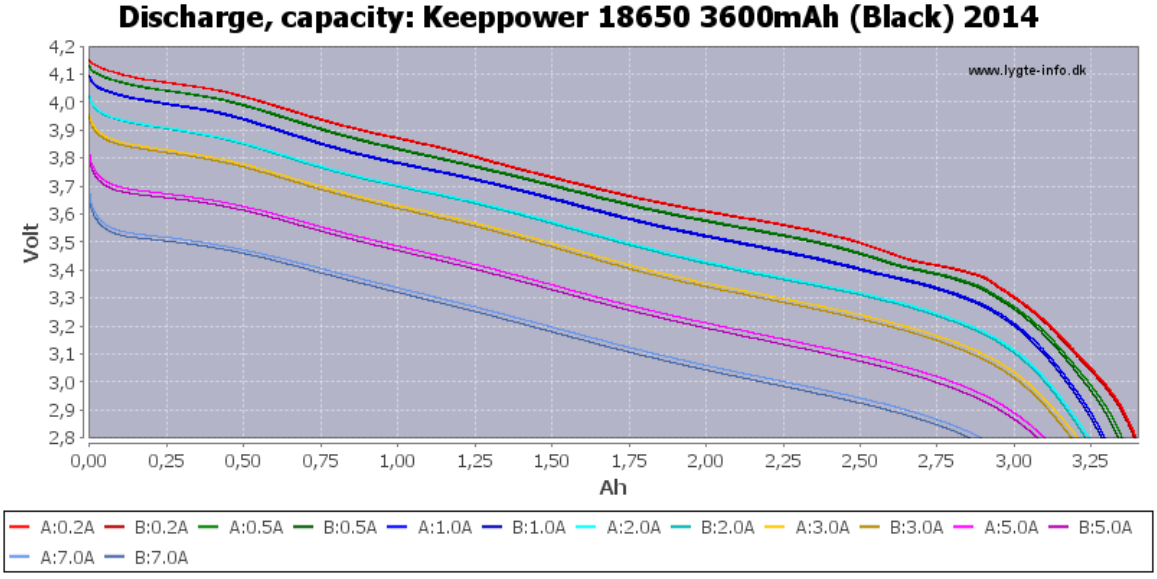


(c) Keeppwer 3600mA battery discharge characteristics

Figure 3-4: An example of an NCA battery [27]

### Lithium Nickel Cobalt Aluminium Oxide - NCA ($LiNiCoAlO_2$)

NCA batteries have been introduced in 1996, they generally provide great performance in terms of energy density, power density and lifetime. This technology follows the LNO topology, in which Al and Co are added to improve its stability characteristics.

The downside of this Li-ion chemistry is its low safety feature (safer than LCO and LNO though) and high cost [47], [6]. An example of NCA battery cells and a typical NCA discharge characteristics can be seen in Fig. 3-4.

NCA can be a very good choice for a GESS, because of its high cycle-life and high specific capacity allowing to charge/discharge the battery at high C-rates, particularly suitable for high power applications. The cost barrier that comes with an NCA battery although yet have to be tackled.

Among the main manufacturers utilizing this technology belong also Panasonic making batteries for Tesla's EVs [14]. Other manufacturers: SAFT, PEVE, AESC.

Manufacturers: Samsung, PEVE, EIG, Hitachi, Sanyo, LG Chem, GS Yuasa, Kokam.

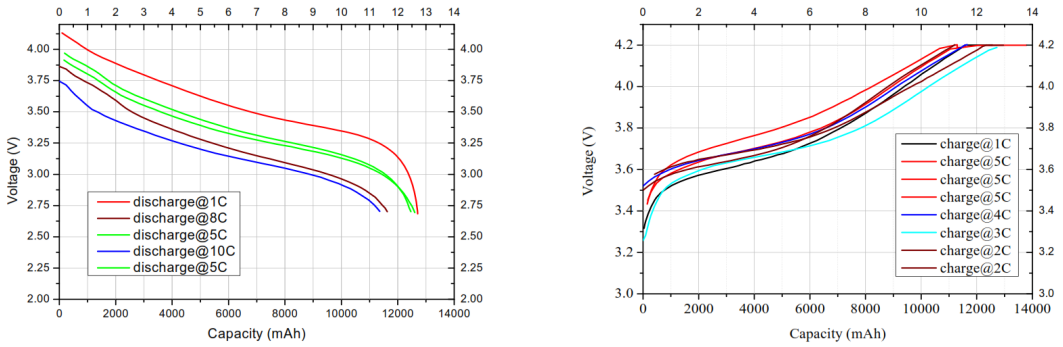


(a) Discharge characteristics (b) Charge characteristics

Figure 3-5: Charge and discharge characteristics of a 12Ah NMC battery [22]

### Lithium Nickel Manganese Cobalt Oxide - NMC or NCM ($LiNiMnCo_2$)

Adding cobalt to the original LNO structure enhances the battery's stability, further providing higher specific energy in comparison to LCO at lower cost since the amount

of cobalt is reduced. Very common technology on the market [47], [6]. An example of charge/discharge curves for this technology is shown in Fig. 3-5.

One of the main providers of this battery type is Samsung SDI that also aims to approach the GESS market as well as the EV market [42]. The current performance and future plans for Samsung SDI batteries can be seen in Fig. 3-6.

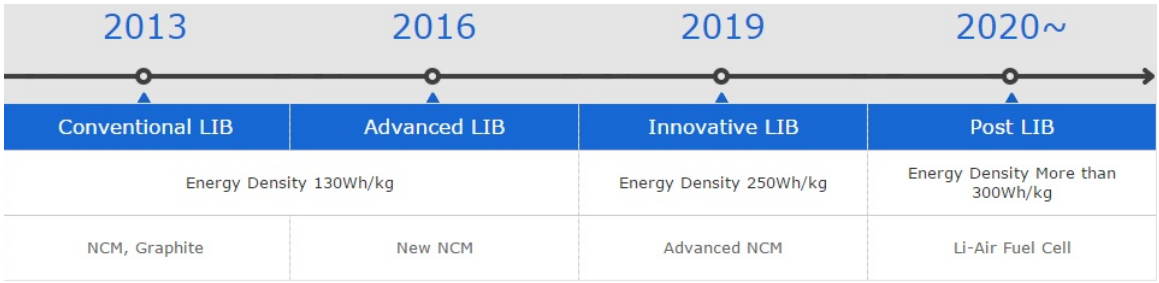


Figure 3-6: Samsung SDI - Battery technology roadmap [42]

### Lithium Manganese Oxide - LMO ($LiMn_2O_4$)

In comparison to the LCO, LMO has higher rated voltage at about 3.8 to 4V with an energy density lower by 20%. Among the main advantages belong: lower cost, high thermal stability providing better safety features, low internal resistance and capability to provide higher charge/discharge rates. The manganese is also low in cost, abundant in the nature and environmentally friendly. LMO are however also regarded as technology with lower cycle life due to its higher capacity loss, and low specific energy as mentioned earlier [47], [6].

For GESSs, the LMO technology has certain potential mainly due to its lower cost and improved safety in comparison to other LIBs. Also in this case, Samsung seems to have noticeable intentions [41].

Manufacturers: Hitachi, Sanyo, Gsyuasa, LG Chem, Samsung, Toshiba, Altairano

### Lithium Iron Phosphate - LFP ($LiFePO_4$)

Lithium Iron Phosphate was discovered in 1996 at the University of Texas. LFP batteries provide high capacity, low cost, flat cell voltage profile and an environmentally friendly structure. Its operation is similar to NCA, but with enhanced safety.

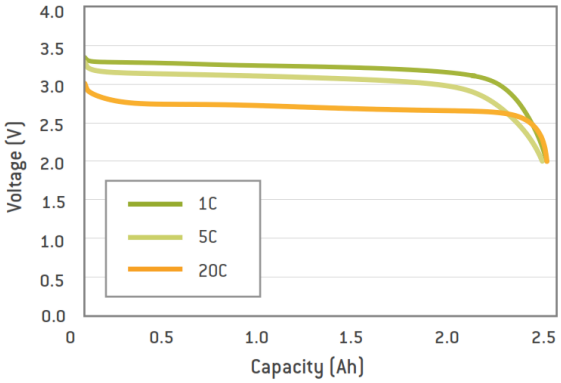


(a) Discharge characteristics at T = 23°C


(b) A123 battery cell

Figure 3-7: An example of a LFP battery - ANR26650m1-B series by A123 Systems [6]

This technology is particularly interesting in automotive and high power stationary applications for the following features: good thermal stability, high safety, very high charge/discharge rate, low self-discharge (although slightly higher than other Li-ion technologies) and high lifetime span. The low nominal voltage of a single cell at around 3.2V however limits the battery's specific energy [47].

An example of an LFP battery cell made by A123 Systems is shown in Fig. 3-7, with a complete data sheet in Appendix D. In this figure, the very high discharge capability of 20C can be also seen.

Manufacturers: A123 Systems, BYD, GS, Yuasa, SAFT, EIG, Lishen

## 3.2 Li-metal Batteries

### Lithium Titanate Oxide - LTO ($Li_4Ti_5O_{12}$)

In this case, the anode consists of a lithium titanate nanocrystals instead of carbon. This allows the battery faster and higher release of ions allowing the flow of higher currents resulting in the battery's faster recharging capability. This technology has good safety and stability features at the cost of lower but flatter voltage level (typically 2.2V). Among the main advantages belong: high rate charge/discharge (up to 10C), while sustaining good thermal stability. They can also operate well at very low temperatures [47].

This technology is still however quite expensive with relatively low specific energy that limits its use in GESSs. Among some of the current applications belong its use in power trains and UPS devices. Manufacturers: Altairnano, EIG, Laclanché

## 3.3 Comparison of the Current LIBs

A comparison of the main features for the current LIBs can be seen in Table 3.1.

Table 3.1: Comparison of various LIB chemistries [47]

| Type | Specific capacity [mAh/g] | Nom. voltage [V] | Specific energy [Wh/kg] | Cycle-life [cycles] | Other features | | |
|---|---|---|---|---|---|---|---|
| | | | | | Safety | Lifetime | Cost |
| LCO | 140 | 3.7 | 110 - 190 | 500 - 1000 | Poor | Average | High |
| LMO | 146 | 3.8 | 100 - 120 | 1000 | Average | Poor | Average |
| NCA | 180 | 3.6 | 100 - 150 | 2000 - 3000 | Low | High | High |
| NMC | 145 | 3.6 | 100 - 170 | 2000 - 3000 | Low | Good | High |
| LFP | 170 | 3.3 | 90 - 115 | >3000 | High | Average | Average |
| LTO | 170 | 2.2 | 60 - 75 | >5000 | High | High | High |

In a graphical way, a comparison of the various lithium chemistries depicted above is shown in Fig. 3-8.

**Conclusion**

With reference to the LIB technologies presented above, there are several that stand out for the GESS application. From the general performance point of view, NCA and NMC seem to provide the best results, mainly due to their high specific energy (i.e. Wh/kg) and reasonable cycle-life. These two are however also quite low in safety and high in cost. With respect to cost, LMO and LFP represent better solution supported by improved safety features. The limited cycle-life of LMO may however put some limitations to its final application. Neglecting the Specific energy parameter that may not be essential for stationary GESS applications, LFP might be chosen as the best GESS option from the currently available technologies for its good lifetime, outstanding safety, high power capabilities and more importantly reasonable cost.

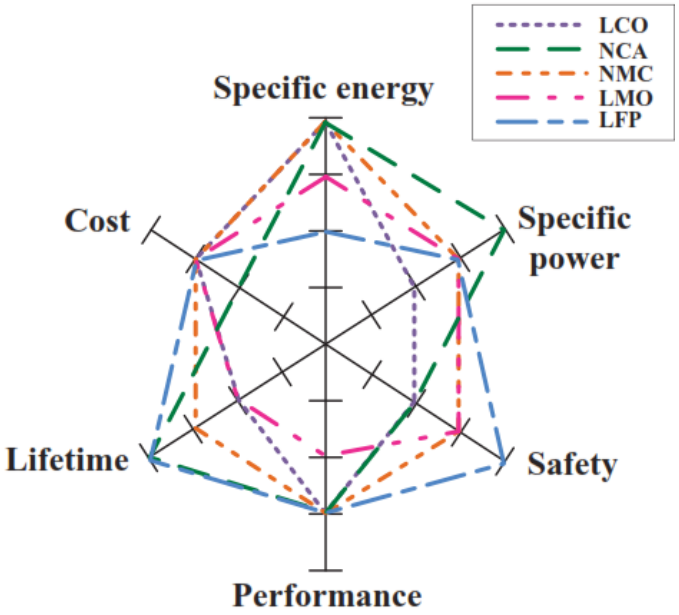


Figure 3-8: Comparison of various Li-ion chemistries [47]

Similarly, in the same sense, if the cost of LTO decreased, its utilization in GESS would be also very reasonable for its high safety, high charge/discharge capability and very long cycle-life.

In general, it shall be then very interesting to observe these technologies on how they develop in terms of cost and performance in the near future. In addition, beside the current LIB technologies, new emerging technologies should be also carefully observed, for the reasons depicted in the next section.

## 3.4 Emerging LIB Chemistries

### Lithium Air - Li-air ($Li_2O_2$)

New emerging technology at its very first stage of development that promises very high energy density almost approaching the one of fossil fuels. The anode is composed from a lithium metal and the cathode is made of a porous carbon, while $O_2$ comes in form of air [47].

### Lithium Sulphur - Li-S ($Li_2S$)

In a similar fashion as in Li-air, the anode of Li-S is also made from lithium metal, while instead of oxygen, sulphur is used to form solid $Li_2S$ instead of gaseous $Li_2O_2$ [47].

At the moment, Li-S provides better cycle-life and higher efficiency than Li-air. Its energy density is however lower than the one of Li-air. Given the generally low cost for sulphur, the Li-S batteries have certain potential to became competitive with other commercially available Li-ion batteries. The development must however overcome various obstacles arising from the sulpur's nature, including: low electric conductivity, or a low vaporization point of sulphur, that contributes to losses of the active material in the battery [47].

Manufacturers: Oxys Energy, Sion Power

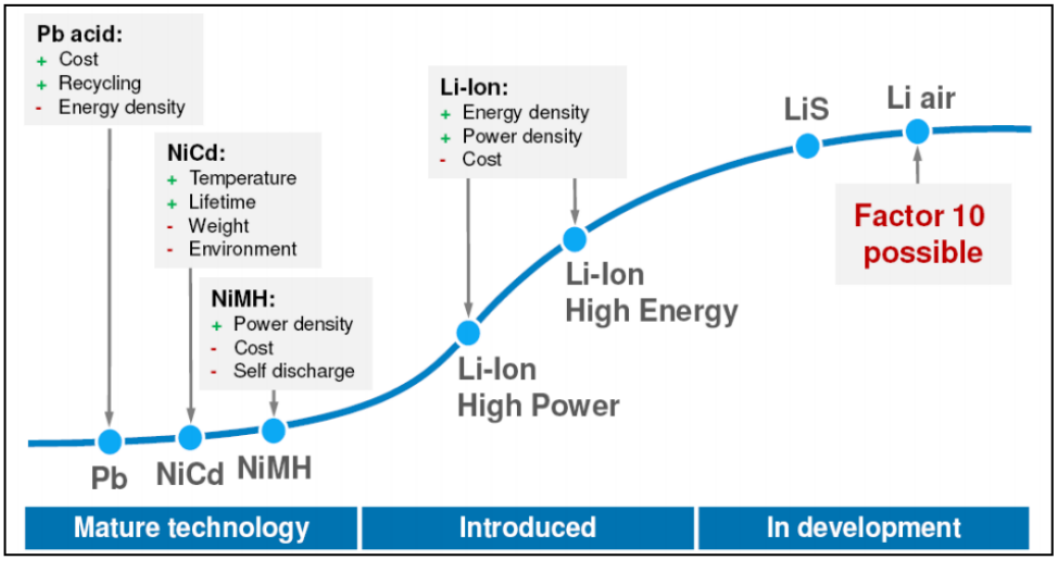


Figure 3-9: An outlook for development of LIBs, where factor 10 means that the future LIBs should reach 10x the energy density of the current LIBs [16]

### Lithium-silicon

Silicon is a very attractive choice of anode material for various reasons, including: very high theoretical charge capacity, high specific energy and more importantly, low cost, given its abundance in the world and already well developed manufacturing facilities.

The obstacles in its implementation however lie in high brittleness of silicon. This can make the silicon anode pulverize because of significant expansion that occurs when the battery is charged/discharged. Furthermore, the high charge capacity of silicon may not be utilized at the moment because of the incapability of the current cathode materials to approach this high charge capacity of silicon [16]. Nonetheless, this technology is well under development at various universities as well as in the industry, where Panasonic considers first designs to be commercialized in customer electronics as soon as in 2020 [16].

# Chapter 4

# Understanding LIB Characteristics

Although a battery may seem as a generally simple device that allows to store and release electric energy, in its essence it is a rather complicated unit, which requires a considerable attention. The main complexity of the battery comes from its internal chemistry and structure that affect its external character and performance, as also portrayed in Chapter 3. In this section it is intended to elaborate on some of the main characteristics of a LIB as a background for the forthcoming chapters that will be regarded to LIB modeling.

## 4.1 Charge and Discharge Characteristics

To get the basic understanding of the battery's behavior a manufacturer data sheet is commonly provided, including its nominal parameters and charge/discharge characteristics or charge/discharge curves, respectively.

For the discharge state, two sets of curves are usually provided, as shown in Fig. 4-1. In case of charging, the basic CC-CV (Constant Current - Constant Voltage) curves are usually given with additional information at what voltage should the CV phase start and at what current should the charging stop. An example of such curves can be seen in Fig. 4-2. This concept of battery charging will be also discussed more in detail later in the report. For charge state a similar set of curves as for discharge state may be also available from some manufacturers although very exceptionally as

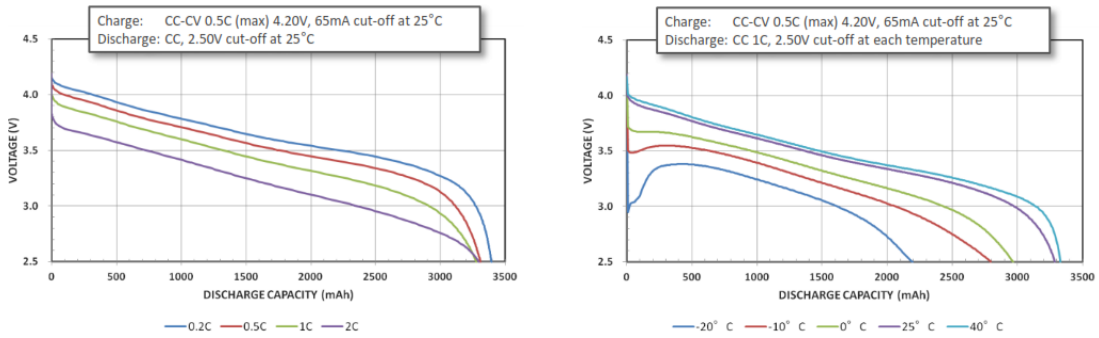


(a) Discharge curves for various C-rates (b) Discharge curves at various temperatures

Figure 4-1: An example of discharge curves describing the battery's behavior during discharge state

the battery manufacturers generally tend to provide very little of information.

A complete data sheet including the curves depicted in Fig. 4-1 and Fig. 4-2 can be seen in Appendix A. Additionally, other charge and discharge characteristics for comparison can be also seen in Appendices B, C, D.

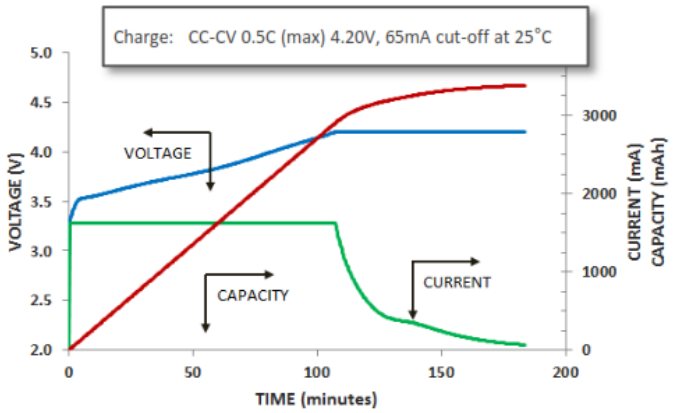


Figure 4-2: Typical LIB charge characteristics

## 4.2 Nominal Parameters

A brief overview of some of the nominal battery parameters is shown below [6] [47]:

- ***Nominal capacity (Rated capacity)*** is the rated value of available capacity in the battery defined by the manufacturer. Since the battery's capacity is subjected to C-rate effect, Temperature effect and Aging effect (all explained later in this chapter) the nominal capacity gives reference information that correspond to certain temperature and charge/discharge current. Commonly defined for temperature between 20-25°C and charge/discharge current of half the nominal value (general case for LCO batteries), but can very with the chemistry. Commonly specified in Ah, mAh, or eventually in Wh, kWh, etc.

- ***Nominal C-rate discharge/charge*** defines at what current is the most optimal to discharge/charge a battery. For example, if a battery has a nominal capacity of 3250mAh and the optimal C-rate discharge current is 0.5C, the battery would be optimally discharged at half of its nominal capacity, or 1625mA respectively as for this particular example. Similarly for the charge state. Generally, it is common to have higher C-rates for discharge than for charge.

- ***Maximum C-rate continuous discharge/charge current*** specifies the maximum value of current that can be applied to the battery.

- ***Maximum C-rate peak (pulse) discharge/charge current***, gives a value of current, eventually a value of power in Watts, that can be applied to a battery for a limited period of time.

- ***Nominal voltage*** provides a reference voltage value. For example: a typical nominal voltage for a LFP battery is around 3.2 - 3.3V, although for a LCO battery it is between 3.6 - 3.7V.

- ***Nominal cell impedance*** states the battery's internal impedance referred to the battery's nominal conditions. It is important to note that the battery's internal

impedance frequently changes in function of C-rate, temperature, state of charge of the battery (SOC) and cycle-life.

- ***Cycle-life*** specifies a number of cycles that the battery can perform in a lifetime. Respectively, a number of cycles that can be performed before the battery capacity falls below certain point relative to the nominal capacity of the battery. This point is also called the End of Life (EOL) and is usually assumed to be 70 or 80% of the nominal capacity. When reaching EOL, the battery is said to be outdated and should be replaced To ensure the longest possible cycle-life of the battery, the daily operational routine should be optimized to minimize the aging effect (described below).

- ***Specific energy (Energy density)*** represents energy stored in the battery over a unit of mass or volume. Usually expressed in Wh/kg or Wh/l.

- ***Specific capacity (Power density)*** provides ratio of Rated (Nominal) capacity over a unit of mass. Example: mAh/g, Ah/kg. The two former parameters play crucial role mainly in the EV industry as there the battery volume and mass can cause significant problems. For the stationary applications the volume and mass of the battery generally do not represent a big obstacle.

- ***Operating temperature*** is a common parameter specifying at which temperature the battery can be utilized. It should be noted that the temperature ranges may vary for charge state, discharge state and for storage off-state.

## 4.3 Battery Phenomenons

### 4.3.1 Rate-dependent capacity (C-rate effect)

This phenomenon is defined by the internal battery chemistry processes and generally describes the fact that the battery cannot be fully charged or discharged if the charging/discharging currents exceed certain C-rate.

In more detail, the active particles inside the battery flow from one electrode to another where they react with the other electrode. At the former electrode, from which the particles left, a diffusion with the battery's electrolyte takes place. Lost of capacity appears when the diffusion process of the active particles lags behind the process of reaction at the other electrode. This is common at higher charge/discharge currents. If a battery is left for some time or charged at sufficiently low current that the diffusion process manage to keep up, the battery's capacity can be fully utilized [36], [57].

This phenomenon can be also seen in Fig. 4-1a, where the full capacity of the battery decreases with the rise of C-rate.

### 4.3.2 Temperature effect

Temperature has a significant impact on the battery. Given that the optimal conditions for a LIB are around 23-25°C, at lower temperatures than that the chemical activity in the battery decreases while the internal resistance increases. At higher temperatures the internal resistance decreases and the full charge capacity is increased. The higher capacity may be however canceled out by the increased self-discharge that arises from the increased internal chemical activity [36], [7], [57]. This phenomenon can be seen in Fig. 4-1b.

An interesting observation of an expected calender lifetime of a battery when exposed to different temperatures and under various State of Charges (SOCs) can be seen in Fig. 4-3a.

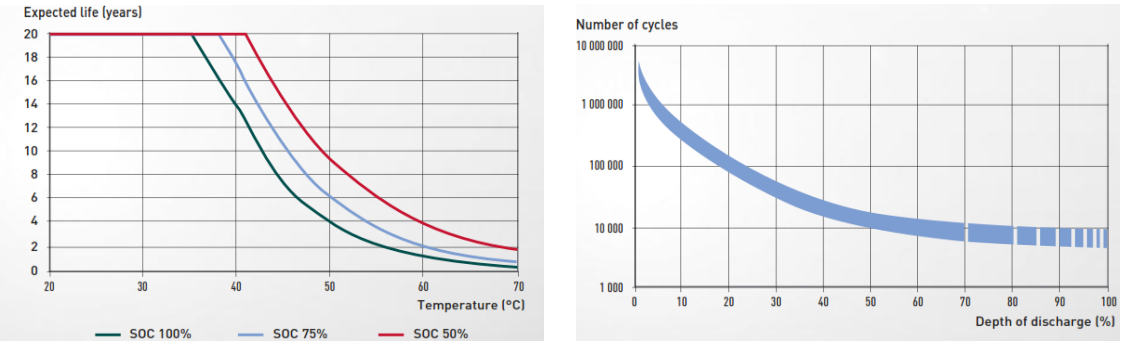


(a) (b)

Figure 4-3: LIB characteristics a) Calendar life vs temperature and SOC, b) Cycle-life vs DOD [37]

### 4.3.3 Self-discharge

Self-discharge of a battery can be defined as an autonomous decrease of battery's charge (SOC respectively) over time without any load being connected to the battery. One of the advantages of Li-ion technology is its low self-discharge in comparison to other battery technologies as also shown in Table 4.1. It is important to note that self-discharge is also dependent on temperature and the battery's SOC, that is: self-discharge increases at higher temperatures and is more profound when battery is more charged [45], [7].

Table 4.1: Self-discharge for various battery types [45], [7]

| Battery type | Alkaline | Lead-acid | Li-ion | Ni-Cd | Ni-MH |
|---|---|---|---|---|---|
| Self-discharge per month | 2-3% | <5% | <5% | 10-15% | 20-30% |

### 4.3.4 Aging effect (Capacity fade)

Aging effect or the Capacity fade effect is a common phenomenon that causes an irreversible loss of the battery capacity with increasing number of charge/discharge cycles. As previously mentioned, the parameter Cycle-life refers particularly to this phenomenon, respectively, it states the expected number of cycles under certain operating conditions [57].

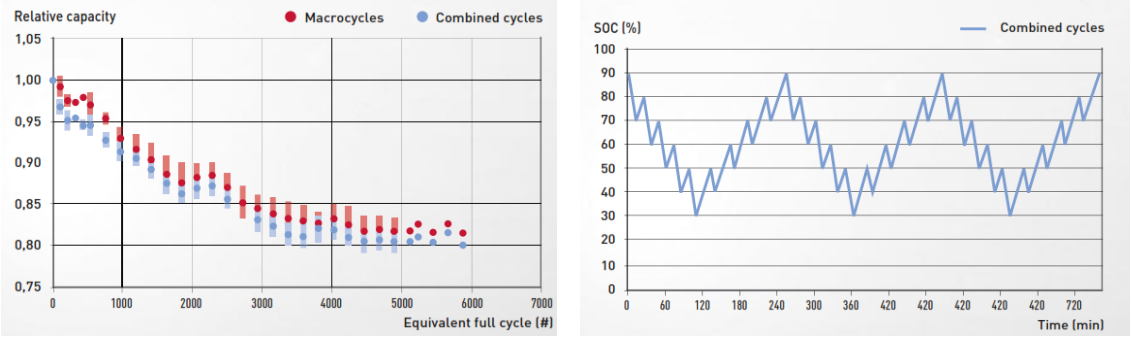


(a) (b)

Figure 4-4: LIB characteristics a) Macrocycle/Combined cycle vs Cycle-life, b) Combined cycle example [37]

Among the main reasons for the capacity loss belong: charging/discharging battery at high C-rates, battery overcharging and battery discharging upto high Depth of Discharge (DOD) (i.e. full or close to full battery discharge). A graph showing the influence of DOD on the battery cycle-life can be seen in Fig. 4-3b.

In physical terms, dealing with battery under such conditions results in electrolyte decomposition, passive film formation and active material dissolution that firstly causes an increase of the battery's internal resistance and finally can develop into a complete battery failure.

Degradation of the battery can be mitigated using various techniques. These include: battery charge and discharge at lower C-rates, discharging a battery with low Depth of Discharge (DOD) and battery charging upto lower cut-off voltage (i.e. lower voltage level for CV phase [20], [36].

Additionally, the influence of different cycling approaches on the battery Cycle-life or the Aging effect respectively, can be seen in Fig. 4-4a. In this figure, the macrocycle approach provides better Cycle-life performance in contrast to the combined cycle approach.

An example of a microcycle can be: from full battery charge (SOC = 100%) the battery is being discharged up to a set value (20% SOC for an instance). Within this period, the battery can be only discharged or left to relax, no charging within this period is however allowed until the set value is reached. The same applied in the

opposite direction. On the other hand, in combined cycle approach, a battery can be charged and discharged throughout the way to the set value as shown in Fig. 4-4b. This is an important information, particularly when planning a daily operational routine of a battery.

## 4.4 Battery SOC and SOH

### Battery SOC

State of Charge (SOC) is a very important information describing the amount of charge (or remaining electrical energy) in a battery. The issue with SOC however comes from the fact that there is practically no way to directly measure it, and only estimation can be used to obtain its approximate value. The precision of the SOC therefore depends on a particular estimation technique used. Another problem also arises from SOC definition, which may not be entirely clear as it will be also seen in Chapter 6.

At the moment, there is an extensive research under way to provide the most accurate estimation technique. An overview of some of the techniques proposed in the literature can be seen in Table 4.2.

As shown in Table 4.2, the estimation techniques can be generally classified into four groups: 1) Direct measurement, 2) Book-keeping estimation, 3) Adaptive systems, 4) Hybrid methods [9].

In the Direct measurement group, each method uses some real measured value of the battery to estimate the SOC. These methods have certain history, although they lack in several aspects: Open circuit voltage method cannot work online, Terminal voltage method gives high error at the end of the discharge curve, and both Impedance methods are very intense on the internal impedance parameter acquisition.

In the second group, the Coulomb counting method and Modified Coulomb counting method belong among the most frequent ones, due to their relative simplicity and reasonable accuracy. In particular, the Coulomb counting method uses integration of the battery's current to obtain SOC value. In case of its modified counterpart,

Table 4.2: SOC estimation techniques - an overview [9]

| Classification | Methodology |
|---|---|
| Direct measurement | Open circuit voltage method |
| | Terminal voltage method |
| | Impedance method |
| | Impedance spectroscopy method |
| Book-keeping estimation | Coulomb counting method |
| | Modified Coulomb counting method |
| Adaptive systems | BP neural network |
| | RBF neural network |
| | Support vector machine |
| | Fuzzy neural network |
| | Kalman filter |
| | Lyapunov-Based method |
| Hybrid methods | Coulomb counting and EMF |
| | Coulomb counting and Kalman filter |
| | Per-unit system and EKF |

the battery's current is slightly scaled to account for Temperature effect and C-rate effect [9]. Both of these SOC estimation approaches can be also seen in the Curve fitting model presented in Chapter 6. In addition, both of these methods are also frequently used in conjunction with other estimating techniques to improve the estimating precision, as also shown in Table 4.2 in the Hybrid methods group.

In terms of the Adaptive system group, this group provides methods that are generally capable to operate online, with the capability to autonomously improve themselves (i.e. to adapt) to the current conditions, based on the battery's terminal voltage and current. As a result, a very accurate SOC estimation can be obtained. In particular, the Kalman filter approach, also including its variations such as: Optimized Kalman Filter (OKF) [17], Extended Kalman Filter (EKF) [55] or Unscented Kalman Filter (UKF) [44]; and the Lyapunov-Based approach [10] seem to provide very accurate and computationally feasible estimation techniques. A good knowledge of the battery in question and its physical possession for a deep analysis is however required to implement these estimation techniques.

### Battery SOH

State of Health (SOH) of a battery could be generally described as information about the battery lifetime, or in other words, the current condition of the battery with respect to its initial condition. Also in this case, definition of SOH is not completely clear [10]. In comparison to SOC, this information may not be as important in regards to the battery's daily routine, although plays a crucial role in the long term perspective.

Given that there is also no direct way to directly measure this parameter, estimation techniques are also used for its acquisition. In a sense described in section Capacity fade, SOH algorithm requires to take into account the battery's operating routine, based on which degradation of the battery can be obtained.

Also for this topic, an extensive research can be found with many approaches presented. Among these, some of the SOC Adaptive algorithms already account for this SOH estimating feature, and seem to provide reasonable results, e.g. Kalman Filter SOH estimation in [31], and Lyapunov-Based method SOH estimation in [10].

## 4.5 Li-ion Battery Pack Concept

With reference to the various LIB chemistries and LIB cells depicted in Chapter 3, a short description of the general battery pack concept is described in this section.

In the most common way, a complete battery pack consists of many small battery cells, such as those described in Chapter 3. These small battery cells are in the most elemental level put into a certain serio-parallel combination to form *a battery module*, and several battery modules are further put in series to create *a battery tray*. Such battery tray then has its own Battery Management System (BMS), which assures that all the batteries are charged and discharged equally (i.e. cell balancing) and that all safety requirements are met (i.e. overheating protection, overcurrent protection, etc.) [35]. In Fig.4-5, en example of a battery tray from Panasonic that consists of 312 18650-type battery cells can be seen.

Moreover, having formed a battery tray, several trays can be put in series to ob-

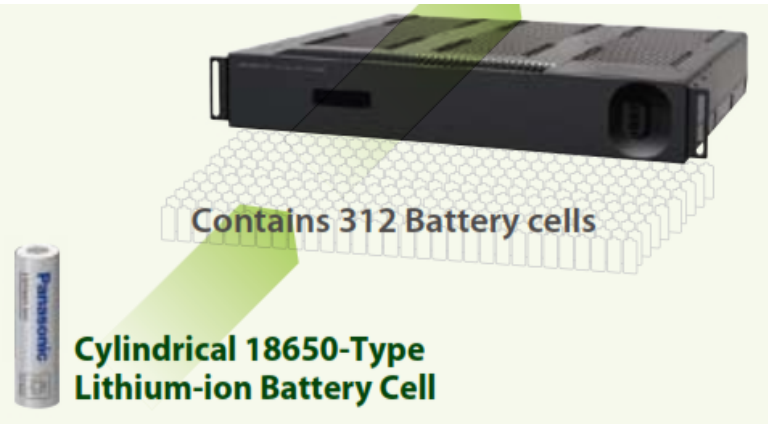


Figure 4-5: LIB tray - Panasonic [33]

tain *a battery rack*. Such battery rack in the end reaches the required voltage level, typically between 500-1000V. Additionally, main battery rack BMS is also added to manage the operation of the entire battery rack. This main BMS therefore communicates with the external equipment (Power Conditioning System) and provides the main information of the complete battery system, such as the battery rack terminal voltage, SOC, SOH, etc. [35].

The definition *Battery pack* may therefore generally refer to any complete assembly, or in some cases also to a single battery tray (Fig. 4-6). In this study, the term battery pack generally refers to a single battery rack, which is specified by number of the fundamental battery cells placed in series and parallel as later shown in Chapter 6.

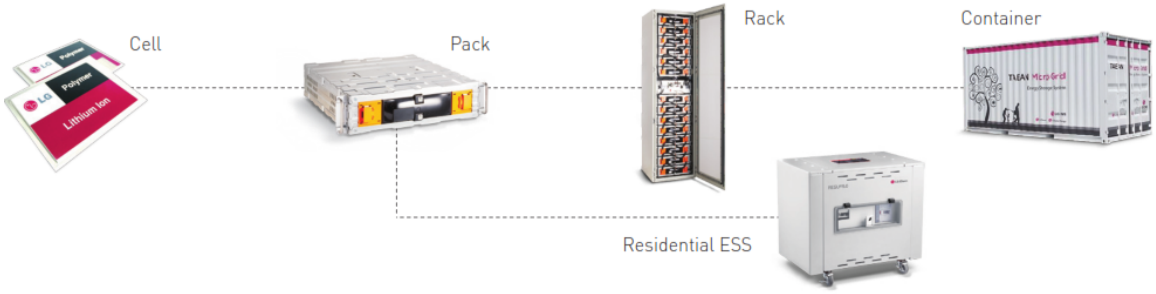


Figure 4-6: LIB Assembly for a GESS by LG Chem [11]

In addition to the battery pack assembly, if high energy storage is required, several battery racks is put in parallel with corresponding number of PCSs. Such assemblies are then typically sold in containers at high power and high energy ratings in units of

MW/MWh. An example of a battery pack assembly from the most elemental level, which is in this case a prismatic LIB cell, up to the container can be seen in Fig. 4-6 as proposed by LG Chem [11].

More information on the battery pack assembly and BMSs can be also found in Appendix E, in which a Li-ion battery pack configuration from Saft is provided. Finally, in AppendixF a typical battery rack data sheet is shown for High Rate (HR) Energy Storage Racks from NEC Energy Systems. An interesting fact can be also noted in this particular case, as inside this battery rack the A123 Systems LFP battery cells (described in Chapter 3, and in Appendix D are used [48].

# Chapter 5

# Battery Modeling - Literature Review

Given the high interest generally developed in the field of batteries and energy storage, initially caused by battery-supplied consumer electronic devices (e.g. mobiles, laptops) and more recently by the progress in the EV and grid energy storage industry, many battery models have been presented in the literature.

As found, these models can be generally classified into four major groups: physical models, empirical models, abstract models and the last group being a mix of any of the three previous types [36], [57].

## 5.1 Physical Models

In their essence, physical models are models representing a battery on its somehow true physical basis, such as modeling of the internal battery chemistry and its electrochemical features. These models are generally very complex, requiring many input parameters and an extensive knowledge of the battery chemical composition, making the model very intense on a computational power. As a result, a very high accuracy is reached, allowing the models to be applied in for example battery-cell development laboratories. Their use is however not beneficial to a simple battery emulator system as these systems are in most cases very sensitive on the model complexity and from

it resulting computational power [36], [57], [25].

Several types of physical models have been reviewed in [25], in which Single Particle Models (SPMs) and Pseudo-2-D Models (P2-D) were used to model a LIB. In Fig 5-1, a linear trend portraying the increasing computational power with the model's accuracy can be observed.

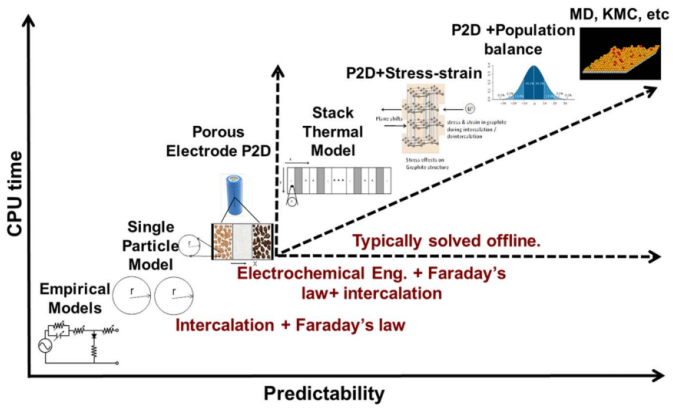


Figure 5-1: Physical battery models - computational power vs model's accuracy

In addition, to allow these models to be implemented in a regular DSPs, a Reduced-order model have been also introduced. These type of models are simplified versions of the complete physical models that still provide certain level of accuracy depending on how much the complete model was simplified [57].

## 5.2 Empirical Models

### Introduction

In contrast to the physical models, empirical models are very simple, with low requirements on computational power. In these models, charge and discharge curves are typically taken and modeled through various mathematical functions; including for example: trigonometric, logarithmic, polynomial, exponential and power law functions [25]. Over time, several approaches using combination of these mathematical functions have been developed, among which probably the most known Shepherd's original model, which will be also introduced in this section, and further analyzed in Chapter 7.

Additionally, different names for this type of models can be also seen in the literature, such as: *Mathematical* models or *Analytical* models [21].

### Shepherd, Unnewehr and Nernst model

An interesting comparison of three different empirical models can be seen in [21]. These are: Shepherd Model (5.1), Unnewehr Universal Model (5.2) and Nernst Model (5.3), as shown in their generic versions.

$$V = V_0 - Ri - \frac{\mu}{SOC} \tag{5.1}$$

$$V = V_0 - Ri - \mu(SOC) \tag{5.2}$$

$$V = V_0 - Ri + \mu_1 ln(SOC) + \mu_2 ln(1 - SOC) \tag{5.3}$$

Where: $V$ is the battery's terminal voltage, $V_0$ is the battery's nominal voltage, $R$ is the internal resistance of the battery, $i$ is the current through the battery (positive for discharge, negative for charge) and $\mu$, $\mu_1$, $\mu_2$ are curve fitting factors particular for each method.

As found, these models vary in accuracy with regard to their application. For example, the Shepherd's model has better prediction of the battery's terminal voltage at continuous current discharge mode, as in comparison to the other two models. This comparison can be also seen in Fig. 5-2. Moreover, the Nernst model performs best when current is being dynamically varied. The Universal model on the other hand seems to provide the most accurate value of SOC among the three models [21].

Nevertheless, the most commonly seen models in the literature are two; the Shepherd's model, also called the *Shepherd's original model*, shown in (7.1) and next *Shepherd's modified model* in (7.2 and 7.3), that is a modified version of the Shepherd's original model.

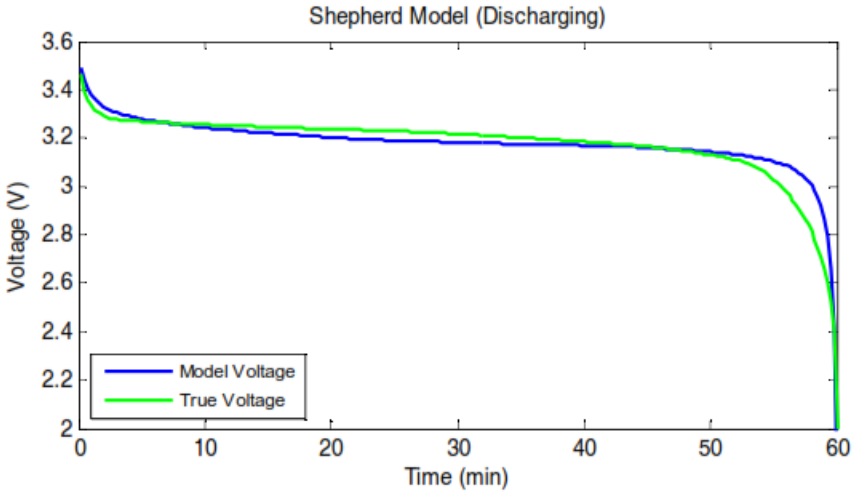


(a)

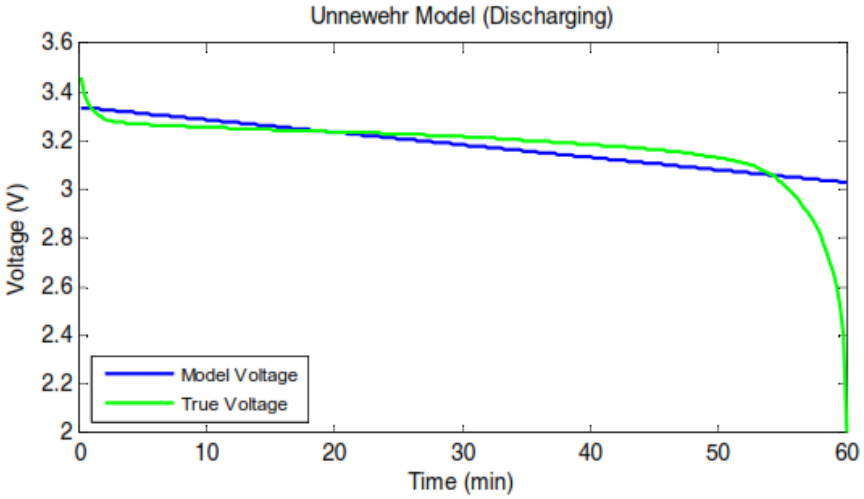


(b)

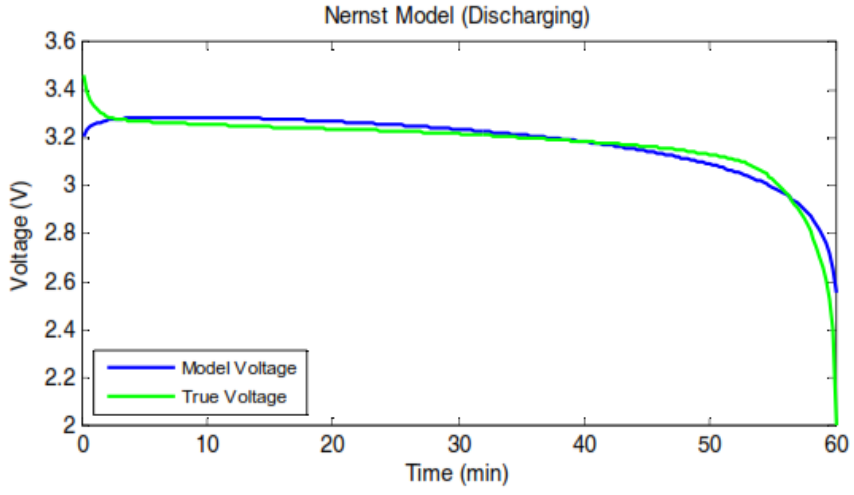


(c)

Figure 5-2: Comparison of three different empirical models in a continuous discharging mode [21]

### Shepherd's original model

Despite the fact that this model has been developed already in 1963 by C. M. Shepherd [43], its original form has persisted over the years up to now and still finds its way to the current research articles, as in [5], [51], [30], [57].

The main advantage of this model lies in its simplicity as only a few parameters need to be extracted from the manufacturer's data sheet. The model developed then represent a reasonable approximation of the battery's behavior, within certain operating conditions. Description of the modeling approach and analysis of this model can be seen in Chapter 7.

### Shepherd's modified model

The modified version of the original Shepherd's model can be seen in (7.2 and 7.3). In this case, two equations are available, one for the discharge mode and the other for the charge mode. This modification then allows to model the battery's behavior with higher accuracy, although still with restriction to certain operating conditions.

This model has found its use for various application, mainly for a simple EV battery models [29], [54], [1]. Interestingly, an implementation of this model can be also seen in a Matlab-Simulink battery model [50] and in a PSIM battery model [34].

Given the certain advantages of the two Shepherd models, their use have been also considered in this study. A thorough analysis of the two models can be seen in Chapter 7.

### Empirical models - conclusion

In conclusion, as already stated before, the simplicity of these models make them well suited for use at low computational power devices, while providing a generally good approximation of the battery's terminal voltage. Severe drawbacks however arise when a more detailed model is required.

In addition, other empirical models have been also proposed in the literature with the aim to improve the overall model or at least some of the model's prediction

capabilities, including: Peukert's law model, Battery efficiency model, Weibull fit model. Any significant improvement of the overall model performance however has not been found in any of these models [36].

## 5.3 Abstract Models (EECMs)

Abstract models use certain elements, to analogically model the battery's behavior. In most cases, this is done trough electrical circuit elements, such as: resistors, diodes and capacitors, upon which an Equivalent Electric Circuit Model (EECM) is created.

In the today's literature the EECMs are taken very seriously and together with empirical models represent the most common choice for a battery system model [25].

EECMs are capable to operate with a reasonable computational power at accuracy higher than the one of the empirical methods. Similarly, as in case of empirical models, EECMs do not generally have any deeper physical/chemical meaning, rather the circuit elements are used to model the battery's external electrical character [25]. The main disadvantage however, in comparison to the purely empirical models is that to obtain an accurate EECM, the model developer must physically posses the real battery as a series of tests is usually needed [57], [40], [12], [56], [10]. An overview of the most common EECMs is provided further in this section.

#### Impedance based EECM

In this approach an Electrochemical Impedance Spectroscopy (EIS) is used to obtain the battery's impedance through imposing small AC currents and measuring its frequency response. The results are then implemented into a special EECM. The disadvantage of this method is the need for a signal generator and the fact that the battery characteristics can be obtained only in the offline state not allowing online parameter re-calibration [57]. An example of the Impedance based EECM can be seen in Fig. 5-3 b).

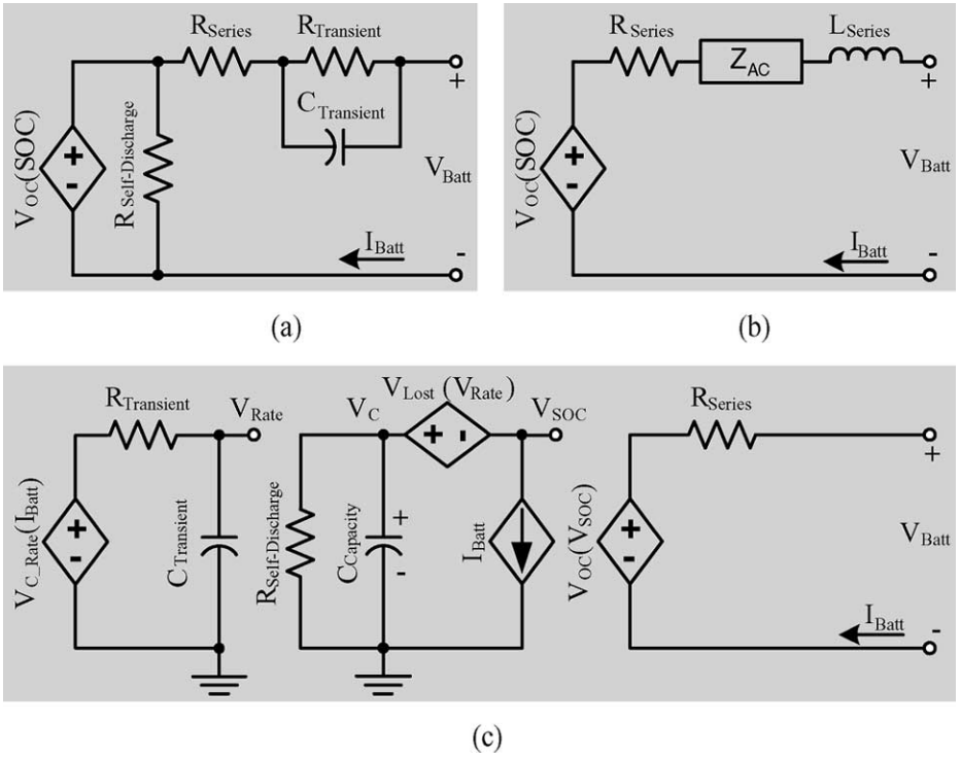


Figure 5-3: EECM - a) Thevenin (RC) model, b) Impedance model, c) Run-time model [12]

### V-I based EECM

In this method the commonly available parameters, such as the battery's current and Open Circuit Voltage (OCV) are used to obtain the model. In general, an ideal controlled voltage source is used to model the battery's OCV. Further, a resistor representing the battery's internal resistance, and non to several RC networks in series modeling the battery's dynamic behavior. Based on the number of RC networks, the n-th order of the EECM is determined. The most common models are the 1st order EECM (also called the Thevenin model or RC model) and the 2nd order EECM (entitled as the Dual Polarization (DP) model). Nevertheless, higher-order models can be also found in the literature. The order of the model is then usually obtained as a compromise between the model's accuracy and complexity [46], [57], [18], [12].

An example of the Thevenin model can be seen in 5-3 a), with the typical series resistor $R_{Series}$ and RC element ($R_{Transient}$, $C_{Transient}$) representing the fast dynamics of the battery. In this particular case, a self-discharge resistor $R_{Self-Discharge}$ is also

included to account for the battery's self discharge. Additionally, an important feature can be also seen in all the models in Fig. 5-3, that is the controlled voltage source dependency on the SOC. As shown, this is particularly the case for the latest models that use a lookup table to capture the non-linear character of the battery's OCV ($V_{OC}(SOC)$.

More traditionally, only a fixed voltage source was used, as a simplified solution to provide the system under examination with sense of the battery's dynamics [12].

### Run-time based models

An example of a *Run-time based model* can be seen in Fig. 5-3 c). These models as from their name have the capability to emulate battery's Run-time or in other words the C-rate effect. Furthermore, they provide a reasonably accurate parameter prediction under the continuous charge/discharge mode. The disadvantage of these models however lies in increased modeling complexity and more importantly in poor accuracy under dynamic conditions [23], [12].

### State of the art EECMs

Combining the EECMs mentioned earlier, that is the Thevenin's model and the Run-time model, it is possible to obtain an EECM, which provides accurate voltage and SOC estimation for both continuous and dynamic conditions, while implementing the Run-time capability [23], [12], [35].

An example of such circuit can be seen in Fig. 5-4. In this figure, on the left side, entitled OCV-SOC characteristic, a controlled current source that is driven by the charging/discharging current is used to charge and discharge the capacitor $C_C$. This capacitor than outputs a value between 0 - 1V as an information of the SOC (0 - 100%) in the battery. Further, a self-discharge resistance $R_d$ can be added to account for the battery's self-discharge. Additionally, in some applications, the current that charges the capacitor can be also further scaled by a temperature correction factor and life-cycle degradation factor [12].

Moving to the right part of this EECM, a lookup table is used to relate the

battery's SOC to the battery's OCV, which consequently drives the controlled voltage source $V_{OC}$. Once the OCV is obtained, the dual RC model (DP model) is used to incorporate the fast and slow dynamics (relaxation effects) and the voltage drop caused by the battery's internal resistance, in this case entitled as $R_b$.

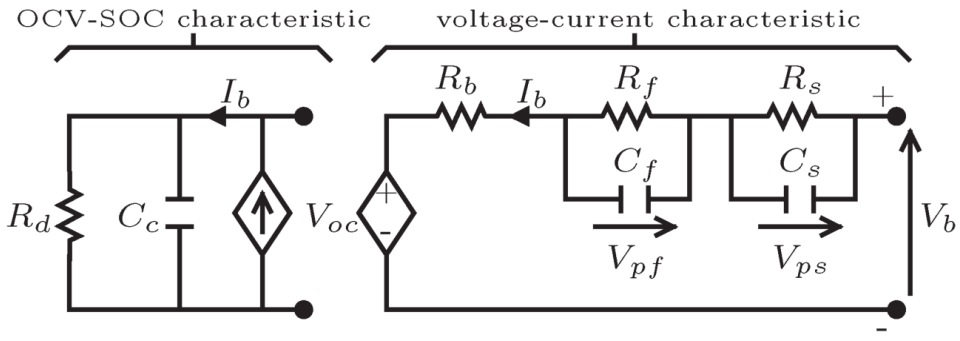


Figure 5-4: State of the art EECM [10]

In principal identical, although more descriptive representation of basically the same circuit can be seen in Fig. 5-5

**EECMs conclusion**

In comparison to the empirical models, the advanced EECMs can prove to provide a good accuracy at a reasonable computational power. Moreover, given that the parameter estimation techniques for these models are well above the level of the empirical models, including SOC estimation, battery terminal voltage estimation, and also the State of Health (SOH) estimation, these models have a great potential in the Battery Management Systems (BMSs).

The main disadvantage of these models however lies in complex acquisition of the internal model parameters, for which several extensive tests must be carried out [56], [40], [10], [19], [4], [24].

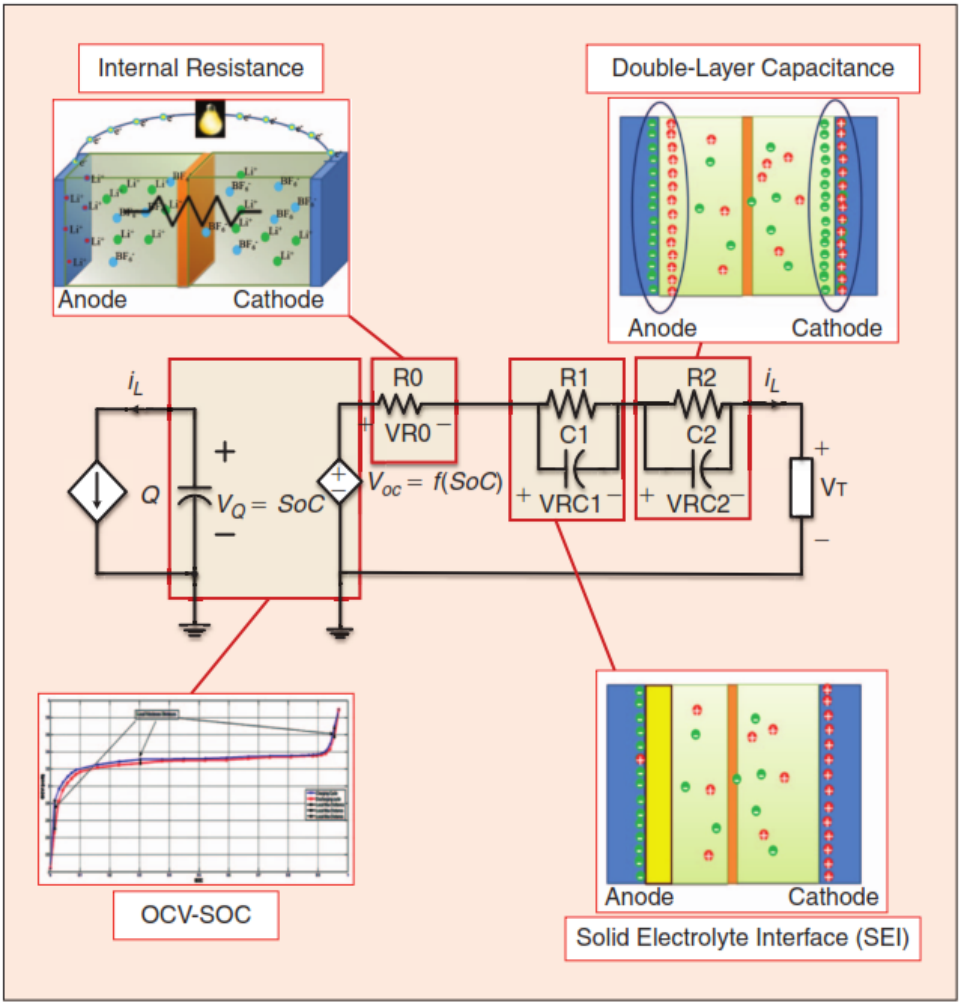


Figure 5-5: Graphical representation of the advanced EECM [35]

## 5.4 Other Models

### Bio-inspired black-box approach

Over the time, other approaches were also considered to model the battery's behavior. Among them belong also the so-called black box bio-approach, in which some sort of intelligent algorithm is used to model a battery, as for example: the wavelet neural network method or the artificial neural network method. In general, these models can provide a reasonable accuracy at the cost of computational power and parameter input intensity. A high level of knowledge of the battery in question is however also needed in this modeling approach [57].

### Other methods

Further, a large number of other methods were also proposed, including: stochastic model, transmission line model or hydrodynamic model. These models however have not got much attention as they are generally focused on improvement of certain parts of a battery model without the capability to sufficiently model a complete battery behavior [57].

### Curve fitting model

Finally, a Curve Fitting Model (CFM) can be used to model a battery or to model the battery's characteristics, respectively. With regards to the previous classification, this approach do not really represent a fully empirical model, nor it is an EECM, but rather utilizes some elements from both. That is: the lookup table approach from the EECMs with use of some empirical relations.

The main principle lies in utilization of two lookup tables portraying the relationship $OCV(SOC)$, providing one reference charge curve and one reference discharge curve. The core of this approach therefore lies in scaling of these reference curves through several C-rate and Temperature factors. As a result, a battery model is developed, providing many features, including [15], [39]:

- Only data sheet based model,
- Temperature effect implemented,
- C-rate effect implemented,
- Reasonable accuracy at manageable computational power.

For these reasons, this approach was considered as the main modeling approach in this study, and its detailed description and analysis will be presented next in Chapter 6.

# Chapter 6

# Curve Fitting Model

## 6.1 BE Physical Implementation

The fundamental idea of the BE lies in measuring of DC current ($I_{DC\text{-}LINK}$) on the DC-LINK (DC bus respectively) and adjusting the DC-LINK voltage ($V_{DC\text{-}LINK}$) with respect to this current. In more complex models, which is also the case in this study, the output voltage $V_{DC\text{-}LINK}$ is also dependent on initial conditions and cell temperature, both manually defined for the purpose of improved battery emulation. An overview of this strategy can be seen in Fig. 6-1.

As shown, the measured value of current ($I_{DC\text{-}LINK}$) is brought to a control algorithm that incorporates this current as an input, altogether with initial conditions, e.g. initial SOC (SOC_INIT) and cell temperature (TEMPERATURE) and outputs a voltage reference value VB_OUT. This value is than translated on the DC-LINK through a controlled voltage source. This voltage therefore represents physical terminal voltage of a battery.

In addition, it should be noted that the control voltage source is used for the purpose of simulation and preliminary system analysis. In reality, VB_OUT is used as a reference for a DC-LINK voltage controller that makes sure that the DC-LINK voltage $V_{DC\text{-}LINK}$ follows the reference VB_OUT. Design of this or any other control loop however is not considered in this study.

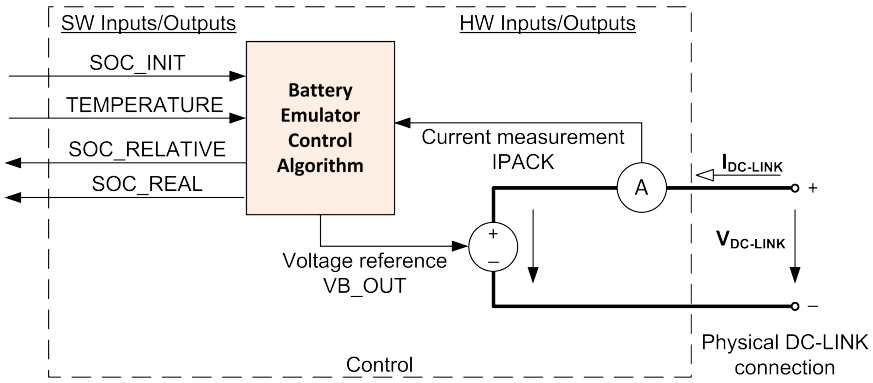


Figure 6-1: BE interface with physical DC-LINK

## 6.2 BE Control Algorithm

### 6.2.1 Overview

To provide a real example of this modeling technique, a real Li-ion battery cell: Panasonic NCR18650B is taken and modeled based on its manufacturer's data sheet that can be found in Appendix A.

An overview of the BE control algorithm can be seen in Fig. 6-2.

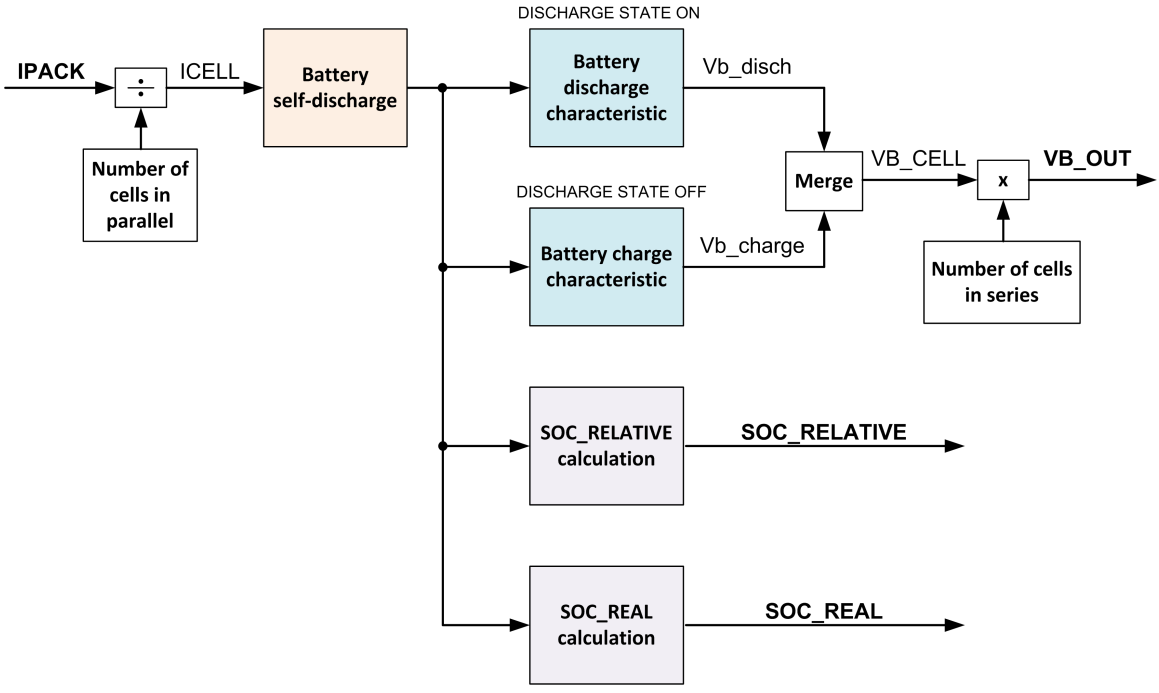


Figure 6-2: BE algorithm overview diagram

With help of this simplified diagram in Fig. 6-2, the control algorithm is split into several parts and described in the following sections.

### 6.2.2 BE self-discharge

In order to implement the self-discharge feature into the model the input current ICELL entering the control is observed for zero or near zero current, defined by a hysteresis. Whenever the current ICELL then falls within this hysteresis, a small positive current (positive = discharge)is applied on the output of the block. If the input current ICELL is outside the hysteresis, the current ICELL is passed on the output without any change.

In this way, whenever there is a near to zero current ICELL, the battery's voltage and SOC will decrease. The value of the so-called "self-discharge current" $\mathrm{ICELL_{SD}}$ is found as a product of the battery's nominal capacity $\mathrm{C_{NOM}}$ in Ah and the value of the battery's daily self-discharge ($\mathrm{SD_{DAILY}}$) as shown in (6.1). In other words, if a battery has 2% of self-discharge per day, which is a common case for Li-ion batteries, it will lose 2% of its nominal capacity in an hour. This feature then allows to speed up the process of analysis. However, since this is only a parameter, the value of self-discharge can be adjusted.

$$ICELL_{SD} = C_{NOM} \cdot SD_{DAILY} \tag{6.1}$$

### 6.2.3 BE discharge characteristics

Probably the most important part of the whole BE model is based on the way the discharge characteristics are modeled, as this reflects the main output of the model: the BE voltage VB_OUT. This method is based on paper [15] and [39].

For this battery modeling approach, it is important to have discharge characteristics of the desired battery. Most importantly the C-rate dependent characteristics, which are given in a way of several curves. An example can be seen in Fig. 6-5. The temperature dependent characteristics are not compulsory but should be included in

case the temperature effect is desired in the model. As already mentioned in the previous chapters, one of the main advantages of this modeling technique include: 1) Model based on data sheet information only, 2) Incorporation of the capacity effect, 3) Incorporation of the temperature effect.

In the following sections, the modeling approach is firstly briefly explained with following description of parameter acquisition for this curve fitting model.

### Introduction

The first step of this method lies in a selection of a reference discharge curve from the battery data sheet information. This curve is then implemented in a lookup table (called: Main Discharge Lookup Table or Main Discharge LUT), having SOD in % (or Capacity in Ah) on the x-axis and the cell voltage on the y-axis (as shown in Fig. 6-3).

The core of this curve fitting technique consists in stretching of this reference curve with respect to the temperature and C-rate, which allows movement of the operation point within the various discharge curves. This feature is allowed through implementation of four correction (scaling) factors K1 - K4, in a way depicted in Fig. 6-3.

The movement of the reference curve in the horizontal direction, in other words, the adjustment for the capacity effect is done with the factors K1 and K2 in a sense shown in (6.2), in which $SOD_{spec}$ is the value pointing on the x-axis of the Main Discharge LUT. Further, $\mathrm{SOD_{INIT}}$ is the initial SOC transferred into initial SOD and the term including $\mathrm{C_{NOM}}$ in denominator serves to adjust the scale from units of Ah into % if the Main Discharge LUT is in % (i.e. x-axis as SOD). Lastly, $i(t)$ is the current value for a single cell also called ICELL.

Hence, when the value of $SOD_{spec}$ is adjusted by either of the two factors, the interpolated voltage that is outputted from the Main Discharge LUT is also adjusted, based on which the capacity effect is incorporated. The entire control procedure

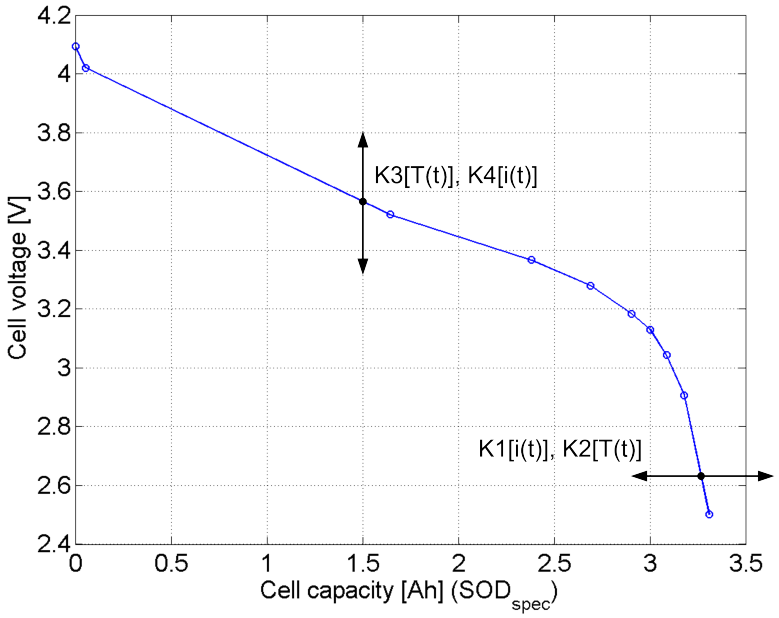


Figure 6-3: Discharge reference curve for 0.5C, demonstration of its adjustment with scaling factors K1-K4

inside the Battery discharge characteristic block can be seen in Fig. 6-4.

$$SOD_{spec} = \frac{100}{C_{NOM}} \int_0^t K1[i(t)] \cdot K2[T(t)] \cdot i(t)dt + SOD_{INIT} \tag{6.2}$$

As also shown in Fig.6-3 and 6-4, the scaling factors K3 and K4 are used to adjust the magnitude of the output voltage. In the following sections, selection of the reference curve and acquisition of the scaling factors is described in detail.

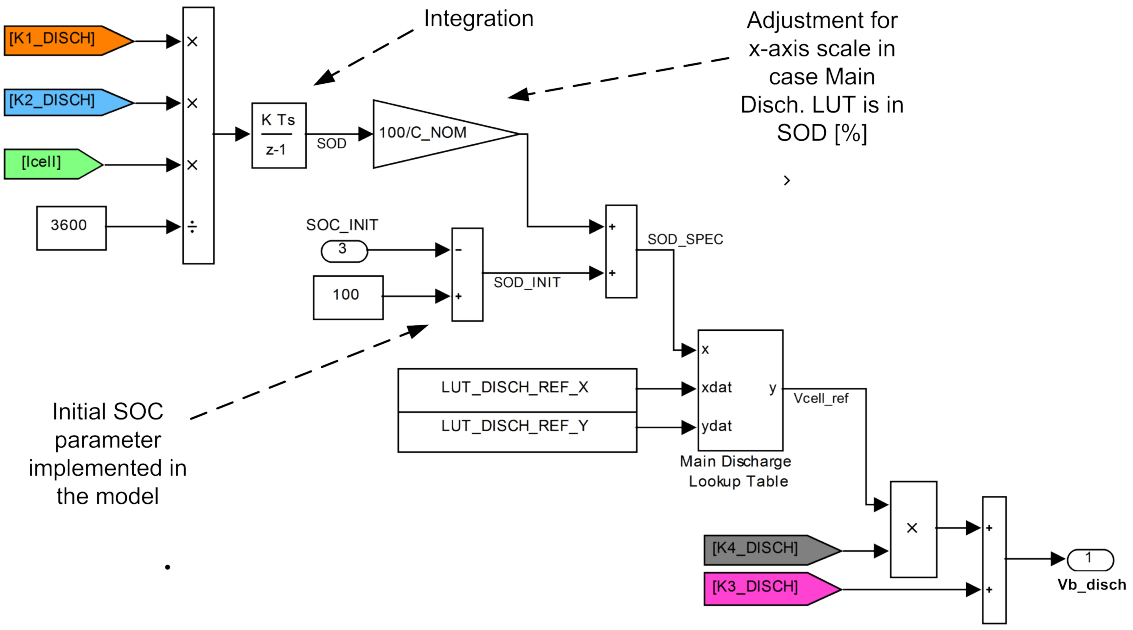


Figure 6-4: BE - Battery discharge characteristic block

### Reference curve selection

Selection of the reference discharge curve should obey several rules: This curve should be the one that most accurately approaches the anticipated operating point of the battery. Eventually, in case a large operational range is required, a curve which most approaches all of the curves withing the operating range should be taken. In this case, with reference to Fig. 6-5, the red 0.5C curve was chosen as it provides a reasonable fit with the other curves. Moreover, if the operating point is assumed only up to 1C for most the time, choosing 1C or 2C curve as the reference curve would not be reasonable. Hence, the chosen reference curve is recorded in Matlab for its further use in a Matlab-Simulink lookup table. The number of points for the curve is chosen as a compromise between the precision and DSP memory/computational power. The reference curve for 0.5C from Fig. 6-5, prepared for its implementation as a lookup table with 2x10 points can be also seen in Fig. 6-3.

A reference curve is also selected for the temperature dependent discharge characteristics if temperature effect is included in the model (Fig. 6-6). In this case, however, this curve is not fully modeled, but only serves to define the reference parameters (i.e.

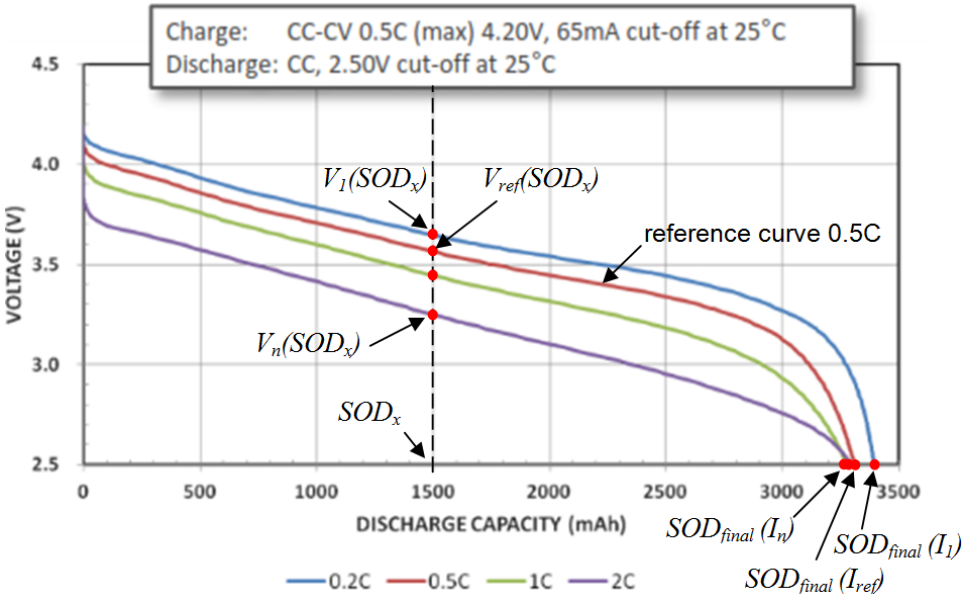


Figure 6-5: Parameter acquisition for current scaling factors K1 and K4

$V_{ref}(SOD_x)$ and $SOD_{final}(T_{ref})$) as it will be explained below.

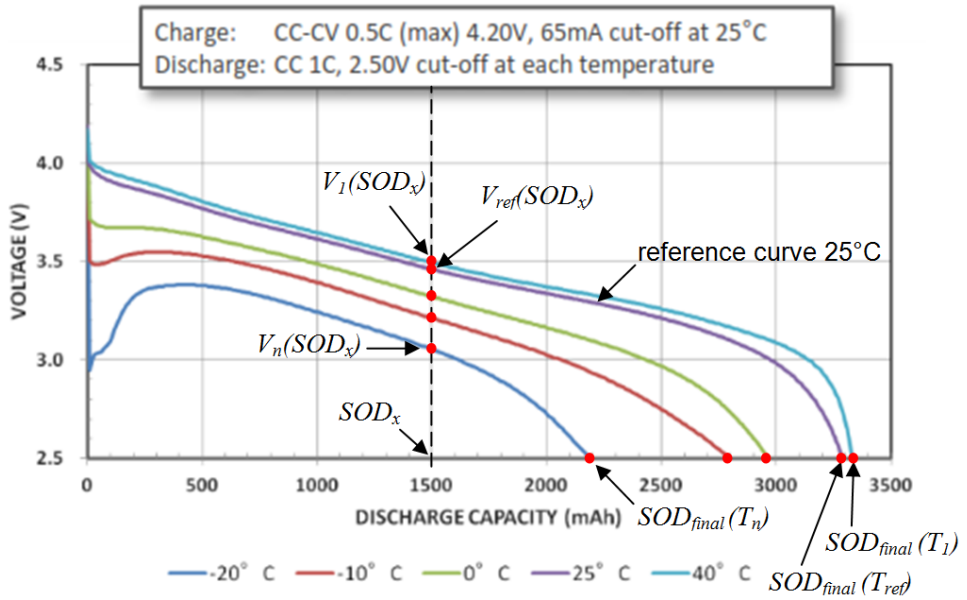


Figure 6-6: Parameter acquisition for temperature scaling factors K2 and K3

Having the reference curves selected, the next step is to obtain the scaling factors that will allow adjustment of the reference curve.

### Scaling factors K1, K2

Two factors are used to scale the reference curve in the horizontal direction: K1 and K2. This feature allows an implementation of the so-called Capacity effect as already described earlier in the study. K1 can be obtained in (6.3) for the values in Fig. 6-5. Similarly, K2 can be found in (6.4) for parameters in Fig. 6-6.

$$K1[I_n] = \frac{SOD_{final}(I_{ref})}{SOD_{final}(I_n)} \tag{6.3}$$

$$K2[T_n] = \frac{SOD_{final}(T_{ref})}{SOD_{final}(T_n)} \tag{6.4}$$

As it can be observed from both discharge characteristics, and also from the results now presented in Fig. 6-7a and 6-7b, the scaling factors K1 and K2 are highly nonlinear. For this reason, they should be implemented in the model through two lookup tables, one for each parameter.

### Scaling factors K3, K4

To scale the reference curve in the vertical direction, in other words to account for voltage drop with regard to the C-rate and temperature applied, K3 and K4 factors are used. K3 can be found according to (6.5) for values depicted in Fig. 6-6. Lastly, K4 is calculated in (6.6) for values determined in Fig. 6-5.

$$K3[T_n] = V_n(SOD_x) - V_{ref}(SOD_x) \tag{6.5}$$

$$K4[I_n] = \frac{V_n(SOD_x)}{V_{ref}(SOD_x)} \tag{6.6}$$

In this case, K3 factor is non-linear, as well as K4 factor (Fig. 6-7c and 6-7d), although in case of K4 factor a linear approximation could be made if a model simplification was desired (red line in Fig. 6-7d). The advantage of using linear function is in less DSP memory used as it is possible to create a linear function with four parameters, instead of using eight parameters, which would be the case for this K4

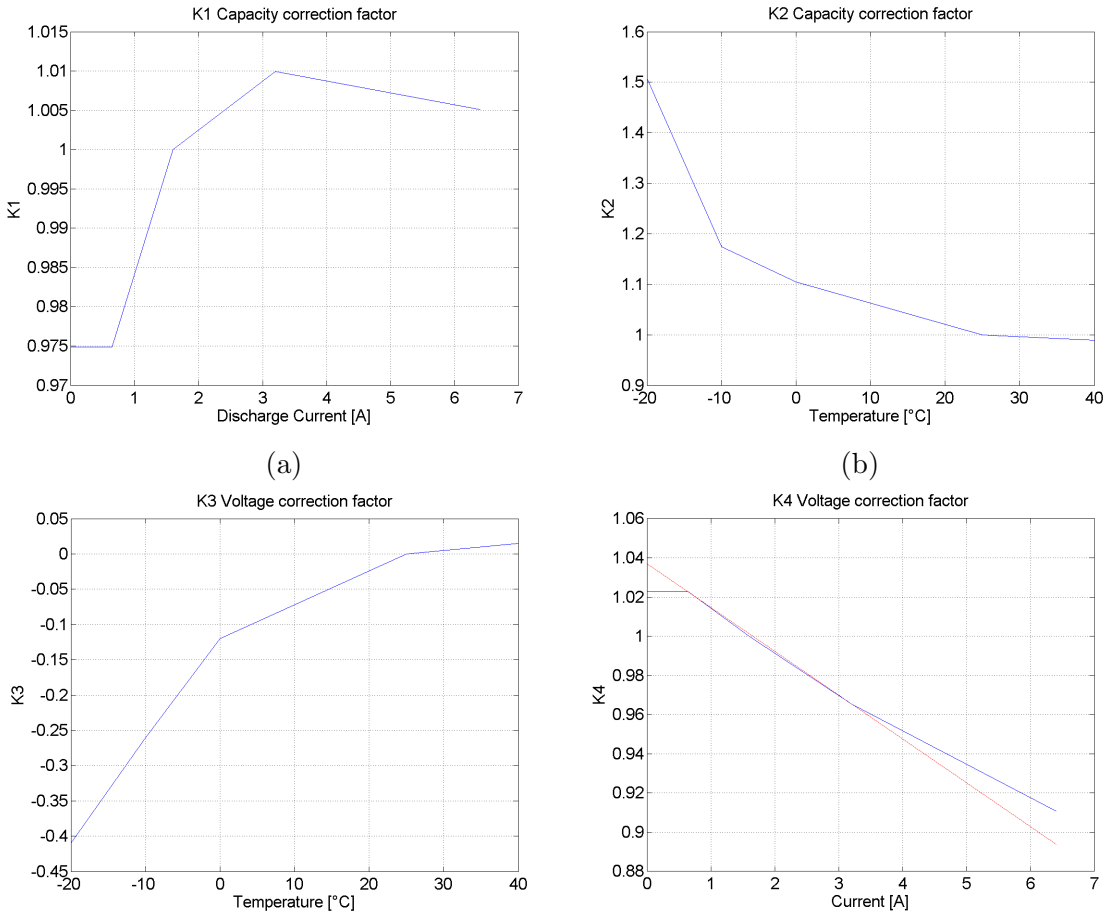


Figure 6-7: Scaling factors K1-K4

factor lookup table. Furthermore, less computation power would be required.

In general, if only a small operating range is required, for example: assuming that only operation at fixed temperature and with limited C-rate is assumed, certain linear approximation could be found also for other factor. Eventually, in case of fixed temperature operation, the temperature dependent factors K2 and K3 may be fully neglected.

An example of lookup table implementation for all four scaling factors regarded for the discharge model depicted in Fig. 6-4 is shown in Fig. 6-8

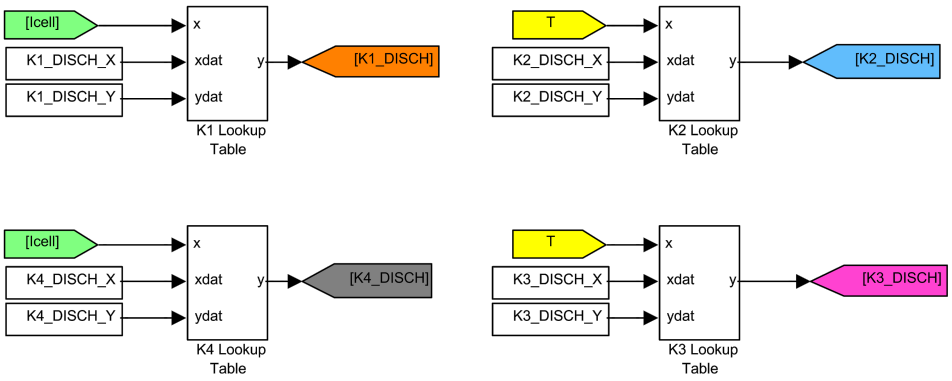


Figure 6-8: K1-K4 lookup tables in Matlab-Simulink

### 6.2.4 BE charge characteristics

To implement the charge characteristics into the complete BE model, practically the same approach as the one described above for discharge characteristics is taken. The main issue however in this case arises from limited information that restricts the accuracy of the charging phase. For the selected battery, the only available characteristic is shown below in Fig. 6-9.

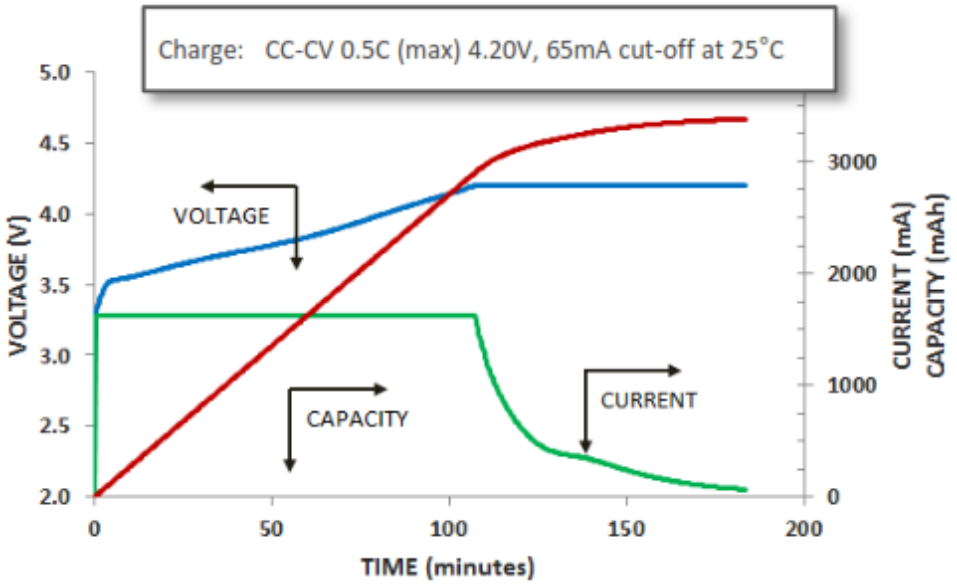


Figure 6-9: Battery charge characteristics

In this figure, a single charging curve can be found for C-rate of 0.5C (blue line). Since there is also need to create the Main charge lookup table, analogically to the

discharge model, this blue curve is extracted and its x-axis scale is adjusted for capacity instead of time. Finally, the extracted charge curve with 2x8 points can be seen with its discharge counterpart in Fig. 6-10.

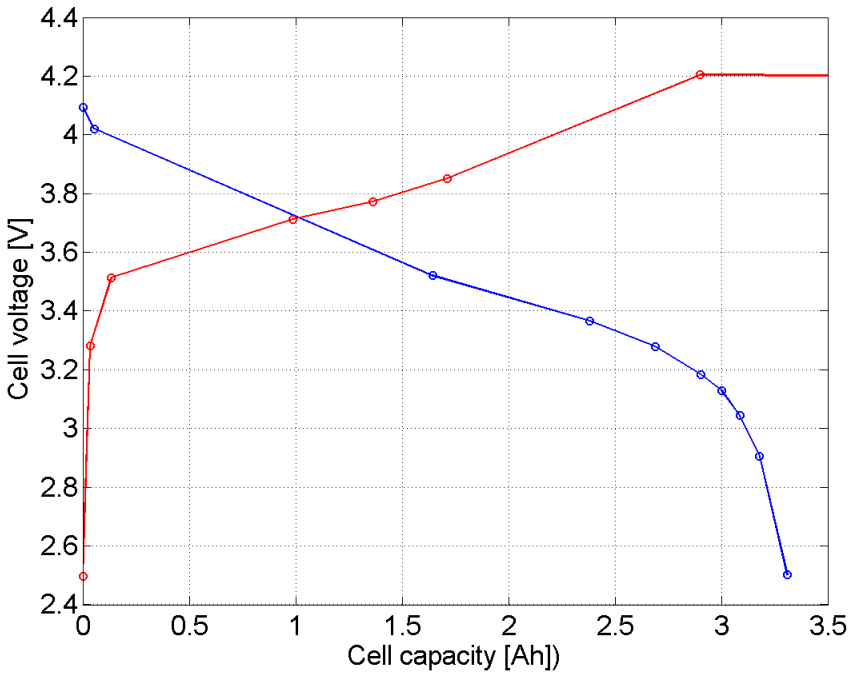


Figure 6-10: The main charge LUT in red, the main discharge LUT in blue

As shown in Fig. 6-10, the reference charge curve reaches the value of 4.2V (charging cut-off voltage) and then sustains this voltage. This phase is very important, but also very difficult to model in the sense of real battery behavior. In real case, when battery is being charged, the charging process is switched from the so-called Constant Current (CC) charging to Constant Voltage (CV) charging. From this the name CC-CV charging. The switch between the two phases is done when the cut-off voltage is reached, and the battery is further kept at this constant voltage, while the current applied to the battery is naturally decreasing in response to the increasing battery internal resistance. CV charging is switched off and the battery is considered to be fully charged when cut-off current is achieved. Both values for cut-off voltage (4.2V) and cut-off current (65mA) can be also seen in Fig. 6-9 in the upper part of the figure.

In this model, for the sake of simplicity, the charge curve is followed up to the

cut-off voltage level with respect to the charge in the battery (SOC), and further kept at this voltage to show the relative behavior. It is then assumed that when a PCS system is connected to the emulator that the charging stops completely at the point of cut-off voltage, leaving the battery not fully charged. In another scenario, it is also considered to rise the slope of the CV phase (part after cut-off voltage) in order to emulate a situation, when the charging system should be capable to recognize over-voltage and switch off charging itself.

As a final option, concept of virtual impedance can be implemented. This concept consists of implementing a voltage change/current change concept into the charging process, which provides certain impedance of the charging model that shall limit the current at the CV phase. One possibility to implement this phenomenon is to include include a resistance on the voltage output of the model, or if the scaling factors are also applied in the charging mode, this resistance is already included. To analyze this concept, a more sophisticated model for PCS must be however also developed in the modeling environment. This particular concept is being currently further analyzed in conjunction with an advanced PCS model.

### 6.2.5 SOC Relative and SOC Real

As already mentioned in Fig. 6-2, there are two SOC values provided by this algorithm. Simply said, the first one provides a value of SOC (%), which is relative to the nominal capacity of the battery (6.7). This however means that for instance: when a battery is discharged at high C-rate and very low temperature, the battery will be fully discharged sooner then expected because of the capacity effect. The $SOC_{RELATIVE}$ will however provide a value, which is relative to the nominal capacity and can be for example 20% SOC, although the battery already cannot provide any more usable energy. To account for this phenomena, the variable $SOC_{REAL}$ was created. This variable is then capable to provide the value of SOC in regards to the real end of discharge/charge period. This was achieved by scaling the nominal capacity $C_{NOM}$, practically in the same way as in the previous case with the voltage characteristic (6.8).

A comparison between the two SOC values will be further elaborated in the section with model results.

$$SOC_{RELATIVE} = \frac{100}{C_{NOM}} \int_0^t i(t)dt + SOC_{INIT} \tag{6.7}$$

$$SOC_{REAL} = \frac{100}{C_{NOM} \cdot K1[i(t)] \cdot K2[T(t)]} \int_0^t i(t)dt + SOC_{INIT} \tag{6.8}$$

### 6.2.6 BE as a battery pack

Given the main purpose of the model that is to serve as a battery pack emulator, a simple division and multiplication operations were added to allow the model the possibility to scale up. Hence, as shown in Fig. 6-2, it is only needed to enter the number of cells in parallel and in series upon which the obtained output characteristics will correspond to the desired battery pack configuration. It should be also noted that in some cases the nominal parameters may not be provided for a single battery cell but for a battery module, in which case a proper recalculation of the scaling up ratios should be done.

## 6.3 Model Performance

In this section, the described model is analyzed through several tests. In particular, in each test a continuous or dynamically changing current is applied on the model (i.e.: ICELL, always shown in the top subfigures). Upon which the model is observed for its SOC output response (both $SOC_{RELATIVE}$ and $SOC_{REAL}$), and for output voltage response (VB_CELL). In this analysis, in order to make the obtained results comparable with the datasheet information (Fig. 6-5 and 6-6) the voltage output is presented for a single battery cell with no battery pack scaling applied.

### Continuous charging/discharging test

In the following tests, the charging starts at predefined value of SOC (i.e. 60%) and continues to charge until 99% of $SOC_{RELATIVE}$. At this point, the discharge is launched until 1% of $SOC_{RELATIVE}$ is reached. The charging is switched on and the whole cycle repeats.

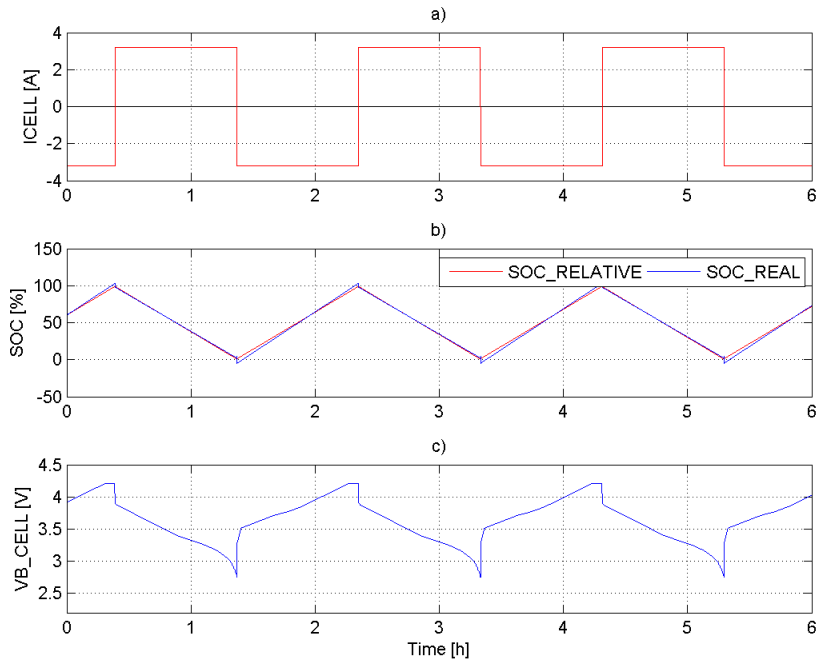


Figure 6-11: Continuous charging/discharging test for 1C at 25°C

Comparing Fig. 6-11 with Fig. 6-12, the difference in capacity effect can be well observed. Also, there is a decrease of the battery's voltage that also correspond to the expected behavior depicted in Fig. 6-6. Moreover, observing Fig. 6-11 with Fig. 6-13, a double of the charging/discharging time can be seen, plus lower voltage drop, both due to the lower C-rate intensity.

In the following figure (Fig. 6-14), a detail on the difference between the two types of SOC is presented. Hence, as shown, when approaching the end of charging, the $SOC_{RELATIVE}$ gives a value of 100% later than $SOC_{REAL}$. This is because according to the $SOC_{REAL}$ the charging should have stopped somewhere near 90% of $SOC_{RELATIVE}$ at which the battery was actually full.

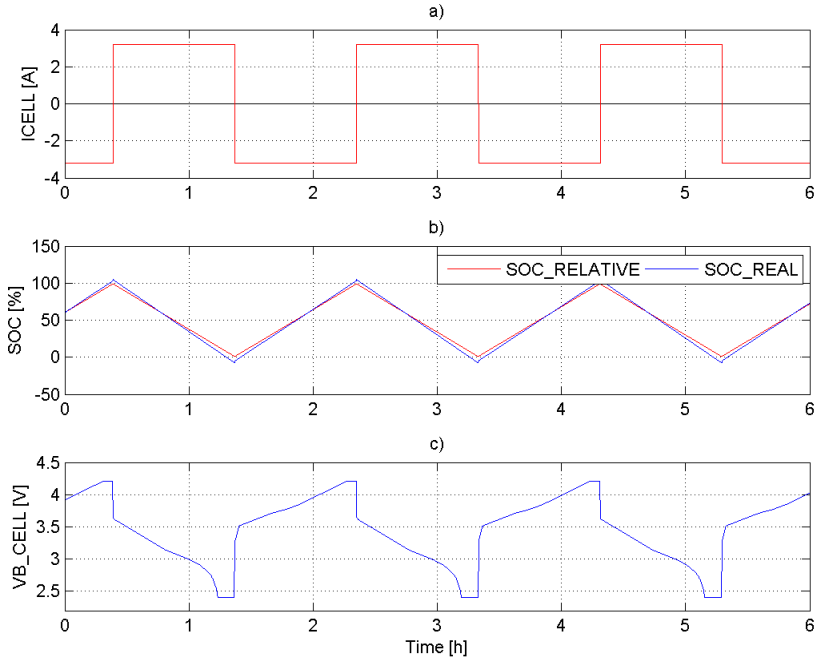


Figure 6-12: Continuous charging/discharging test for 1C at -10°C

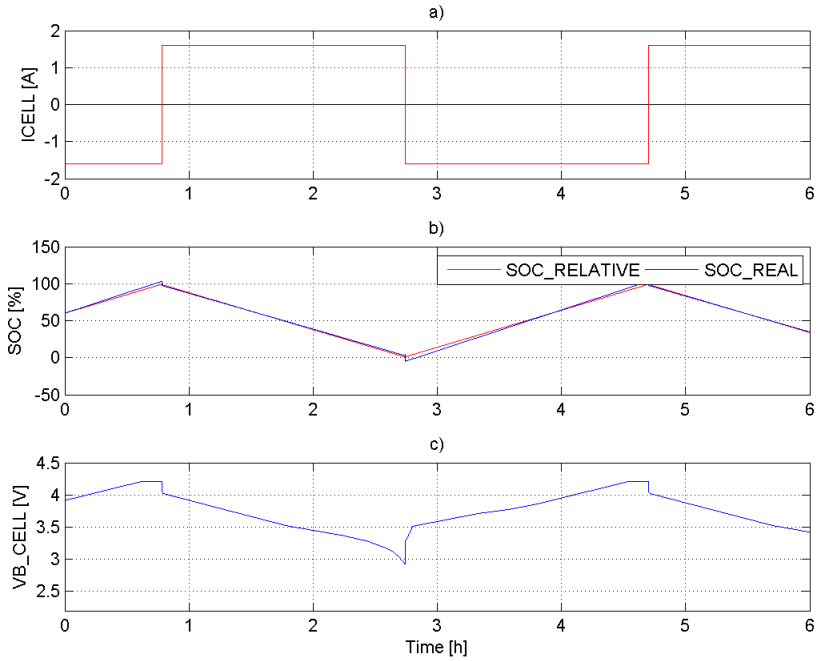


Figure 6-13: Continuous charging/discharging test for 0.5C at 25°C

On the other side, since the battery is discharged at 0.5C, which is the nominal value for discharge that corresponds to the battery's nominal capacity (as shown in Fig. 6-5) the two SOC values meet at the end of discharge.

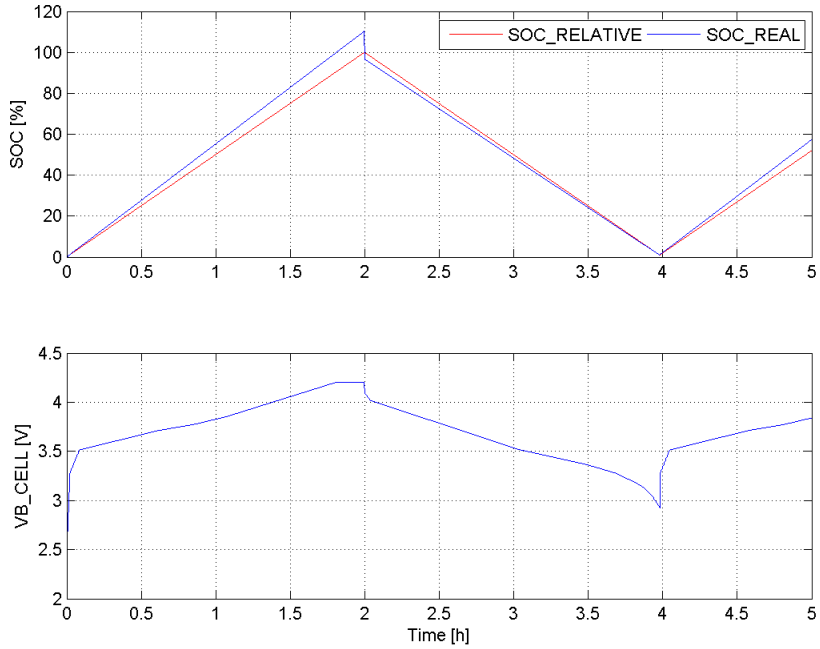


Figure 6-14: Detail - continuous charging/discharging test for 0.5C at 25°C

**Dynamic charging/discharging test**

In this part, dynamic charging/discharging is applied to the BE and its response is observed similarly to the previous analysis. Since the the two following figures (i.e. Fig. 6-15 and 6-16), are simulated for two very different temperatures, the capacity effect can be well recognized from both the BE voltage and also the $SOC_{REAL}$.

## 6.4 BE - Direct C-code Generation

With the BE model fully working in Matlab-Simulink as presented above, now, in order to approach the model to its real implementation in a DSP, the model is optimized for a direct C-code generation. For this purpose, Matlab-Simulink Embedded Coder

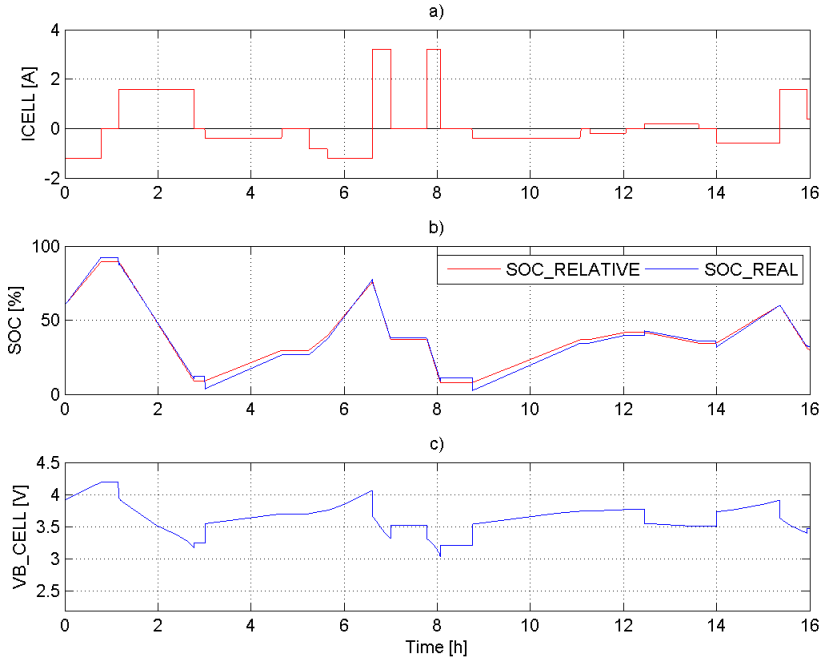


Figure 6-15: Dynamic charging/discharging test for maximum of 1C-rate at 25°C

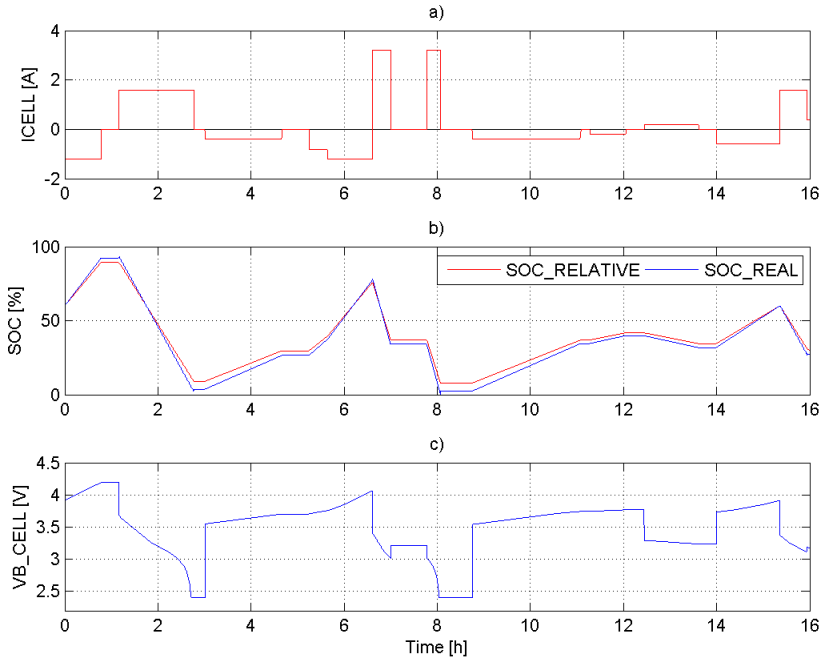


Figure 6-16: dynamic charging/discharging test for maximum of 1C-rate at -10°C

is used. In this section, several general rules are stated with some model examples. It should be also noted that the C-code is optimized for a fixed point DSP from Texas Instrument C2000 family. Moreover, to make the code more efficient, the model is based on IQMath mathematical operations. Certain parts of the C-code will be also presented in Appendix G.

### 6.4.1 C-code optimization rules

#### Matlab parameter specification

Since the model is to be run on a fixed point DSP platform, all the parameters earlier mentioned, must be typed as a fixed point numbers. This is done in Matlab m-file, from which the model parameters are taken and loaded into the BE model in Simulink. Hence, all the relevant parameters should be typed as fixed point numbers. These include for example: Battery cell nominal capacity ($C_{NOM}$), Model initial SOC ($SOC_{NOM}$), Number of cells in series/parallel (S_CELLS/P_CELLS), but also other, such as the Main Discharge/Charge LUT parameters, scaling factor parameters K1 - K3 and so on.

The way to type the parameters consists of using a Matlab function "fi" that specifies the desired parameter in: value, signedness, word-length, and fraction-length. An example of a 32bit parameter with fraction length of 18 digits (corresponding to IQ18) is shown for parameter $C_{NOM}$ below in Fig. 6-17.

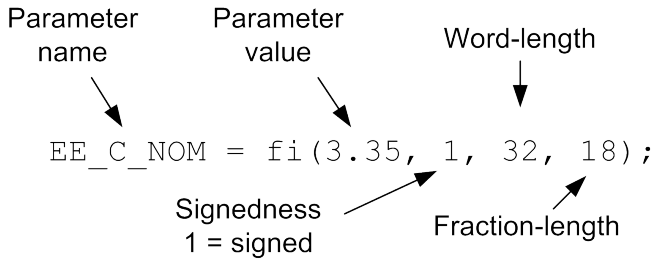


Figure 6-17: Description of fixed point number formulation in Matlab [28]

Moreover, to give to the parameters some sort of unity and separation from other parameters that may be included in the DSP, a prefix "EE_" is used for all BE related parameters.

### Embedded Coder parameter specification

Second step is to specify the way in which the parameters are inserted in the code, the so-called Storage class. These could be as: Inlined parameters or Tunable parameters. In Inlined parameter setting, the parameter's value is inserted into the code and cannot be tuned. For this reason, the Tunable options is chosen. Furthermore, four possibilities are available for this setting as shown in Fig. 6-18.

For this application, the ExportedGlobal option is chosen as it allows to implement the parameter in the code with a reasonable clarity, while the parameter initialization is done directly in the same program .c-file, without any need to provide the parameters externally.

| Storage Class | Generated Variable Declaration and Code |
|---|---|
| SimulinkGlobal (Auto) | typedef struct _Parameters_tunable_sin Parameters_tunable_sin;<br><br>struct _Parameters_tunable_sin {<br>  real_T Kp;<br>};<br><br>Parameters_tunable_sin tunable_sin_P = {<br>  3.14<br>};<br>.<br>.<br>tunable_sin_Y.Out1 = rtb_u * tunable_sin_P.Kp; |
| ExportedGlobal | real_T Kp = 3.14;<br>.<br>.<br>tunable_sin_Y.Out1 = rtb_u * Kp; |
| ImportedExtern | extern real_T Kp;<br>.<br>.<br>tunable_sin_Y.Out1 = rtb_u * Kp; |
| ImportedExtern Pointer | extern real_T *Kp;<br>.<br>.<br>tunable_sin_Y.Out1 = rtb_u * (*Kp); |

Figure 6-18: Parameter storage class specification [28]

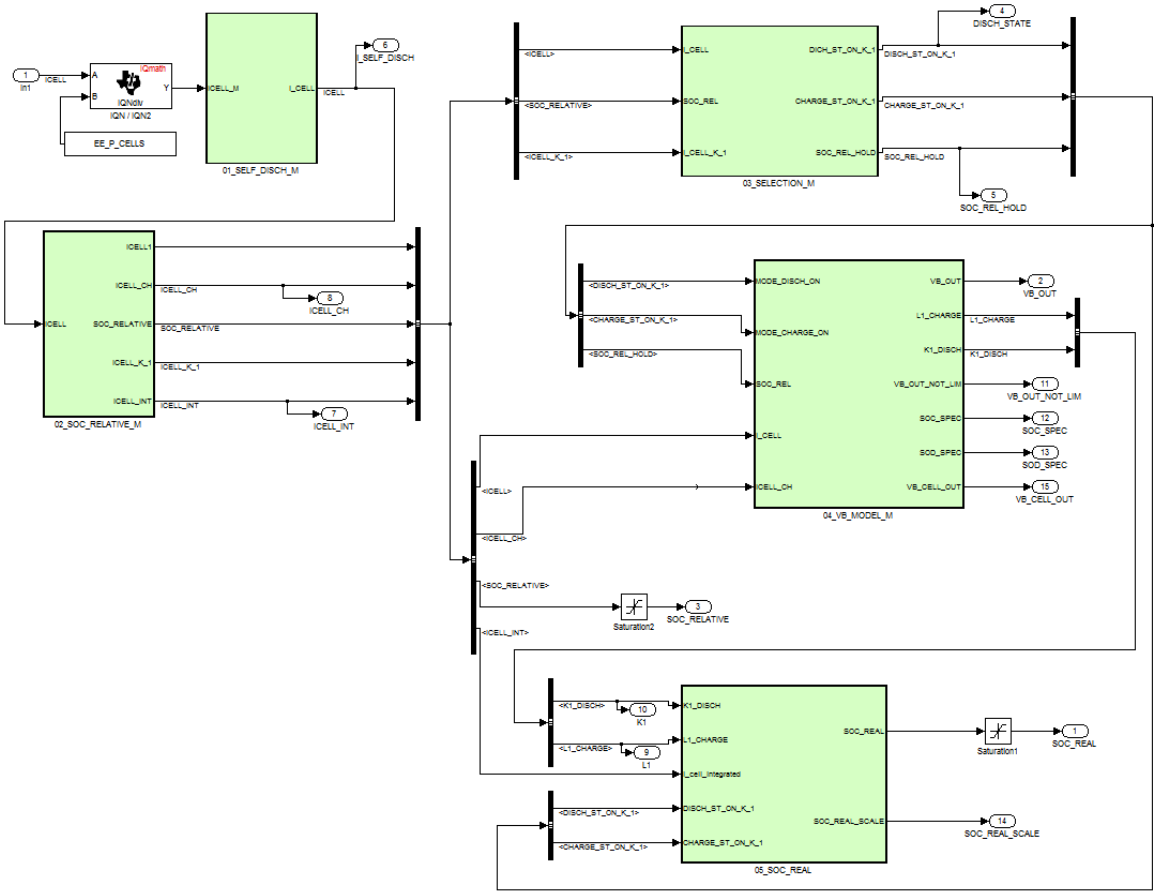


Figure 6-19: BE model first level block connections

### Simulink BE model reorganization

With the input parameters initialized and ready for the code, what remains is to adjust the BE Simulink model so it generates the code with clarity and minimum of errors. The following changes are considered: wiring style, IQMath implementation, if-statement reorganization and LUT and linear function mask adaptation.

### Wiring

To avoid any problems in the code flow it is recommended to wire all blocks with wires, with minimum or preferably no use of floating objects. Floating object is a block that is not connected with any wires (an example of floating object is when only GOTO and FROM connections are used). For this reason, all the blocks are wired, but caution, no wires should cross. Hence, to do so and to sustain certain

level of clarity, use of bus objects is highly advised. Moreover, when buses are used, the named interconnecting signals also keep their names in the generated code, which makes the code more readable. Use of subsystems to avoid wire crossing is also recommended (allows to leave from the block through an outport and return to a different place in the same block with an inport). An example of the wiring system with various buses can be seen in Fig. 6-19.

### IQMath implementation

To include the element of IQMath into the model, two blocks from the DSP C2000 Simulink library are used; IQNmpy, IQNdiv. Both blocks can be seen in Fig. 6-20, where the $SOD_{SPEC}$ is being calculated as part of the discharge voltage curve calculation. With respect to IQMath implementation, it should be also noted that the whole model is kept within IQ18 (32bit operation). This value was chosen for its reasonable accuracy within the model. Its unity is then kept throughout the model to limit any precision losses. Moreover, in this regards, further adjustments were made, such as using division blocks before multiplication blocks (where beneficial) to avoid any signal saturation.

### If-statement rearrangement

Given that there were several if-statement in the original BE model, mainly implemented through Matlab function subsystem blocks, these had to replaced and rear-

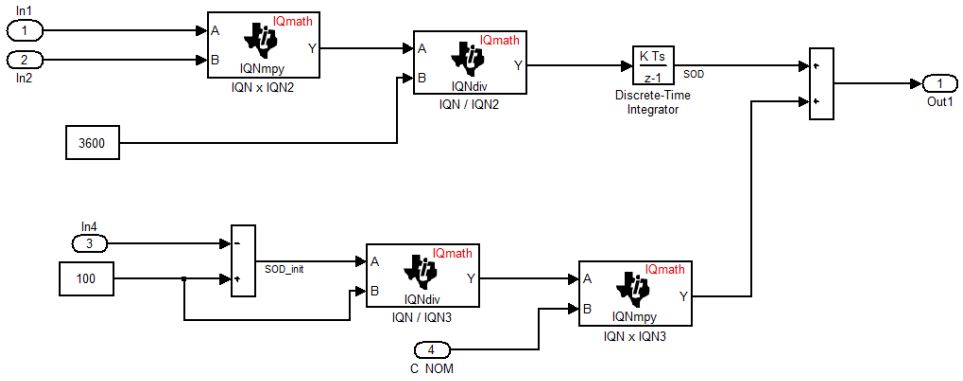


Figure 6-20: IQMath implementation in calculation of $SOD_{SPEC}$

ranged so they could be properly translated into the C-code. This was done in two ways: 1) Use of If block, Action port (inserted into the driven subsystem), Merge block and Merge block (to explicitly define range of the statement), shown in Fig. 6-21. 2) Use of two enabled subsystems driven by boolean logic (when one is on, other is off), with result merged in Merge block, shown in Fig. 6-22.

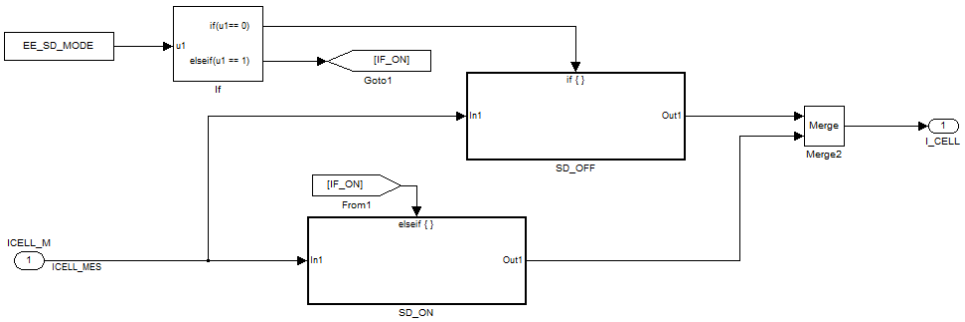


Figure 6-21: Switch on/off for a self-discharge feature in the model - an example of an If-condition with an If block

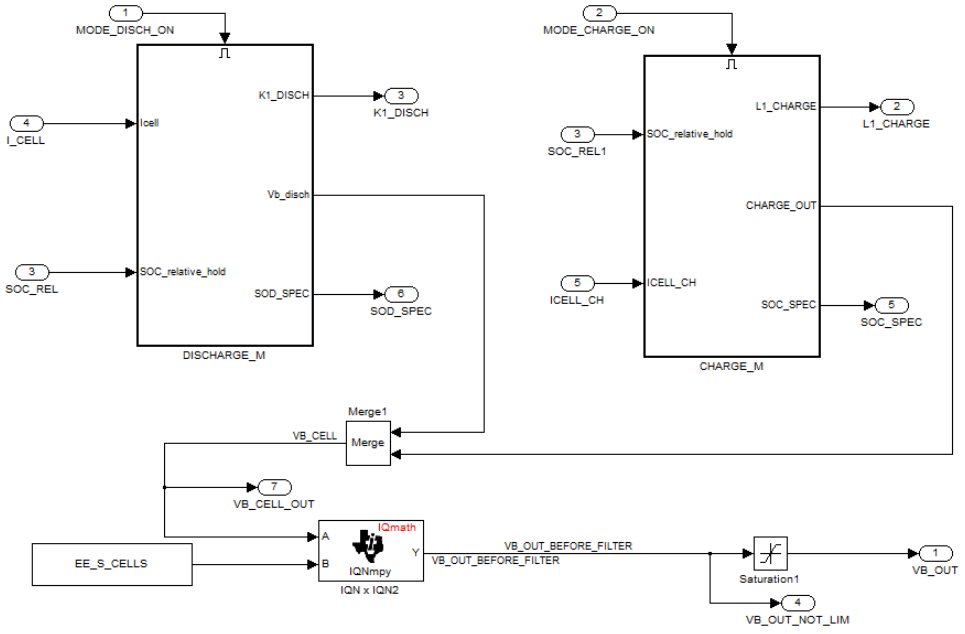


Figure 6-22: Selection between the charge/discharge mode - an example of an If-condition with two enabled systems

### LUT and Linear function as Reusable code

An interesting feature that can be enabled through a proper model setting is the possibility to generate a reusable code. In other words, if the model has one function implemented more than ones, it is possible to generate it as a separate function with its arguments in the code, which can allow significant savings in DSP memory and help to clarify the code.

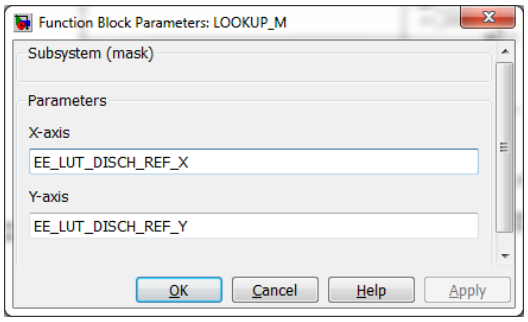


(a)

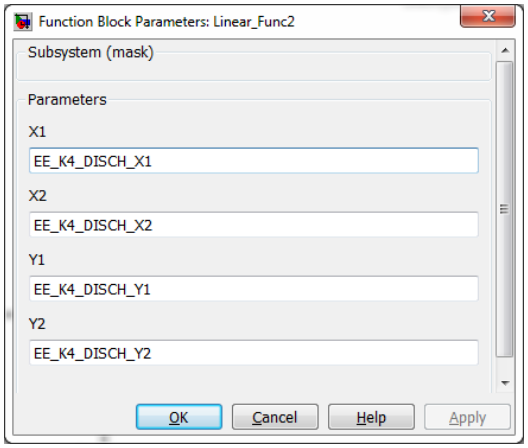


(b)

Figure 6-23: Masked subsystems for the purpose of reusable code generation, a) Masked LUT b) Masked linear function

In our case, there are several LUTs and several linear functions within the code. Some linear functions are used instead of lookup tables for reference curve scaling parameters to save DSP memory and increase execution speed. The code reuse is then activated by creating a mask of the desired subsystem (i.e. a LUT block or a linear function subsystem). This masked subsystem is then distributed within the entire model in desired positions and its parameters, which can be accessed through the mask, are filled individually with respect to the position and exact purpose of the block. In this way, the Embedded Coder is capable to recognize multiple use of the masked block and generates a reusable function. Hence, two masks were created, one for a linear function and one for a LUT. It should be also noted that in order to generate a reusable function for a lUT, the input parameters should have the same dimensions.

### Code generation options

Besides all the adjustments of the BE model stated above there is also need to specify certain optimization parameters under the Simulink - Tools - Code generation - Optimization option. In this option, the following fields should be checked: Block reduction ON, Implement logic signals as Boolean data ON, Optimize using the specified minimum and maximum values ON, Remover code from floating-point to integer conversion ON, Signal storage reuse ON, Inline invariant signals ON, Pack boolean data into bitfields ON. More options can be selected, depending on a particular application with reference to Matlab Help in [28].

### Code generation report

Upon a successful code generation for the BE model (or any other), a Code generation report appears. This report then can provide a great interface between the generated code and the actual Simulink model. The code generation report generated for the BE model can be seen in Fig. 6-24. There, on the left bottom, it can be seen that

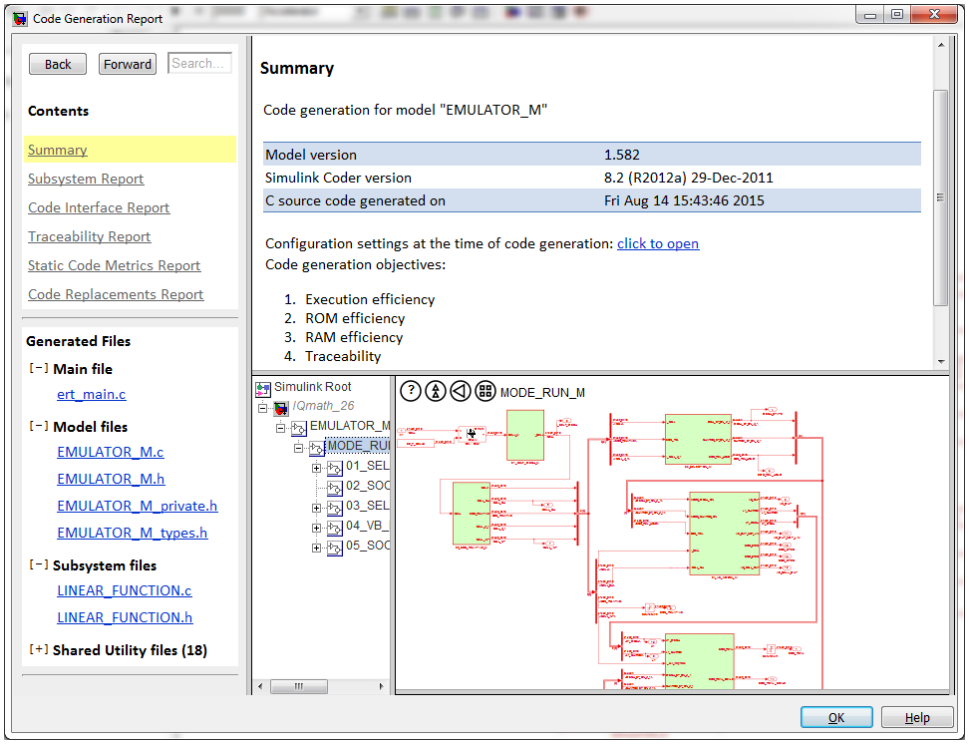


Figure 6-24: Introduction page of the Code generating report

the generated code consists of a single main file, for main model files, two subsystem files and 18 shared utility files. These utility files however do not add many lines to the code, having no more than 40 lines each in average. An example of the main code algorithm that is in the EMULATOR_M.c file can be seen in Appendix G.

In addition, the code generation report can be also accessed through most of the today's web browsers that allows the designer to share the code in a very useful way.

### 6.4.2 BE C-code based model validation

One of the advantages of the direct C-code generating process is the fact that the adjusted model can be run throughout its development, allowing to recognize and eliminate most of the development problems (bugs). Certain level of troubleshooting may be however also required prior to the final DSP implementation.

To evaluate the function of the algorithm inside the DSP, a special SW tool is used to interface the code. The code is then run while its inputs are being varied, particularly the ICELL variable (no Temperature effect included in this particular case). In response to the input ICELL, model output variables: VB_OUT and SOC_RELATIVE are observed. Moreover, other parameters can be also taken out from the model as far as they are wired as outputs. This possibility was utilized for several internal state variables (e.g. SOC_SPEC, SOD_SPEC) in order to analyze some of the internal code process. To verify the model function, an example of continuous discharge and charge at 1C can be seen in Fig. 6-25. A dynamic response of the model can be seen in Fig. 6-26.

### 6.4.3 Conclusion

In this chapter, the Curve Fitting Model was developed and analyzed. From the model's performance point of view, this model is considered as very accurate, due to the fact that the model characteristics are implemented directly from real LIB characteristics. Moreover, a scaling technique is also used to provide an estimation of SOC (i.e. SOC_RELATIVE), that allows to predict the moment of the battery's

full charge or full discharge. Finally, the model was also successfully implemented in a fixed-point DSP, through the Embedded Coder platform and its direct C-code generation capability; allowing the algorithm to be easily integrated in any research or/and industrial test bench.

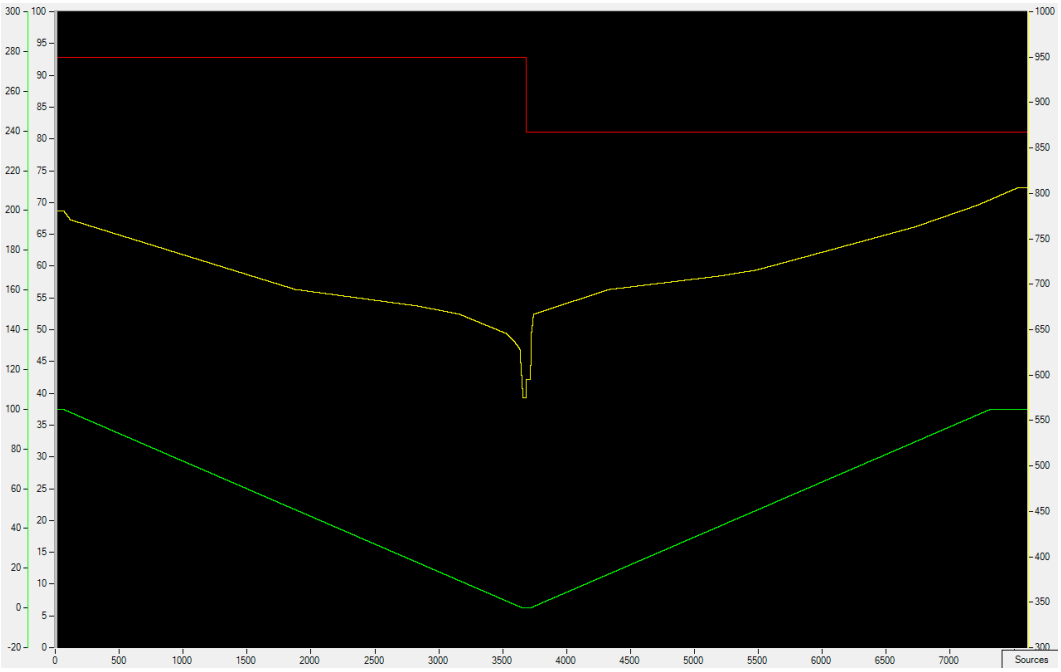


Figure 6-25: Discharge and charge process at constant rate of 1C, as measured inside the DSP, red line - current ICELL, yellow line - VB_OUT (referred to the y-axis on the right side), green line - SOC_RELATIVE (referred to the first y-axis on the left side)

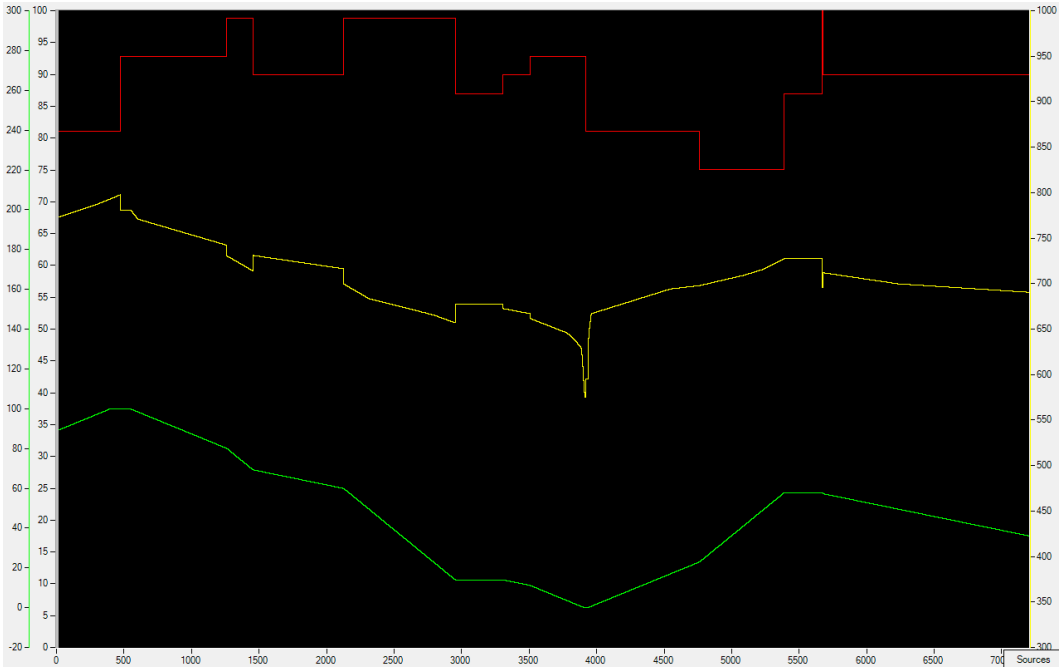


Figure 6-26: Discharge and charge process at dynamic rate between -2C and 2C, as measured inside the DSP, red line - current ICELL, yellow line - VB_OUT (referred to the y-axis on the right side), green line - SOC_RELATIVE (referred to the first y-axis on the left side)

# Chapter 7

# Shepherd's Battery Model

Following the introduction of the two most commonly used Shepherd's models in Chapter 5, the two models were also developed to analyze their possible use for the BE. Please note that this part of the study, that is the development of the two Shepherd's models was initially done before the Curve fitting model. In the final report however, its evaluation is positioned after, so all three models could be compared altogether.

In this chapter, firstly the two models are presented in their empirical form. Secondly, since both models use the same parameters, a single process of parameter acquisition is shown for both models. Following this part, the equation modeling in Simulink is presented. Finally, a comparison of the two models and the Curve fitting model is shown and the observations are discussed.

### Introduction

An equation for the Shepherd's original model can be seen below in (7.1).

Shepherd's original model:

$$V = V_0 - K\frac{Q}{Q - it} - Ri + A \cdot e^{(-B \cdot it)} \tag{7.1}$$

The Shepherd's modified model that consists of two equations, one for charge mode and the other for discharge mode is shown in (7.2 and 7.3).

Shepherd's modified model - discharge mode equation:

$$V = V_0 - K\frac{Q}{Q - it}it - K\frac{Q}{Q - it}i - Ri + A \cdot e^{(-B \cdot it)} \tag{7.2}$$

Shepherd's modified model - charge mode equation:

$$V = V_0 - K\frac{Q}{Q - it}it - K\frac{Q}{it - 0.1Q}i - Ri + A \cdot e^{(-B \cdot it)} \tag{7.3}$$

In these equations: $V$ - battery terminal voltage, $V_0$ - battery nominal voltage, $R$ - battery internal resistance, $i$ - current through the battery (positive for discharge, negative for charge), $Q$ - nominal capacity of the battery cell, $it$ - current integrated over time, and $K$, $A$ and $B$ are curve fitting coefficients, which will be elaborated on in the following sections with reference to [5], [51], [30], [29], [54], [1].

In regard to the equations above, it can be observed that the Shepherd's modified equations include one more term, often called *Polarization resistance*. Practically, this term helps to adjust the final part of the discharge voltage curve where the voltage decreases at high slope. On the other side, this Polarization resistance term also helps to increase the voltage curve at the beginning of the charging process. It should be also noted that this term has quite high significance particularly for battery cells with low internal resistance ($\mu\Omega$). If the battery cell internal resistance have higher values ($m\Omega$), as it is also the case for the battery cell under study, the Polarization resistance term does not make a big difference.

## 7.1 Parameter Acquisition

As already stated, the strong point of this empirical approach is the low requirement on the parameter input. In particular, only several points must be taken to model discharge characteristics of a battery. As shown in Fig. 7-1a, a discharge characteristic is firstly split into sections, forming the so-called: Exponential area and Nominal area. Having this separation, the curve parameters can be taken, as depicted in Fig. 7-1b. As shown, the same battery cell was also considered for this modeling approach.

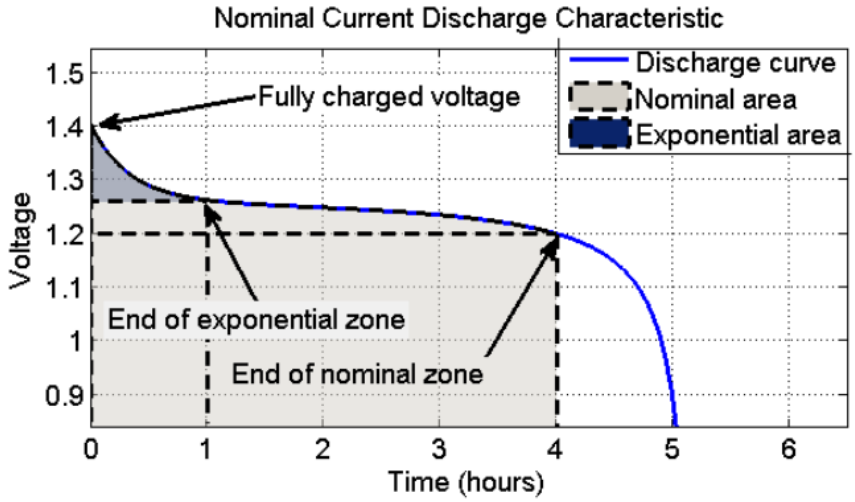


(a) General section separation of a battery discharge characteristic prior to parameter extraction [51]

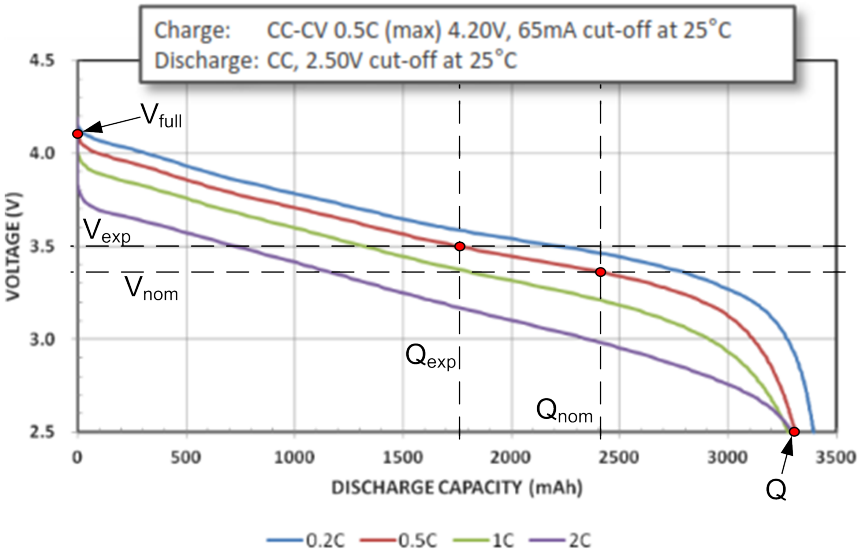


(b) Parameter extraction directly for the required battery cell

Figure 7-1: Parameter acquisition

The obtained parameters are: $V_{full}$, $V_{exp}$, $V_{nom}$, $Q_{exp}$, $Q_{nom}$, and $Q$. From these, only $Q$ can be directly put into the equations (7.1, 7.2, and 7.3), while the other parameters are used to obtain the remaining equation variables; $A$, $B$, $K$, and $V_0$, as shown in (7.4, 7.5, and 7.6) in the same order.

$A$ - Exponential zone amplitude parameter (V)

$$A = V_{full} - V_{exp} \tag{7.4}$$

$B$ - Exponential zone time constant inverse ($Ah^{-1}$)

$$B = \frac{3}{Q_{exp}} \tag{7.5}$$

$K$ - Polarization voltage (V)

$$K = \frac{(V_{full} - V_{nom} + A \cdot e^{-B \cdot Q_{nom}} - 1) \cdot (Q - Q_{nom})}{Q_{nom}} \tag{7.6}$$

$V_0$ Battery constant voltage (V)

$$V_0 = V_{full} + K - A + R \cdot i \tag{7.7}$$

The internal resistance of the battery cell $R$ can be usually found from a battery data sheet. However, if this information is not given, an approximate value of the internal resistance $R$ shall be found from the C-rate discharge characteristics, in the following way:

$$R = \frac{\delta V}{\delta I} \tag{7.8}$$

Where, $\delta V$ is voltage difference between two discharge curves taken at the same SOD, and $\delta I$ is difference of the currents at which the two discharge curves were taken.

With all the parameters taken, the model equations can be implemented in Matlab-Simulink.

## 7.2 Matlab-Simulink Models

Below, in Fig. 7-2 and Fig. 7-3, the two models can be observed as modeled in Matlab-Simulink. An interesting feature in context of this modeling approach has been also presented in [1], where the author adjusted the model equations for in total four battery types; Ni-Cd, NiMH, Lead-Acid, and Li-ion. A very generic representation of four battery types were therefore available within a single simple model.

In this regards

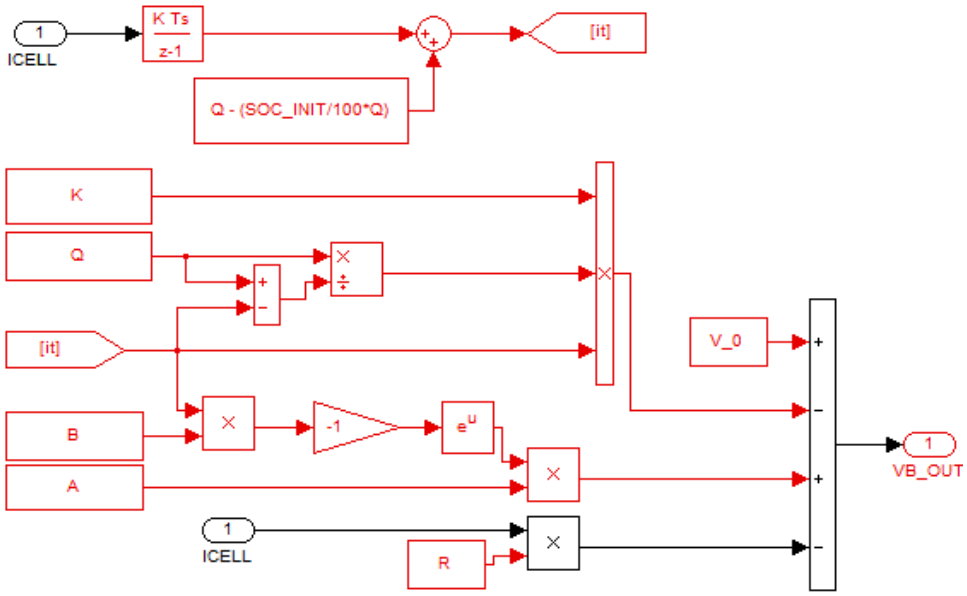


Figure 7-2: Shepherd's original model in Simulink

Additionally, a parameter SOC_INIT can be also observed in the two models as shown in Fig. 7-2 and Fig. 7-3, which similarly as in the Curve fitting model represent the initial value of SOC.

## 7.3 Shepherd's Model Analysis

With three models developed up to now; two Shepherd's models and one curve fitting model, all three are compared for their continuous and dynamic performance in this section. It this regard, it is considered that the fitting curve model provides the most accurate approximation, to which the other two models tend to approach.

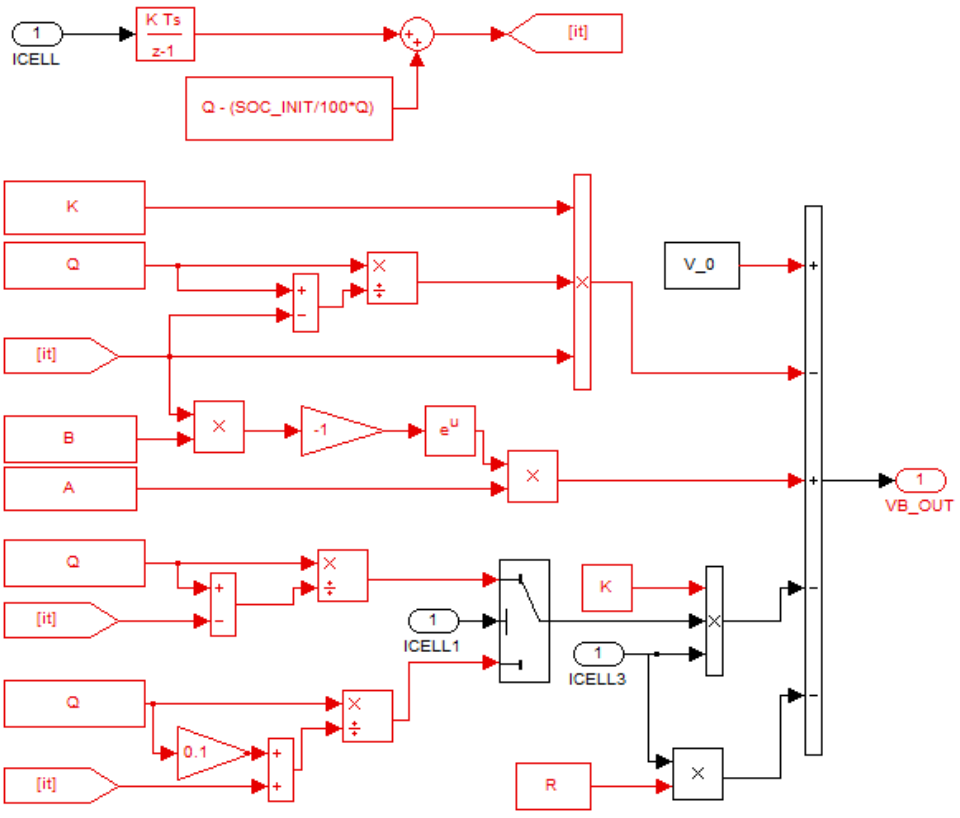


Figure 7-3: Shepherd's modified model in Simulink

### Continuous charge/discharge analysis

To evaluate the performance in the continuous current mode, the charge/discharge voltage curves of all three models are taken at three different C-rate values; 1C, 0.5C and 0.2C (Fig. 7-4, 7-5 and 7-6, respectively).

Hence, as it can be observed, both Shepherd models provide certain approximation of the output voltage value (VB_OUT). This approximation then meets with the required value in some places depending on several factors; a) to which discharge curve were the Shepherd's models fitted, and b) what is the actual charge/discharge C-rate. In this context, either of the two Shepherd's models may be of a high interest if the C-rate operation point were very narrow.

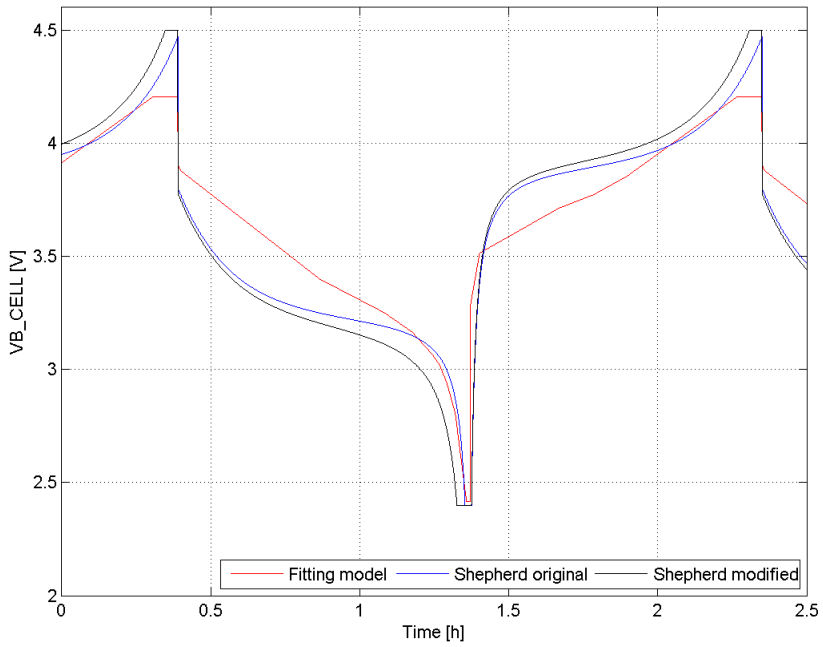


Figure 7-4: Comparison of VB_OUT for all three models in continuous charging/discharging mode at 1C

### Dynamic charge/discharge analysis

A comparison of the three models in a dynamic mode can be seen in Fig. 7-7. As shown, the drawback of the Shepherd's models in dynamic charge/discharge mode is really significant.

## 7.4 Conclusion

In this chapter, the two Shepherd's models: Shepherd's original model and Shepherd's modified model, were analyzed for their potential use in the BE. As found, the two models provide certain approximation of the charge/discharge curve a continuous mode of operation, although lack in accuracy in the dynamic charging/discharging mode. Therefore, considering that the BE shall be exposed mainly to the dynamic conditions that are present in electric systems with RESs, their performance would not be sufficient.

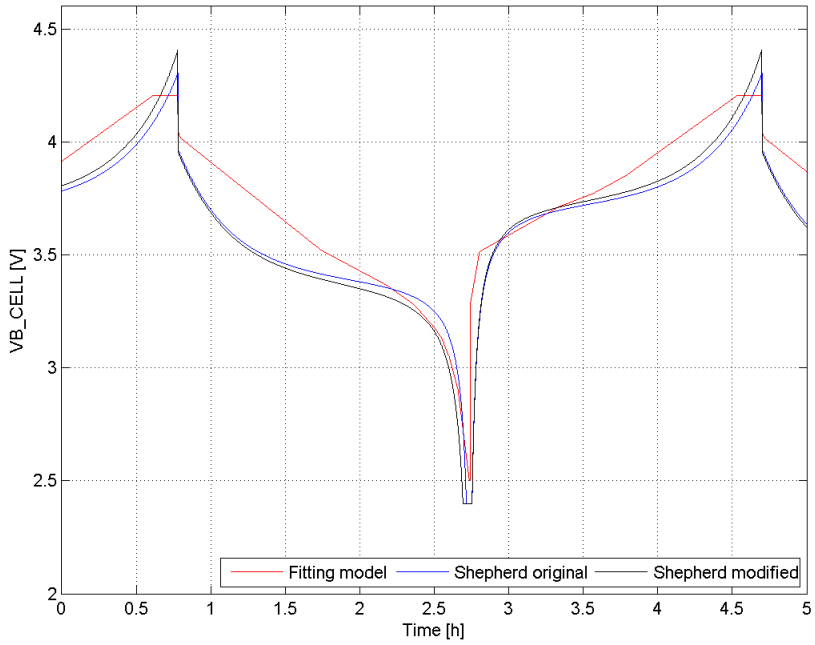


Figure 7-5: Comparison of VB_OUT for all three models in continuous charging/discharging mode at 0.5C

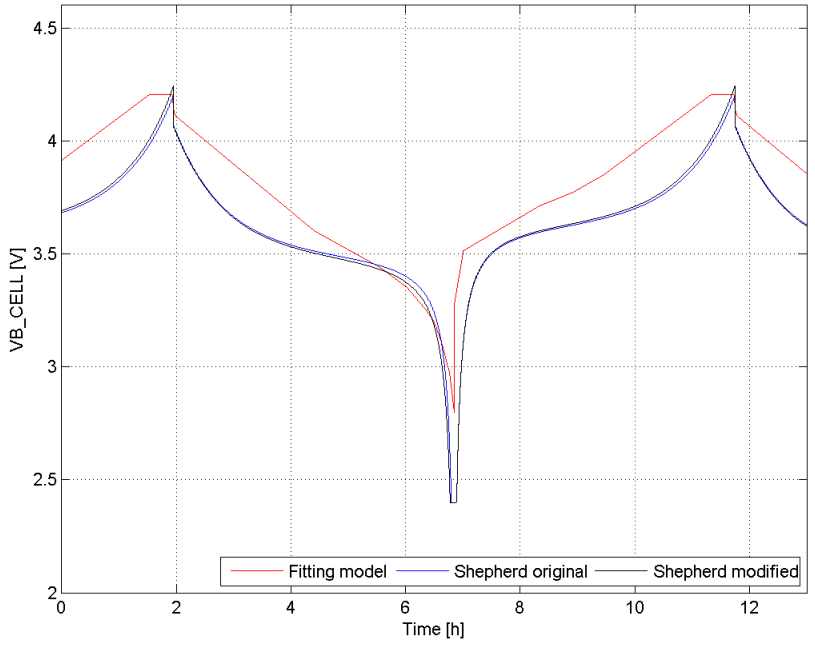


Figure 7-6: Comparison of VB_OUT for all three models in continuous charging/discharging mode at 0.2C

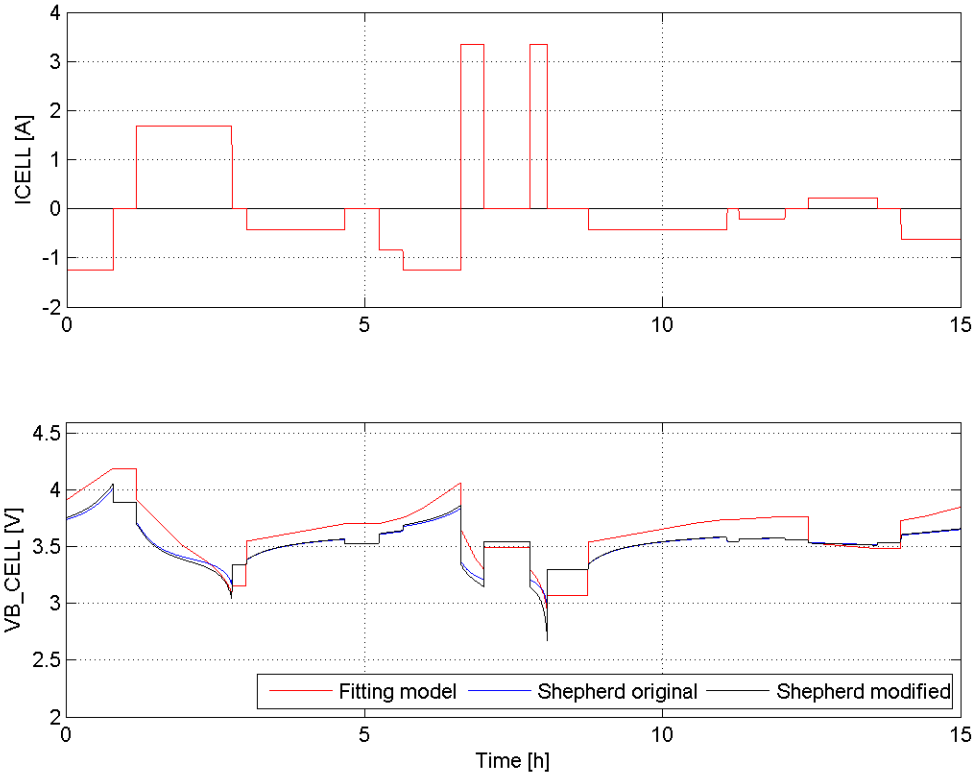


Figure 7-7: Comparison of VB_OUT for all three models in dynamic charging/discharging mode

# Chapter 8

# Conclusion and Future Work Recommendations

## 8.1 Conclusion

Following the progress of this Master thesis, several conclusions can be made with regard to each chapter:

Firstly, the general motivation for LIBs have been justified at the very beginning (Chapter 2). As presented, LIBs have the potential to be a very effective distributed GESS technology in both high power and high energy applications. The main obstacle up to now has been the high cost for LIBs, although this shall also change in the near future as the cost for LIBs is foreseen to fall significantly. As also shown, an observation of other battery technologies should be also in place, including Na-S (Sodium-Sulphur) and more importantly VR (Vanadium Redox) that may prove to be a big competitor to LIBs mainly in high energy applications.

With regard to a particular LIB technology, after a revision of the currently most common LIBs in Chapter 3, the Lithium Iron Phosphate (LFP) technology seem to be the most attractive due to its relatively low cost, high lifetime and high power capability. Another possibly attractive technologies that are however yet significantly restricted by their cost are: NCA (Lithium Nickel Cobalt Aluminium Oxide), NMC (Lithium Nickel Manganese Cobalt Oxide) and LTO (Lithium Titanate Oxide). Sev-

eral LIB technologies under development have been also presented, among which the Li-silicon seem to be a very interesting option for the future.

Prior to the modeling phase, the most important characteristics and phenomenons of a LIB have been also described (Chapter 4). Among these: C-rate effect, Temperature effect and Aging effect, that all help to understand the complexity of a single LIB.

In Chapter 5, a literature review of the current battery models is provided. As presented, the empirical models and the curve fitting model shall provide a reasonable accuracy within certain limits at low computational power, while based only on a manufacturer's data sheet.

Based on this literature review, two empirical models, i.e. Shepherd's original model and Shepherd's modified model are analyzed in Chapter 7. As found, these models provide certain accuracy at the continuous mode of operation, however lack in precision in the dynamic mode. For this reason, the Curve fitting model is further analyzed.

In Chapter 6, the Curve fitting model is built in Matlab-Simulink and consequently converted into C-code through the Embedded Coder SW platform (Mathworks).

As found, the model provides satisfying results that can effectively emulate a battery pack system in both dynamic and continuous mode, while incorporating the battery's temperature effect, C-rate effect and self-discharge effect. All of that based only on real LIB data sheet information.

Moreover, as stated, the final version of the Curve fitting model is optimized for direct C-code generation. Finally, upon optimization of the model, the model proves to function very well in a fixed-point DSP, while utilizing IQmath operations at precision of IQ18.

## 8.2 Future Work Recommendations

The following points are considered for future work development on the Curve fitting model:

- Comparison of the Curve fitting model with a real LIB,
- Implementation of dynamics for the output voltage (VB_OUT),
- Analysis of the final charging phase (CV phase), particularly with emphasis on the virtual impedance concept,
- Consideration of more advanced SOC estimation techniques,
- Incorporation of aging effect and SOH estimation,
- Implementation of temperature feedback based on the battery operation,
- Improvement of algorithm precision through implementation of various IQMath ranges.

In general, further observation of the battery industry in the forthcoming years shall be also very interesting, in particular: which LIB technology will prove in the end as the most effective and how will the cost for LIBs progress.

# Appendix A

# Panasonic Li-ion (LCO) Battery Cell NCR18650B

Panasonic

# Lithium Ion NCR18650B

## Features & Benefits

- High energy density
- Long stable power and long run time
- Ideal for notebook PCs, boosters, portable devices, etc.

* At temperatures below 10°C, charge at a 0.25C rate.

## Specifications

| | |
|---|---|
| Rated capacity(1) | Min. 3200mAh |
| Capacity(2) | Min. 3250mAh<br>Typ. 3350mAh |
| Nominal voltage | 3.6V |
| Charging | CC-CV, Std. 1625mA, 4.20V, 4.0 hrs |
| Weight (max.) | 48.5 g |
| Temperature | Charge*: 0 to +45°C<br>Discharge: -20 to +60°C<br>Storage: -20 to +50°C |
| Energy density(3) | Volumetric: 676 Wh/l<br>Gravimetric: 243 Wh/kg |

(1) At 20°C (2) At 25°C (3) Energy density based on bare cell dimensions

## Dimensions

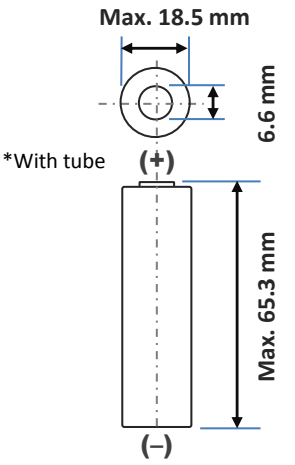


For Reference Only

## Charge Characteristics

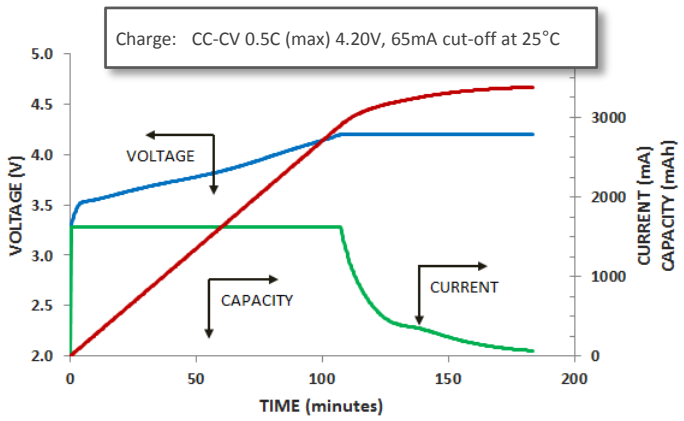


## Cycle Life Characteristics

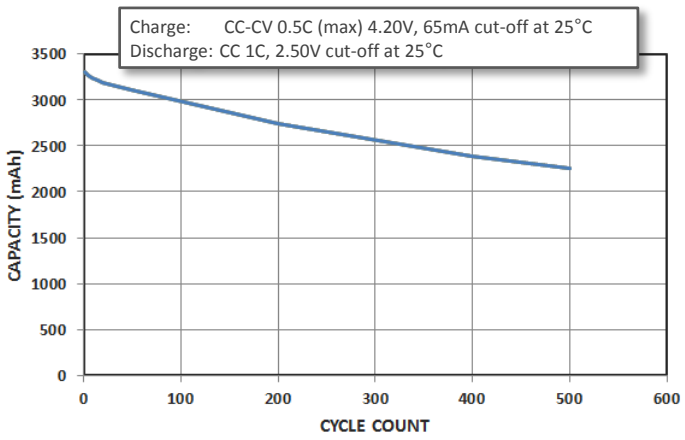


## Discharge Characteristics (by temperature)

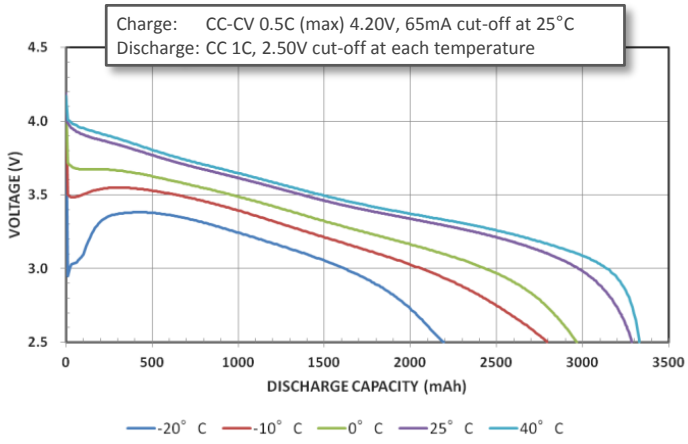


## Discharge Characteristics (by rate of discharge)

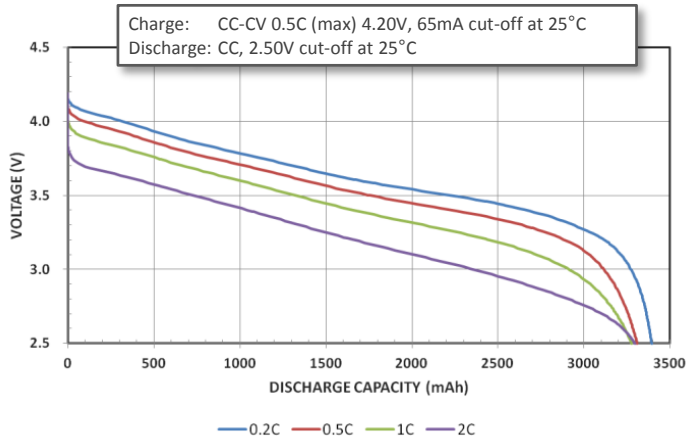


The data in this document is for descriptive purposes only and is not intended to make or imply any guarantee or warranty.

For more information on how Panasonic can assist you with your battery power solution needs, visit us at www.panasonic.com/industrial/batteries-oem, e-mail secsales@us.panasonic.com, or call (469) 362-5600.

VERSION 13.11 R1 | Copyright© 2012 SANYO Energy (U.S.A.) Corporation. All Rights Reserved.

# Appendix B

# Saft Li-ion (LCO) Battery Cell MP 176065

# Rechargeable lithium-ion battery
# MP 176065 Integrat*ion*™


## High performance
## Medium Prismatic cell

**Saft always supplies MP cells in assemblies or as customized battery system constructions**

### Benefits

- A broad operating temperature range
- Extended autonomy and life for mobile systems
- Recommended for ruggedized designs
- Easy integration into compact and light systems
- Used in potentially explosible atmospheres
- Reliability and peace of mind
- Aluminium casing
- Very high energy density *(375 Wh/l and 178 Wh/kg)*
- Unrivalled low temperature performance

### Key features

- Excellent charge recovery after long storage, even at high temperature
- Maintenance-free
- Long cycle life *(over 70 % initial capacity after 600 cycles, C charge rate, C/2 rate 100 % DoD at 20°C)*
- Restricted for transport *(Class 9)*
- Compliant with IEC 61960 standard
- Underwriters Laboratories *(UL)* Component Recognition *(File Number MH 12609)*

### Main applications

- Mobile asset tracking
- Rack-mount telecom batteries
- Small UPS
- Future soldier equipment
- Portable radios
- Portable defibrillators
- Professional portable lighting
- Electric bikes and personal mobility

### Electrical characteristics

| | |
|---|---|
| Nominal voltage (1.4 A rate at 20°C) | 3.75 V |
| Typical capacity 20°C (at 1.4 A 20°C 2.5 V cut-off) | 6.8 Ah |
| Nominal energy | 26 Wh |

### Mechanical characteristics (sleeved 100 % charged cell)

| | |
|---|---|
| Thickness *(Thickness tends to increase with cycling, typically obtained after 600 cycles. Consult Saft) (At beginning of life 18.6 mm)* | 20.3 mm |
| Width max | 60.5 mm |
| Height max (including protection circuit) | 70 mm |
| Typical weight (including protection circuit) | 143 g |
| Lithium equivalent content | 2.04 g |
| Volume | 68 $cm^3$ |

### Operating conditions

| | |
|---|---|
| Charge method | Constant Current/Constant Voltage |
| End charge voltage | 4.20 +/– 0.05 V |
| Maximum recommended charge current** | 7.0 A (~C rate) |
| Charge temperature range* | –20°C to +60°C |
| Charge time at 20°C | To be set as a function of the charge current:<br>C rate → 2 to 3 h<br>C/2 rate → 3 to 4 h<br>C/5 rate → 6 to 7 h |
| Maximum continuous discharge current** | 14 A (~2C rate) |
| Pulse discharge current at 20°C | up to 30 A (~4C rate) |
| Discharge cut-off voltage | 2.5 V |
| Discharge temperature range* | –50°C to +60°C |

* *For optimized charging below 0°C, 60°C and discharging at –50°C, consult Saft.*
** *Electronic protection circuits within battery packs may limit the maximum charge/discharge current allowable. Consult Saft.*

**September 2009**

# MP 176065 Integration™

## Battery assembly

In order to operate properly, individual Li-ion cells are mechanically and electrically integrated in battery assemblies specific to each application. The battery assembly incorporates electronics for performance, thermal and safety management.

## Technology

- Graphite-based anode
- Lithium Cobalt oxide-based cathode
- Electrolyte: organic solvents
- Built-in redundant safety protections *(shutdown separator, circuit breaker, safety vent)*
- Batteries assembled from MP cells feature an electronic protection circuit

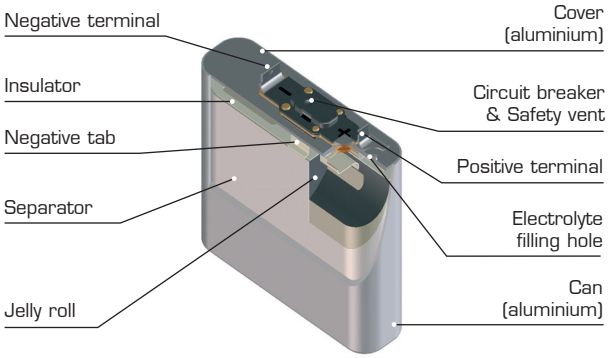


## Built-in protection devices ensure safety in case of:

- Exposure to heat
- Exposure to direct sunlight for extended periods of time
- Short circuit
- Overcharge
- Overdischarge

## When handling Saft MP batteries:

- Do not disassemble
- Do not remove the protection circuit
- Do not incinerate

## Transportation and storage:

- Store in a dry place at a temperature preferably not exceeding 30°C
- For long-term storage, keep the battery within a 30 ± 15 % state of charge

**Capacity versus current at +20°C**

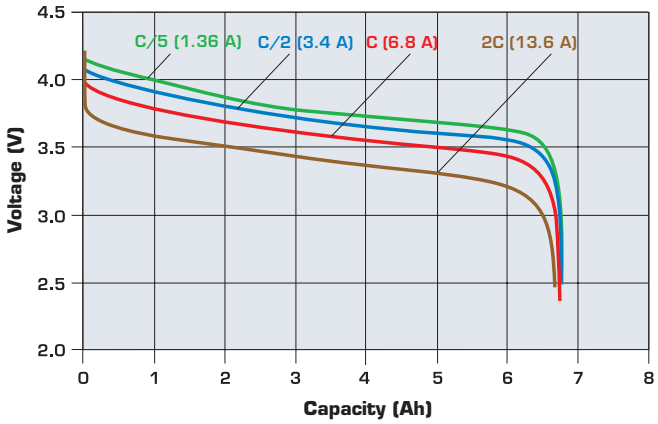


**Typical discharge profiles (1.36 A - C/5 rate)**

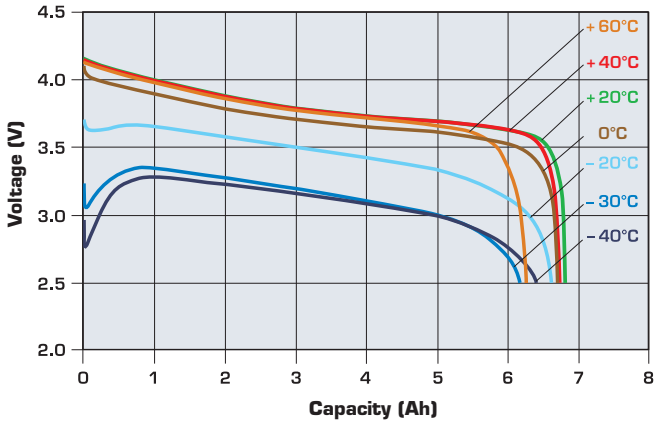


**Charge characteristics to 4.2 V at +20°C**

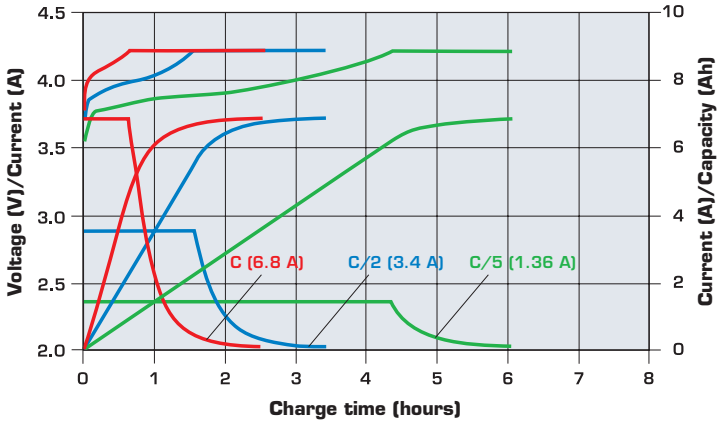


**Saft**
**Specialty Battery Group**
12, rue Sadi Carnot
93170 Bagnolet - France
Tel.: +33 (0)1 49 93 19 18
Fax: +33 (0)1 49 93 19 69

313 Crescent Street
Valdese, NC 28690 - USA
Tel.: +1 (828) 874 41 11
Fax: +1 (828) 879 39 81

**www.saftbatteries.com**

Doc. N° 54049-2-0909

Information in this document is subject to change without notice and becomes contractual only after written confirmation by Saft.

Published by the Communications Department.

Photo credit: Saft.

Société anonyme au capital de 31 944 000 €
RCS Bobigny B 383 703 873

Produced by Arthur Associates Limited.

# Appendix C

# Boston Power Li-ion (LCO) Battery Cell Sonata 5300

# Sonata® 5300 Rechargeable Lithium-ion Cell

Boston-Power's Sonata 5300 is a high performance lithium-ion rechargeable cell. Its exceptional energy density, industry-leading cycle life, fast charge capability, and industry leading safety features make the Sonata 5300 an ideal solution for industrial, medical, military, notebook computer sensor, and other portable power applications.

## Specifications



| | | |
|---|---|---|
| Nominal capacity [1] | | 5300 mAh |
| Nominal energy [1] | | 19.3 Wh |
| Nominal voltage | | 3.65 V |
| Energy density | Gravimetric | 202 Wh/kg |
| | Volumetric | 490 Wh/L |
| Nominal cell impedance (1kHz, AC) | | 23 mΩ |
| Cycle life to 80% capacity | | >1000 cycles |
| Standard charging method | Constant current (CC) | 3.7A (0.7C) to 4.2V |
| | Constant voltage (CV) | 4.2V to 50 mA |
| Recommended fast charge | | 8.0A (1.5C) to 4.2V |
| Nominal cell weight | | 95 g |
| Operating temperature | Charge | -20 to 60°C |
| | Discharge | -40 to 70°C |
| Storage temperature | | -40 to 60°C |

[1] Standard discharge 0.2C to 2.75 V

## Certifications

UN 38.3, UL1642, IEC62133, Directive 2006/66/EC, ROHS 2002/95/EC
In process: Nordic Ecolabel

## Cycle Life at 100% Depth of Discharge (DOD)

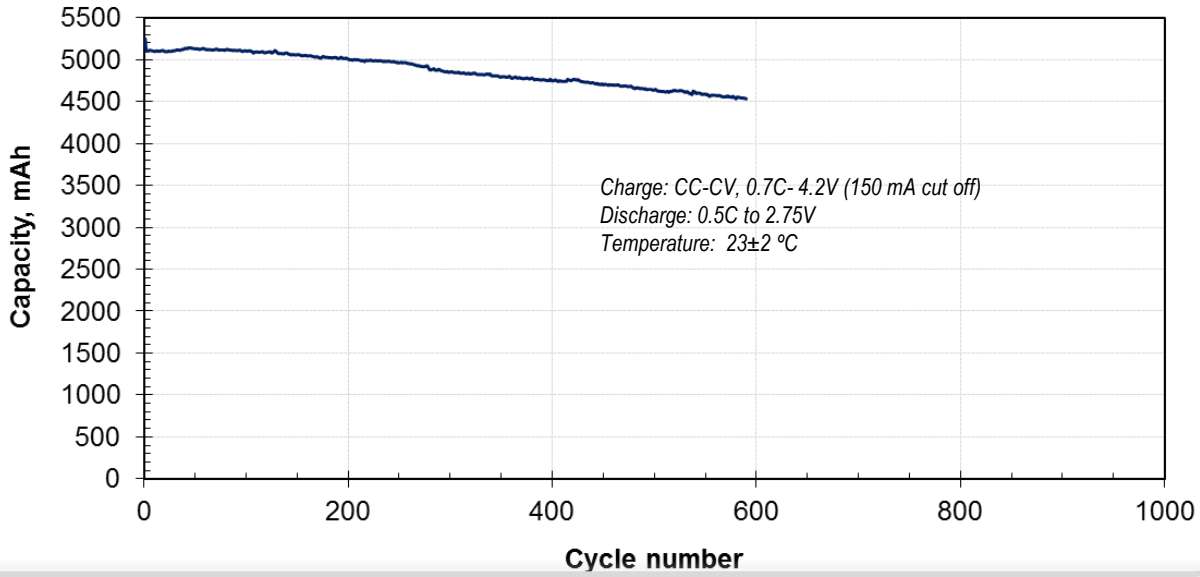

## Discharge Capacity

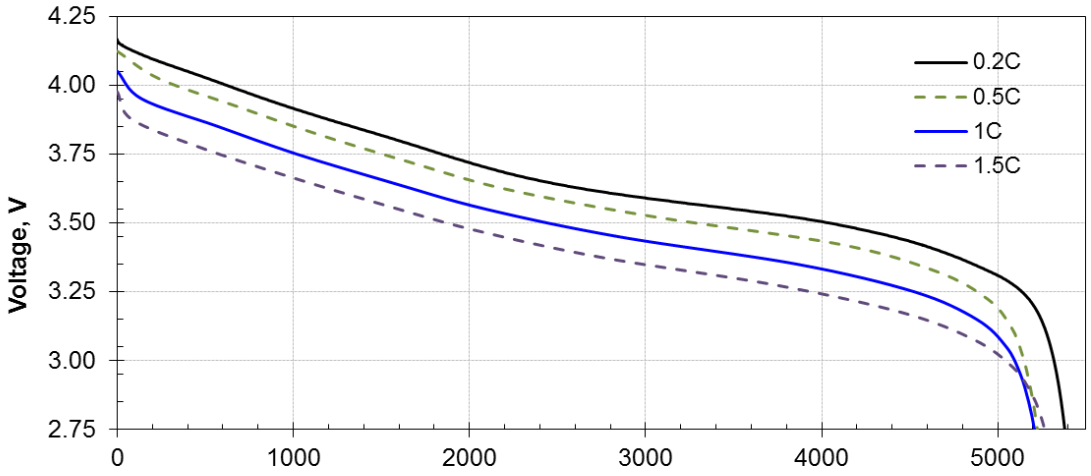


## Temperature Discharge Curve (0.5C)

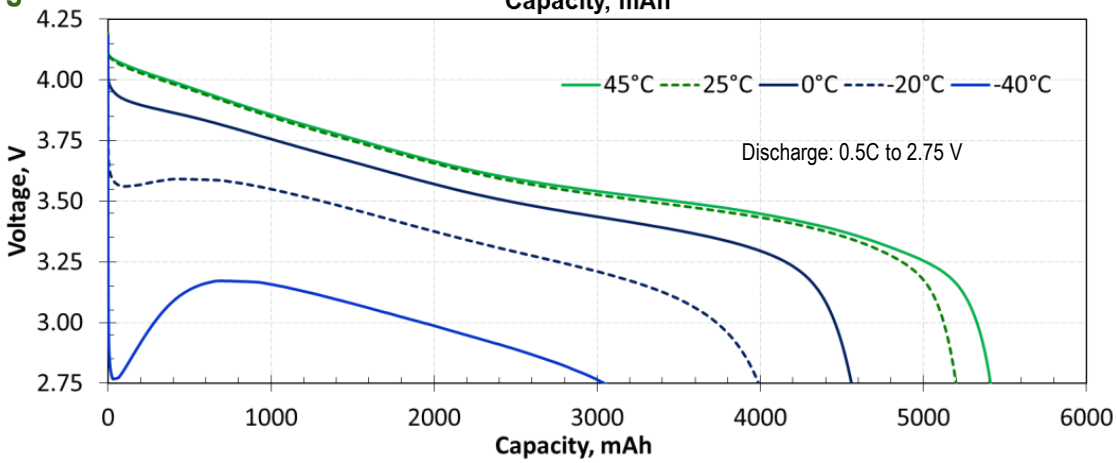


## Charge Curve (0.7C)

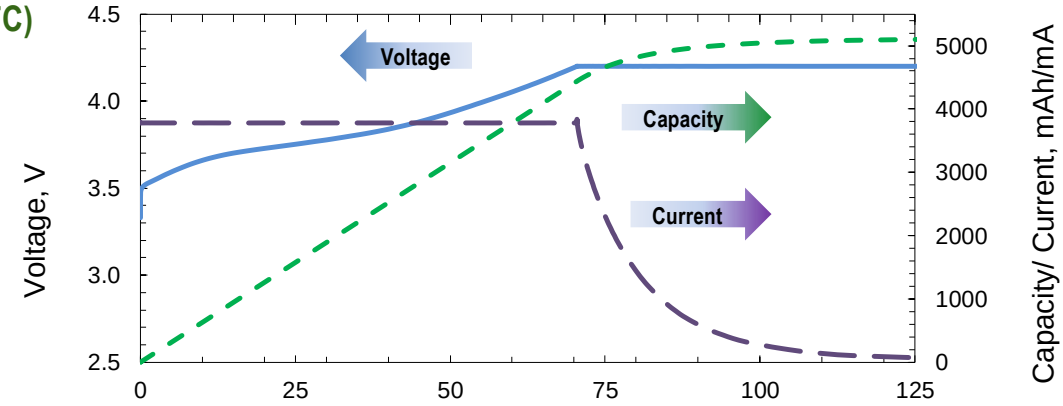


Temperature: 23°C ± 2°C
Standard Charge



www.boston-power.com

**USA**
Boston-Power, Inc.
2200 West Park Drive
Westborough, MA 01581-3961, USA
Phone: +1.508.366.0885

**China**
Boston-Power Battery (Shenzhen) Co., Ltd.
Jinrun Bldg., Tairan 9th Rd.
CheGongMiao, Futian District
Shenzhen 518040, China

**Taiwan**
Boston-Power Battery
(Taiwan) Co., Ltd.
89 Song Ren Road, Suite 11C
Taipei, 110, Taiwan

Performance may vary depending on, but not limited to cell usage and application. If cells are used outside specifications, performance may diminish.
All specifications are subject to change without notice. Some data reflects expected performance for product in development. All information provided herein is believed, but not guaranteed to be accurate.

©2011, Boston-Power, Inc. All rights reserved. No portion of this material may be copied or reproduced, in any manner, without the express written consent of Boston-Power. The Boston-Power logo, Swing, Sonata, Swing Tempo and Swing Key are all trademarks or registered trademarks of Boston-Power, Inc. which retains sole rights to their use.

# Appendix D

# A123 Systems Li-ion (LFP) Battery Cell ANR26650m1B

# Nanophosphate® High Power Lithium Ion Cell
# ANR26650*m1-B*

## KEY FEATURES AND BENEFITS


- Excellent abuse tolerance and superior cycle life from A123's patented Nanophosphate® lithium ion chemistry
- High power with over 2,600 W/kg and 5,800 W/L, 10 seconds, 50% SOC
- High usable energy over a wide state of charge (SOC) range

| ANR26650*m1-B* Cell Specifications | |
|---|---|
| Cell Dimensions (mm) | ø26 x 65 |
| Cell Weight (g) | 76 |
| Cell Capacity (nominal/minimum, Ah) | 2.5/2.4 |
| Voltage (nominal, V) | 3.3 |
| Internal Impedance (1kHz AC typical, mΩ) | 6 |
| HPPC 10 Sec Discharge Pulse Power 50% SOC | 200 W |
| Recommended Standard Charge Method | 1C to 3.6V CCCV, 45 min |
| Recommended Fast Charge Method to 80% SOC | 4C to 3.6V CC, 12 min |
| Maximum Continuous Discharge (A) | 70 |
| Maximum Pulse Discharge (10 seconds, A) | 120 |
| Cycle Life at 10C Discharge, 100% DOD | >1,000 cycles |
| Operating Temperature | -30°C to 55°C |
| Storage Temperature | -40°C to 60°C |

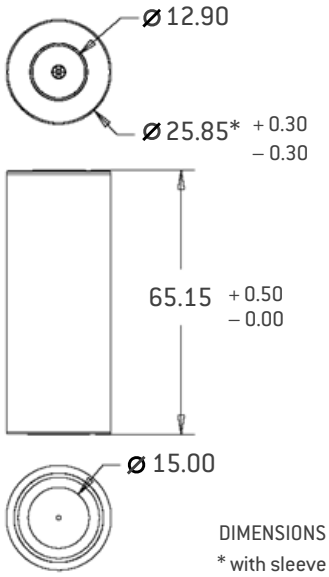


DIMENSIONS IN MM
* with sleeve 25.96 +/- 0.50 mm

## APPLICATIONS

### Transportation

Advanced energy storage for electric drive vehicles

### Commercial

Enabling next-generation commercial products

### Electric Grid

Dynamic energy solutions for a smarter grid



©2011 A123 Systems, Inc. All rights reserved.
MD100113-01

# Nanophosphate® High Power Lithium Ion Cell

## ANR26650*m1-B*

1C Discharge Characteristics at High and Low Temperatures

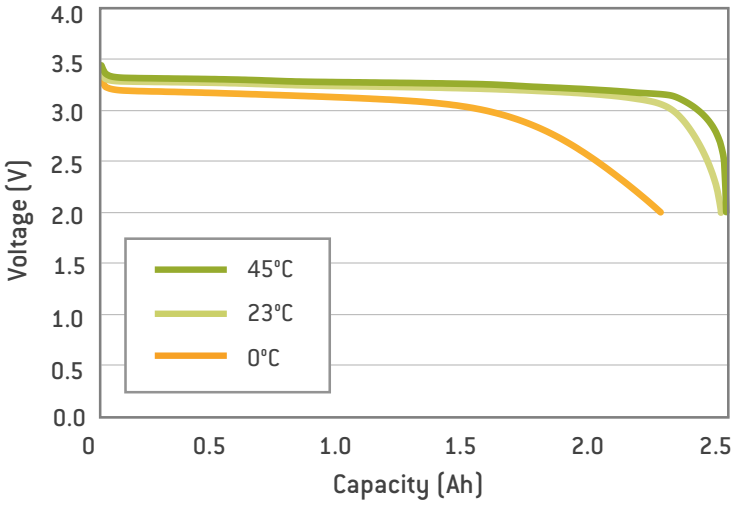


Discharge Characteristics at 23°C

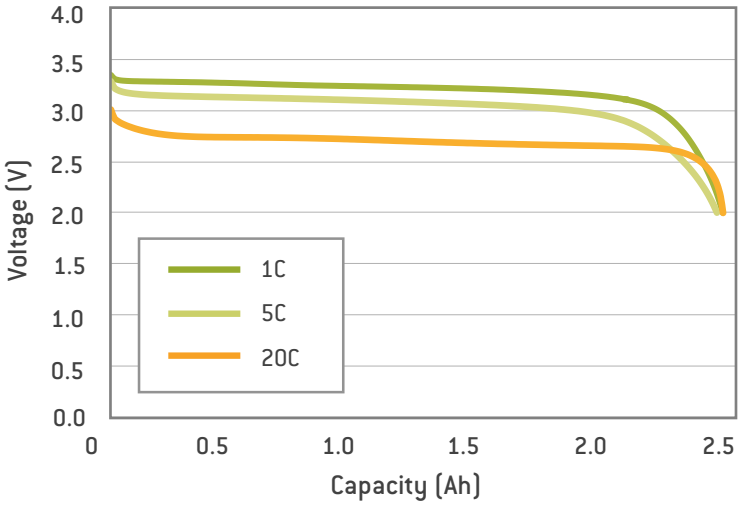


Cycle Life Performance, 100% DOD, Various Temperatures and Discharge Rates

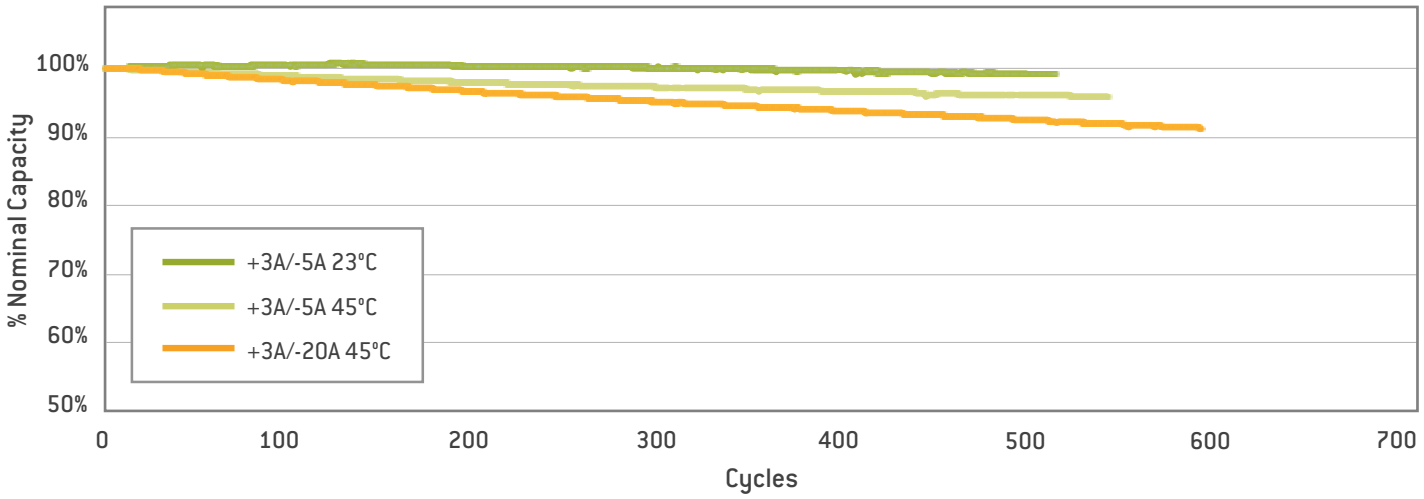


Preliminary Specifications. Performance may vary depending on use conditions and application.
A123 Systems makes no warranty explicit or implied with this datasheet. Contents subject to change without notice.


CORPORATE HEADQUARTERS
A123 Systems, Inc.
200 West Street
Waltham, MA 02451
(617) 778-5700
www.a123systems.com


A123 SYSTEMS


©2011 A123 Systems, Inc. All rights reserved.


MD100113-01

# Appendix E

# Saft Li-ion Battery Pack Assembly

# Lithium-ion battery systems

## Solar photovoltaic (PV) — Energy Storage Systems (ESS)

## The system approach for outstanding performance and safety

**Saft's Li-ion battery technology has established an unrivalled track-record in space vehicle and satellite programs that represent the most demanding and performance-critical environment for any battery. The same rigorous design and manufacturing principles have been applied as Saft has introduced Li-ion batteries across a number of sectors including aircraft, vehicles, rail, telecoms, data centers, industrial standby and energy storage.**

**Saft has a unique capability that spans the entire lithium-ion (Li-ion) battery design, development and manufacturing chain from individual cells, through battery modules to fully integrated battery systems. In the majority of ESS applications for PV installations a Saft battery system offers the optimum route for ensuring the highest levels of performance, availability and safety over a long service life.**

### What are the key battery system functions?

A Li-ion battery system provides a number of key functions in an ESS application:

- Deliver power and energy as required
- Ensure safe system start-up, sleep mode, shut down (connection with charger)
- Ensure battery operation in optimum conditions
  - Supervise voltage, current, temperature at system, module, cell levels
  - Indicate in real time the available charge and discharge power / current to the inverter
  - Ensure balancing of cells, modules, strings
  - Provide alerts when operating conditions are "out of normal"
  - Put the battery into safe operation mode in case of an anomaly
- Present information to the user / inverter system
  - Operational parameters in real time (current, voltage, temperature)
  - State of Charge (SOC) and State of Health (SOH)
  - Alerts
- Ensure safe operation
  - Detect anomalies
  - Send alarms to trigger corrective action (e.g. reduce charge voltage, lower power...)
  - Disconnect the battery (interrupt charge / discharge) if a critical threshold is reached and put the battery into a safe mode condition
  - Re-connect battery and allow charge/discharge if the anomaly has cleared

saft

# VL Li-ion cells

A Li-ion cell comprises:

- A positive electrode made from lithiated metal oxides ($LiNiCoAlO_2$, $LiFePO_4$...)
- A negative electrode generally made of carbon material
- An electrolyte made of lithium salts dissolved in organic cabonates
- A separator made of porous polymeric materials (for insulation between the electrodes and to allow the ionic exchanges)

When the battery is charged, the lithium atoms in the cathode become ions and migrate through the electrolyte toward the carbon anode where they combine with external electrons and are deposited between carbon layers as lithium atoms. This process is reversed during discharge.

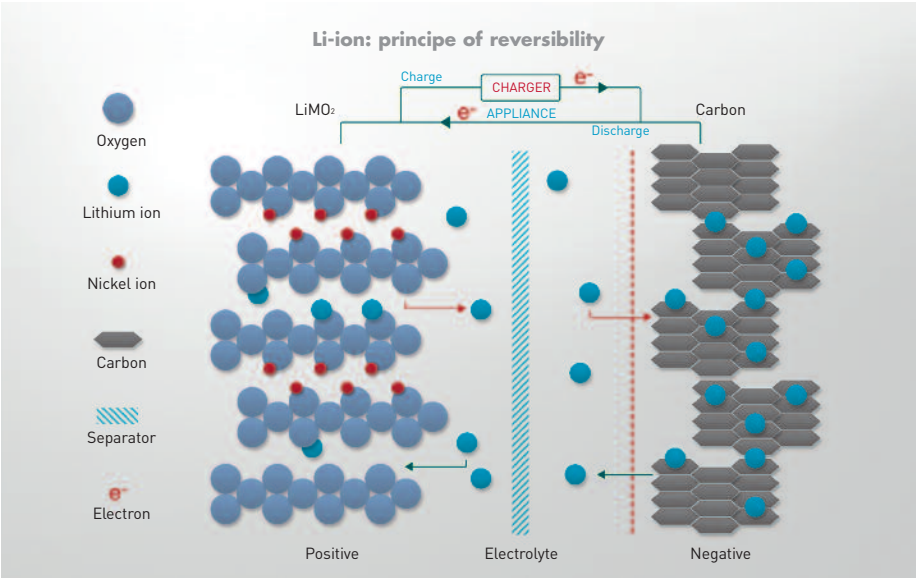


Saft Li-ion cells are manufactured on a volume basis at factories in Jacksonville, US and Nersac, France. An R&D centre in Bordeaux also supports the development of new battery technologies.

Saft ESS batteries are based on cylindrical format VL cells available in 3 different versions to suit various power and energy requirements.

# Synerion® Li-ion battery modules

Saft Synerion® Li-ion battery modules integrate a number of cells assembled in series and/or parallel configuration to provide the required voltage and capacity. They are available in 24 V or 48 V versions from 2 to 12 kW.

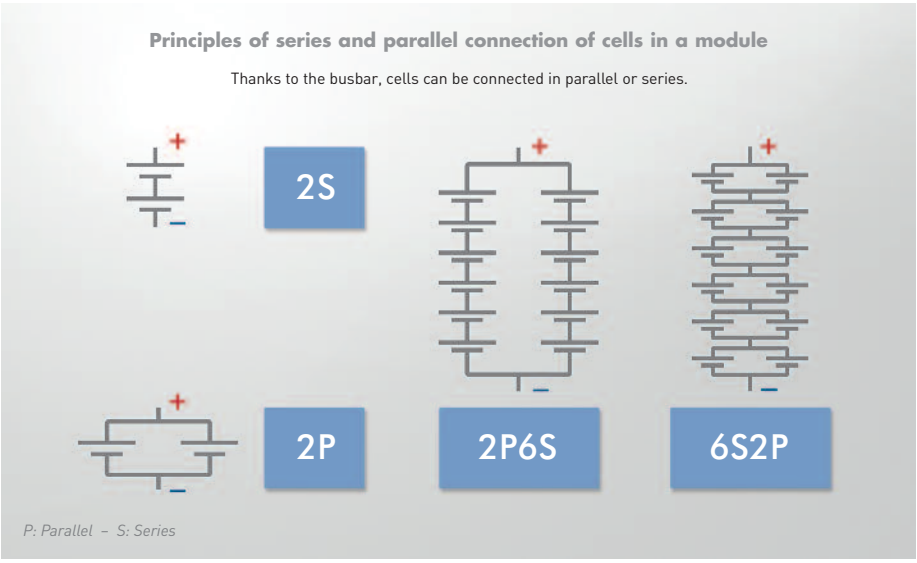



The bus bar provides the electrical interconnection between the individual cells and also carries the circuits and components for managing charge/discharge management (the bus bars often integrate the SMU function as well).

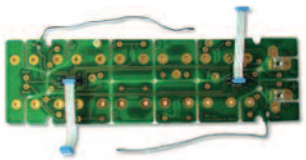

Each module incorporates an electronic contol board known as the SMU (safety monitoring unit). Its finctions are:

- monitoring the individual cell voltage during charge and discharge
- monitoring battery internal temperature
- balancing cells
- data communication with the BMU (Battery Management Unit)

## Keeping things in balance

Although Li-ion cells are manufactured to the very highest quality standards there are always slight variations in their characteristics, especially the rate of self-discharge. The SMU balancing function uses a resistor to discharge the cells with the highest voltage to bring them to a uniform level.

# Intensium® Max battery systems

In Saft's Intensium® battery systems, Synerion modules are connected in series and associated with one BMM (Battery Management Module). The BMM contains two main functions: BMU (battery management unit – to manage all the battery functions) and an EDU (electrical disconnect unit – to enable the safe disconnect of a single string). It is responsible for:

- Operations supervision (U,I)
- Charge/discharge management →IMR/IMD
- Thermal management
- Warnings/alarms
- SOC (State of Charge)
- SOH (State of Health)
- First level safety
- Watchdog
- Blackbox
- Maintenance/Diagnostics

Several strings can be connected in parallel through an MBMM (Master BMM, managing the parallel connection and balancing between strings)
This architecture ensures a high level of redundancy and maintainability: it is possible to disconnect a single string whilst all others continue operation.
The BMM and MBMM provide superior CAN Bus communication capability by delivering key information on the battery operation to the charger and the next level Energy Management System.
This includes its SOC and SOH, available power and energy and, if necessary, warnings and relevant information for maintenance.
Saft also provides a tool for battery diagnostics: it can be connected to the BMM and provides in-depth data on components and operation history – helping identify, isolate and repair quickly any component defect.

## Saft has developed three main battery system ranges for PV installations

### Intensium® Home

Integrated energy storage system for residential applications

### Intensium® Smart

Energy storage to support smart grid applications

### Intensium® Max

A containerised system that provides energy storage capacity of up to 1 MWh or power of up to 1.8 MW in a standard 20 foot container that integrates Li-ion battery modules, power management and control interfaces, air conditioning and safety devices in a comprehensive package, delivered to site ready to install and commission.

**Components: Master Battery Management Module**

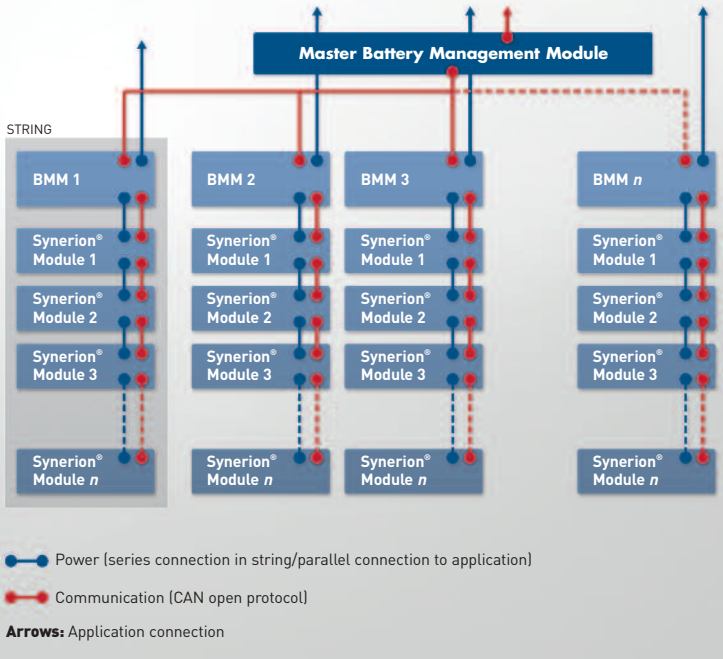

## Total system support

Saft's scope of supply extends well beyond the system to include:

- Pre-project support: modelling the behaviour of both the battery and the entire system over its projected lifetime enables accurate and reliable simulation of each customer application – a vital capability to ensure the optimum sizing of the ESS
- After sales: installation, commissioning, maintenance contracts, spare parts

## Leading the way in ESS

Saft battery systems continue to lead the way in ESS:

- First ESS project at MW scale in 2003
- First ESS project with Li-ion systems in 2007
- First ESS containerised Li-ion storage system delivered in 2012

Currently, with over 50 MWh of containerised systems installed or on order, Saft has one of the largest installed bases of battery system manufacturer.



## Useful acronyms

| | Full name | Comprising | Functions |
|---|---|---|---|
| **BMC** | Battery Management Controller | BMU plus casing | Cell management |
| **BMM/BMS** | Battery Management Module/System | BMU/BMC plus EDU | Cell protection and management |
| **BMU** | Battery Management Unit | SMU plus managing electronics | Cell management and communication |
| **CAN Bus** | Controlled Area Network Bus | | Communication between modules and BMM, and BMM or MBMM to charger |
| **EDU** | Electrical Disconnect Unit | | Enables the safe disconnection of a single battery string |
| **MBMM** | Master Battery Management Module | Several BMCs plus EDUs | Management of modules in series or in parallel |
| **SMU** | System Management Unit | | U and T, data acquisition and balancing |

**Saft**
12, rue Sadi Carnot
93170 Bagnolet - France
Tel. : +33 1 49 93 19 18
Fax : +33 1 49 93 19 64
www.saftbatteries.com

Document N° 21894-2-0514
Edition: May 2014

Data in this document is subject to change without notice and becomes contractual only after written confirmation.

Photo credits: Saft, Fotolia.
Studio DT - R299/B

© Saft – Société par Actions Simplifiée au capital de 31 944 000 €
RCS Bobigny B 383 703 873

# Appendix F

# NEC High Rate (HR) Energy Storage Racks

NEC ENERGY SOLUTIONS

# High Rate (HR) Energy Storage Racks

The High Rate (HR) Energy Storage Rack from NEC Energy Solutions is a fully integrated battery storage system offering reliable energy storage for a wide range of high rate, high power applications including grid stabilization.

The HR Energy Storage Rack is a basic building block of NEC Energy's GBS™ integrated grid-scale energy storage systems. The racks can also be configured as standalone DC sources for a multitude of customized grid and commercial applications. The HR Energy Storage Rack is a standardized product that delivers best-in-class performance and inherent multi-layer safety for the most demanding energy storage scenarios.

### HR Energy Storage Racks include:

- HR Battery Modules utilizing NEC's industry-proven technology (6 for the 700V design; 8 for the 950V design)
- Battery Management System (BMS) that continuously monitors voltage, temperature, and system conditions and performs cell balancing
- Nested safety features provide layered protection at the cell, module, BMS, and rack level
- CAN bus communications between BMS and high-level system controls

## EXAMPLE APPLICATIONS

### Grid Storage/Grid Stabilization

HR Energy Storage Racks support third party systems and can be furnished in NEC's Grid Battery Storage System (GBS™) for high power and stabilization applications such as:

- Frequency-regulation services
- Voltage stabilization/VAR support
- Renewable firming/stabilization
- Power balancing (or bridging)
- Spinning reserve
- Inrush control (e.g., light rail, trolley, etc.)

| Rack Level Specifications | 700V HR | 950V HR |
|---|---|---|
| **Battery Type** | Lithium ion (Nanophosphate™) | |
| **Nominal Voltage** | 700 VDC | 950 VDC |
| **Operating Voltage Range** | 545–750 VDC | 750–1050 VDC |
| **Max. Charge/Discharge Power** | 102 kW (1 full cycle/day) | 136 kW (1 full cycle/day) |
| **Continuous Charge/Discharge Power** | 51 kW | 68 kW |
| **Available Energy (Nominal)** | 26 kWh** | 34 kWh** |
| **Nominal Capacity** | 40 Ah | |
| **Maximum Discharge Current** | 160 A | |
| **Usable State of Charge (SOC)** | 0–100% | |
| **Round Trip Efficiency** | 97% (1C), 98% (C/2) | |
| **Cycle Life** (1C charge / 1C discharge, to 80% BOL @ 23°C) | >9,500 cycles (100% DOD) | |
| **Operating Temperature** | -40 to 60°C** | |
| **Shipping/Storage Temperature Range** | -40 to 60°C | |
| **Communications** | CAN bus | |
| **DC Contactor Interlock** | Yes | |
| **Dimensions (W x D x H)** | 600 x 1070 x 2150 mm (24 x 47 x 85 in) | 600 x 1070 x 2438 mm (24 x 47 x 96 in) |
| **Weight** | 686 kg / 1512 lbs | 872 kg / 1923 lbs |

** Recommended temp range for optimal battery performance is 15°C–30°C

## STANDARDS AND COMPLIANCE

**IEC 62133**, Secondary cells and batteries containing alkaline or other non-acid electrolytes – Safety
**UL 1642**, Lithium Batteries

© 2015 NEC Energy Solutions Inc. All rights reserved.

050415HR-Rev01

## HIGH PERFORMANCE

The HR Energy Storage Rack delivers an unparalleled combination of cycle life, calendar life and energy performance. Multi-year testing of the cells and modules, under both realistic and extreme conditions, confirms life expectancy of > 9,000 cycles.

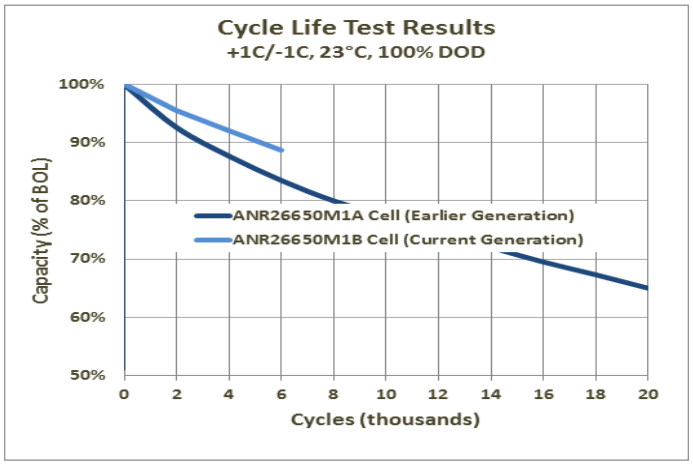


## NESTED SAFETY DESIGN

The HR Energy Storage Rack is engineered for the utmost safety, enabled by the intrinsically safe design, fusing at the cell, module and rack levels, extensive fault monitoring down to the module level and automatic opening of the dual contactors upon power loss or safety cover removal.

## BATTERY MODULE FEATURES

HR Energy Storage Racks contain field-replaceable battery modules with on-board intelligence that communicates with the BMS and:

- Monitor voltage on every cell bank and provide independent module voltage measurements
- Measure representative cell temperatures
- Maintain cells in optimum state-of-charge and help prevent overvoltage conditions
- Monitor overvoltage conditions and signal shutdown if detected

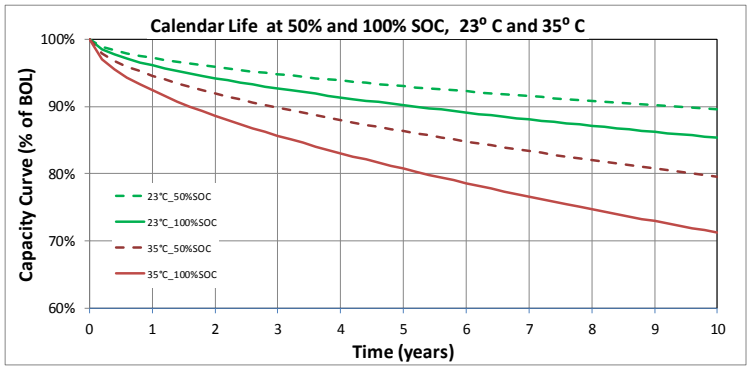


## BMS FEATURES

The HR Energy Storage Rack's BMS continuously monitors voltage, temperature, and current to initiate protective actions if any unsafe condition is detected. Each BMS has automated independent control of two separate contactors that disconnect and de-energize an individual rack from the external DC bus if needed. These contactors mechanically default open (OFF) if the control link from the contactor to the BMS is lost, or, if power to the BMS is interrupted. The BMS also contains a high voltage rack level fuse to supplement contactor overcurrent protection. The BMS offers communications through a configurable CAN bus interface for integration with a larger system, as well as a separate local serial communications interface for local diagnostics.

## RACK-LEVEL FEATURES

- Supports standalone, single rack applications, or scalable multi-rack megawatt (MW) systems
- Built-in rigging/lifting points
- May be installed to Seismic Demand Spectrum (SDS) 1 or 2
- DC Bus Contactor(24V)

NEC ENERGY SOLUTIONS

**NEC Energy Solutions, Inc.**
155 Flanders Road
Westborough, MA 01581

Phone: +1.508.497.7319
Email: contact@neces.com
Web: **www.neces.com**

Performance may vary depending on use conditions and application. NEC Energy Solutions, Inc. makes no warranty explicit or implied with this data sheet. Contents subject to change without notice.

© 2015 NEC Energy Solutions Inc. All rights reserved.

# Appendix G

# BE C-code (EMULATOR_M.c)

```c
/*
 * File: EMULATOR_M.c
 *
 * Code generated for Simulink model 'EMULATOR_M'.
 *
 * Model version                  : 1.584
 * Simulink Coder version         : 8.2 (R2012a) 29-Dec-2011
 * TLC version                    : 8.2 (Dec 29 2011)
 * C/C++ source code generated on : Fri Aug 21 15:41:21 2015
 *
 * Target selection: ert.tlc
 * Embedded hardware selection: Texas Instruments->C2000
 * Code generation objectives:
 *    1. Execution efficiency
 *    2. ROM efficiency
 *    3. RAM efficiency
 *    4. Traceability
 * Validation result: Not run
 */

#include "EMULATOR_M.h"
#include "EMULATOR_M_private.h"


/* Block signals and states (auto storage) */
D_Work_EMULATOR_M EMULATOR_M_DWork;

/* External inputs (root inport signals with auto storage) */
ExternalInputs_EMULATOR_M EMULATOR_M_U;

/* External outputs (root outports fed by signals with auto storage) */
ExternalOutputs_EMULATOR_M EMULATOR_M_Y;

/*
 * Output and update for action system:
 *    '<S12>/DISCH_ST_IF_M'
 *    '<S12>/DISCH_ST_IF_OFF_M'
 */
void EMULATOR_M_DISCH_ST_IF_M(boolean_T rtu_0, int32_T rtu_1, boolean_T *rty_out,
  int32_T *rty_out1)
{
  /* Inport: '<S14>/In1' */
  *rty_out = rtu_0;

  /* Inport: '<S14>/In2' */
  *rty_out1 = rtu_1;
}

/* Model step function */
void EMULATOR_M_step(void)
{
  /* local block i/o variables */
  int32_T rtb_IQNIQN2;
  int32_T rtb_Sum5;
  int32_T rtb_VB_CHARGE;
  int32_T rtb_IQNIQN2_i;
  int32_T rtb_IQNIQN2_h;
  int32_T rtb_SOD;
  int32_T rtb_ICELL;
  int32_T rtb_IQNIQN2_c;
  int32_T rtb_Sum1;
  int32_T rtb_IQNIQN2_k;
```

```
int32_T rtb_IQNIQN1;
int32_T rtb_IQNIQN4;
int32_T rtb_IQNIQN3;
int32_T rtb_IQNxIQN2;
int32_T rtb_IQNIQN1_f;
int32_T rtb_IQNxIQN3;
int32_T rtb_IQNxIQN2_b;
int32_T rtb_IQNIQN3_h;
int32_T rtb_Saturation1_f;
int32_T rtb_IQNxIQN3_g;
int16_T rtb_Switch1;
boolean_T rtb_RelationalOperator_o;
int32_T rtb_UD_ICELL;

/* Saturate: '<S1>/Saturation3' incorporates:
 *  Inport: '<Root>/ICELL'
 */
if (EMULATOR_M_U.ICELL >= EE_ICELL_PACK_MAX) {
  rtb_Saturation1_f = EE_ICELL_PACK_MAX;
} else if (EMULATOR_M_U.ICELL <= EE_ICELL_PACK_MIN) {
  rtb_Saturation1_f = EE_ICELL_PACK_MIN;
} else {
  rtb_Saturation1_f = EMULATOR_M_U.ICELL;
}

/* End of Saturate: '<S1>/Saturation3' */

/* C28x IQmath Library (stiiqmath_iqdiv) - '<S2>/IQN // IQN2' */
{
  rtb_IQNIQN2 = _IQ18div (rtb_Saturation1_f, EE_P_CELLS);
}

/* Outputs for Atomic SubSystem: '<S2>/01_SELF_DISCH_M' */
/* If: '<S3>/If' incorporates:
 *  Constant: '<S3>/Constant5'
 *  Inport: '<S11>/In1'
 *  Inport: '<S8>/In1'
 *  Logic: '<S9>/Logical Operator'
 */
if (!(EE_SD_MODE != 0L)) {
  /* Outputs for IfAction SubSystem: '<S3>/SD_OFF' incorporates:
   *  ActionPort: '<S8>/Action Port'
   */
  EMULATOR_M_DWork.Merge2 = rtb_IQNIQN2;

  /* End of Outputs for SubSystem: '<S3>/SD_OFF' */
} else {
  if (EE_SD_MODE != 0L) {
    /* Outputs for IfAction SubSystem: '<S3>/SD_ON' incorporates:
     *  ActionPort: '<S9>/Action Port'
     */
    /* Abs: '<S9>/Abs1' */
    if (rtb_IQNIQN2 < 0L) {
      rtb_UD_ICELL = -rtb_IQNIQN2;
    } else {
      rtb_UD_ICELL = rtb_IQNIQN2;
    }

    /* End of Abs: '<S9>/Abs1' */

    /* RelationalOperator: '<S9>/Relational Operator' incorporates:
     *  Constant: '<S9>/Constant1'
```

```
     */
    rtb_RelationalOperator_o = (rtb_UD_ICELL >= EE_SD_ICELL_ABS);

    /* Outputs for Enabled SubSystem: '<S9>/ELSE' incorporates:
     *  EnablePort: '<S10>/Enable'
     */
    if (!rtb_RelationalOperator_o) {
      /* C28x IQmath Library (stiiqmath_iqmpy) - '<S10>/IQN x IQN1' */
      {
        EMULATOR_M_DWork.Merge2 = _IQ18mpy (EE_C_NOM, EE_SELF_DISCH_DAILY);
      }
    }

    /* End of Outputs for SubSystem: '<S9>/ELSE' */

    /* Outputs for Enabled SubSystem: '<S9>/IF' incorporates:
     *  EnablePort: '<S11>/Enable'
     */
    if (rtb_RelationalOperator_o) {
      EMULATOR_M_DWork.Merge2 = rtb_IQNIQN2;
    }

    /* End of Outputs for SubSystem: '<S9>/IF' */
    /* End of Outputs for SubSystem: '<S3>/SD_ON' */
  }
}

/* End of If: '<S3>/If' */
/* End of Outputs for SubSystem: '<S2>/01_SELF_DISCH_M' */

/* Outport: '<Root>/I_SELF_DISCH' */
EMULATOR_M_Y.I_SELF_DISCH = EMULATOR_M_DWork.Merge2;

/* Outputs for Atomic SubSystem: '<S2>/02_SOC_RELATIVE_M' */
/* DiscreteIntegrator: '<S4>/Discrete-Time Integrator' */
rtb_SOD = EMULATOR_M_DWork.DiscreteTimeIntegrator_DSTATE_i;

/* Inport: '<S4>/ICELL' */
rtb_ICELL = EMULATOR_M_DWork.Merge2;

/* C28x IQmath Library (stiiqmath_iqdiv) - '<S4>/IQN // IQN1' */
{
  rtb_IQNIQN1_f = _IQ18div (rtb_SOD, EE_C_NOM);
}

/* C28x IQmath Library (stiiqmath_iqmpy) - '<S4>/IQN x IQN1' */
{
  EMULATOR_M_Y.ICELL_CH = _IQ18mpy (rtb_ICELL, (((int32_T)-262144L)));
}

/* C28x IQmath Library (stiiqmath_iqdiv) - '<S4>/IQN // IQN2' */
{
  rtb_IQNIQN2_c = _IQ18div (EMULATOR_M_Y.ICELL_CH, ((int32_T)943718400L));
}

/* C28x IQmath Library (stiiqmath_iqmpy) - '<S4>/IQN x IQN3' */
{
  rtb_IQNxIQN3 = _IQ18mpy (rtb_IQNIQN1_f, ((int32_T)26214400L));
}

/* Sum: '<S4>/Sum1' incorporates:
 *  Constant: '<S4>/Constant8'
```

```
 */
rtb_Sum1 = rtb_IQNxIQN3 + EE_SOC_INIT;

/* UnitDelay: '<S4>/UD_ICELL' */
rtb_UD_ICELL = EMULATOR_M_DWork.UD_ICELL_DSTATE;

/* Update for DiscreteIntegrator: '<S4>/Discrete-Time Integrator' */
EMULATOR_M_DWork.DiscreteTimeIntegrator_DSTATE_i += mul_s32_s32_s32_sr33
  (858993459L, rtb_IQNIQN2_c);

/* Update for UnitDelay: '<S4>/UD_ICELL' */
EMULATOR_M_DWork.UD_ICELL_DSTATE = rtb_ICELL;

/* End of Outputs for SubSystem: '<S2>/02_SOC_RELATIVE_M' */

/* Outputs for Atomic SubSystem: '<S2>/03_SELECTION_M' */
/* Switch: '<S5>/Switch1' incorporates:
 *  RelationalOperator: '<S5>/FixPt Relational Operator'
 *  UnitDelay: '<S5>/Unit Delay1'
 */
if (EMULATOR_M_DWork.UnitDelay1_DSTATE > 0) {
  rtb_Switch1 = EMULATOR_M_DWork.UnitDelay1_DSTATE;
} else {
  rtb_Switch1 = (rtb_ICELL != rtb_UD_ICELL);
}

/* End of Switch: '<S5>/Switch1' */

/* If: '<S5>/If' incorporates:
 *  Constant: '<S5>/Constant8'
 *  If: '<S12>/IF_COND_B'
 *  Inport: '<S13>/In2'
 *  RelationalOperator: '<S12>/Relational Operator'
 *  RelationalOperator: '<S12>/Relational Operator1'
 *  RelationalOperator: '<S12>/Relational Operator2'
 *  RelationalOperator: '<S12>/Relational Operator3'
 *  UnitDelay: '<S5>/Unit Delay2'
 */
if (rtb_Switch1 == 0) {
  /* Outputs for IfAction SubSystem: '<S5>/INIT_STATE_M' incorporates:
   *  ActionPort: '<S13>/Action Port'
   */
  /* Switch: '<S13>/Switch' incorporates:
   *  Constant: '<S13>/Constant1'
   *  Constant: '<S13>/Constant6'
   */
  if (rtb_ICELL > 0L) {
    EMULATOR_M_DWork.Merge_c = TRUE;
  } else {
    EMULATOR_M_DWork.Merge_c = FALSE;
  }

  /* End of Switch: '<S13>/Switch' */
  EMULATOR_M_DWork.Merge1 = EE_SOC_INIT;

  /* End of Outputs for SubSystem: '<S5>/INIT_STATE_M' */
} else {
  /* Outputs for IfAction SubSystem: '<S5>/DISCH_ST_ON_DECISION_M' incorporates:
   *  ActionPort: '<S12>/Action Port'
   */
  if ((rtb_ICELL > 0L) && (rtb_UD_ICELL <= 0L) &&
      (!EMULATOR_M_DWork.UnitDelay2_DSTATE)) {
```

```
    /* Outputs for IfAction SubSystem: '<S12>/DISCH_ST_IF_M' incorporates:
     *  ActionPort: '<S14>/Action Port'
     */

    /* If: '<S12>/IF_COND_B' incorporates:
     *  Constant: '<S12>/Constant2'
     */
    EMULATOR_M_DISCH_ST_IF_M(TRUE, rtb_Sum1, &EMULATOR_M_DWork.Merge_c,
      &EMULATOR_M_DWork.Merge1);

    /* End of Outputs for SubSystem: '<S12>/DISCH_ST_IF_M' */
  } else {
    if ((0L > rtb_ICELL) && (0L <= rtb_UD_ICELL) &&
        EMULATOR_M_DWork.UnitDelay2_DSTATE) {
      /* Outputs for IfAction SubSystem: '<S12>/DISCH_ST_IF_OFF_M' incorporates:
       *  ActionPort: '<S15>/Action Port'
       */

      /* If: '<S12>/IF_COND_B' incorporates:
       *  Constant: '<S12>/Constant1'
       */
      EMULATOR_M_DISCH_ST_IF_M(FALSE, rtb_Sum1, &EMULATOR_M_DWork.Merge_c,
        &EMULATOR_M_DWork.Merge1);

      /* End of Outputs for SubSystem: '<S12>/DISCH_ST_IF_OFF_M' */
    }
  }

  /* End of Outputs for SubSystem: '<S5>/DISCH_ST_ON_DECISION_M' */
}

/* End of If: '<S5>/If' */

/* RelationalOperator: '<S5>/Relational Operator1' incorporates:
 *  Constant: '<S5>/Constant1'
 */
rtb_RelationalOperator_o = !EMULATOR_M_DWork.Merge_c;

/* Update for UnitDelay: '<S5>/Unit Delay1' */
EMULATOR_M_DWork.UnitDelay1_DSTATE = rtb_Switch1;

/* Update for UnitDelay: '<S5>/Unit Delay2' */
EMULATOR_M_DWork.UnitDelay2_DSTATE = EMULATOR_M_DWork.Merge_c;

/* End of Outputs for SubSystem: '<S2>/03_SELECTION_M' */

/* Outputs for Atomic SubSystem: '<S2>/04_VB_MODEL_M' */
/* Outputs for Enabled SubSystem: '<S6>/CHARGE_M' incorporates:
 *  EnablePort: '<S16>/Enable'
 */
if (rtb_RelationalOperator_o) {
  if (!EMULATOR_M_DWork.CHARGE_M_MODE) {
    /* InitializeConditions for Atomic SubSystem: '<S16>/CHARGE_MATH' */
    /* InitializeConditions for DiscreteIntegrator: '<S18>/Discrete-Time Integrator'
    EMULATOR_M_DWork.DiscreteTimeIntegrator_DSTATE_k = 0L;

    /* End of InitializeConditions for SubSystem: '<S16>/CHARGE_MATH' */
    EMULATOR_M_DWork.CHARGE_M_MODE = TRUE;
  }

  /* Outputs for Atomic SubSystem: '<S16>/Linear_Func1' */
  LINEAR_FUNCTION(EMULATOR_M_Y.ICELL_CH, &EMULATOR_M_Y.L1, EE_L1_CHARGE_X1,
```

```
                    EE_L1_CHARGE_Y2, EE_L1_CHARGE_Y1, EE_L1_CHARGE_X2);

  /* End of Outputs for SubSystem: '<S16>/Linear_Func1' */

  /* Outputs for Atomic SubSystem: '<S16>/CHARGE_MATH' */
  /* DiscreteIntegrator: '<S18>/Discrete-Time Integrator' */
  rtb_UD_ICELL = EMULATOR_M_DWork.DiscreteTimeIntegrator_DSTATE_k;

  /* C28x IQmath Library (stiiqmath_iqmpy) - '<S18>/IQN x IQN1' */
  {
    rtb_IQNIQN3_h = _IQ18mpy (EMULATOR_M_Y.ICELL_CH, EMULATOR_M_Y.L1);
  }

  /* C28x IQmath Library (stiiqmath_iqdiv) - '<S18>/IQN // IQN2' */
  {
    rtb_IQNIQN2_h = _IQ18div (rtb_IQNIQN3_h, ((int32_T)943718400L));
  }

  /* C28x IQmath Library (stiiqmath_iqdiv) - '<S18>/IQN // IQN3' */
  {
    rtb_IQNIQN3_h = _IQ18div (EMULATOR_M_DWork.Merge1, ((int32_T)26214400L));
  }

  /* C28x IQmath Library (stiiqmath_iqmpy) - '<S18>/IQN x IQN2' */
  {
    rtb_IQNxIQN2 = _IQ18mpy (rtb_IQNIQN3_h, EE_C_NOM);
  }

  /* Outport: '<Root>/SOC_SPEC' incorporates:
   *  Sum: '<S18>/Sum1'
   */
  EMULATOR_M_Y.SOC_SPEC = rtb_UD_ICELL + rtb_IQNxIQN2;

  /* Update for DiscreteIntegrator: '<S18>/Discrete-Time Integrator' */
  EMULATOR_M_DWork.DiscreteTimeIntegrator_DSTATE_k += mul_s32_s32_s32_sr33
    (858993459L, rtb_IQNIQN2_h);

  /* End of Outputs for SubSystem: '<S16>/CHARGE_MATH' */

  /* Outputs for Atomic SubSystem: '<S16>/LOOKUP_M' */

  /* Dynamic Look-Up Table Block: '<S19>/Main Lookup Table'
   * Input0  Data Type:  Fixed Point    S32  2^-18
   * Input1  Data Type:  Fixed Point    S32  2^-18
   * Input2  Data Type:  Fixed Point    S32  2^-18
   * Output0 Data Type:  Fixed Point    S32  2^-18
   * Saturation Mode: Saturate
   * Lookup Method: Linear_Endpoint
   *
   */
  LookUp_S32_S32_SAT( &(EMULATOR_M_DWork.VB_CELL), EE_LUT_CH_REF_Y,
                     EMULATOR_M_Y.SOC_SPEC, EE_LUT_CH_REF_X, 9U);

  /* End of Outputs for SubSystem: '<S16>/LOOKUP_M' */
} else {
  if (EMULATOR_M_DWork.CHARGE_M_MODE) {
    EMULATOR_M_DWork.CHARGE_M_MODE = FALSE;
  }
}

/* End of Outputs for SubSystem: '<S6>/CHARGE_M' */
```

```
/* Outputs for Enabled SubSystem: '<S6>/DISCHARGE_M' incorporates:
 *  EnablePort: '<S17>/Enable'
 */
if (EMULATOR_M_DWork.Merge_c) {
  if (!EMULATOR_M_DWork.DISCHARGE_M_MODE) {
    /* InitializeConditions for Atomic SubSystem: '<S17>/DISCH_MATH' */
    /* InitializeConditions for DiscreteIntegrator: '<S21>/Discrete-Time Integrator'
    EMULATOR_M_DWork.DiscreteTimeIntegrator_DSTATE = 0L;

    /* End of InitializeConditions for SubSystem: '<S17>/DISCH_MATH' */
    EMULATOR_M_DWork.DISCHARGE_M_MODE = TRUE;
  }

  /* Outputs for Atomic SubSystem: '<S17>/Linear_Func1' */
  LINEAR_FUNCTION(rtb_ICELL, &EMULATOR_M_Y.K1, EE_K1_DISCH_X1, EE_K1_DISCH_Y2,
                  EE_K1_DISCH_Y1, EE_K1_DISCH_X2);

  /* End of Outputs for SubSystem: '<S17>/Linear_Func1' */

  /* Outputs for Atomic SubSystem: '<S17>/DISCH_MATH' */
  /* DiscreteIntegrator: '<S21>/Discrete-Time Integrator' */
  rtb_UD_ICELL = EMULATOR_M_DWork.DiscreteTimeIntegrator_DSTATE;

  /* C28x IQmath Library (stiiqmath_iqmpy) - '<S21>/IQN x IQN2' */
  {
    rtb_IQNxIQN3_g = _IQ18mpy (rtb_ICELL, EMULATOR_M_Y.K1);
  }

  /* C28x IQmath Library (stiiqmath_iqdiv) - '<S21>/IQN // IQN2' */
  {
    rtb_IQNIQN2_i = _IQ18div (rtb_IQNxIQN3_g, ((int32_T)943718400L));
  }

  /* Sum: '<S21>/Sum3' incorporates:
   *  Constant: '<S21>/Constant10'
   */
  rtb_IQNxIQN3_g = 26214400L - EMULATOR_M_DWork.Merge1;

  /* C28x IQmath Library (stiiqmath_iqdiv) - '<S21>/IQN // IQN3' */
  {
    rtb_IQNIQN3 = _IQ18div (rtb_IQNxIQN3_g, ((int32_T)26214400L));
  }

  /* C28x IQmath Library (stiiqmath_iqmpy) - '<S21>/IQN x IQN3' */
  {
    rtb_IQNxIQN3_g = _IQ18mpy (rtb_IQNIQN3, EE_C_NOM);
  }

  /* Outport: '<Root>/SOD_SPEC' incorporates:
   *  Sum: '<S21>/Sum1'
   */
  EMULATOR_M_Y.SOD_SPEC = rtb_UD_ICELL + rtb_IQNxIQN3_g;

  /* Update for DiscreteIntegrator: '<S21>/Discrete-Time Integrator' */
  EMULATOR_M_DWork.DiscreteTimeIntegrator_DSTATE += mul_s32_s32_s32_sr33
    (858993459L, rtb_IQNIQN2_i);

  /* End of Outputs for SubSystem: '<S17>/DISCH_MATH' */

  /* Outputs for Atomic SubSystem: '<S17>/LOOKUP_M' */

  /* Dynamic Look-Up Table Block: '<S22>/Main Lookup Table'
```

```
    * Input0  Data Type:  Fixed Point    S32  2^-18
    * Input1  Data Type:  Fixed Point    S32  2^-18
    * Input2  Data Type:  Fixed Point    S32  2^-18
    * Output0 Data Type:  Fixed Point    S32  2^-18
    * Saturation Mode: Saturate
    * Lookup Method: Linear_Endpoint
    *
    */
  LookUp_S32_S32_SAT( &(rtb_VB_CHARGE), EE_LUT_DISCH_REF_Y,
                      EMULATOR_M_Y.SOD_SPEC, EE_LUT_DISCH_REF_X, 9U);

  /* End of Outputs for SubSystem: '<S17>/LOOKUP_M' */

  /* Outputs for Atomic SubSystem: '<S17>/Linear_Func2' */
  LINEAR_FUNCTION(rtb_ICELL, &rtb_Sum5, EE_K4_DISCH_X1, EE_K4_DISCH_Y2,
                  EE_K4_DISCH_Y1, EE_K4_DISCH_X2);

  /* End of Outputs for SubSystem: '<S17>/Linear_Func2' */

  /* C28x IQmath Library (stiiqmath_iqmpy) - '<S17>/IQN x IQN1' */
  {
    EMULATOR_M_DWork.VB_CELL = _IQ18mpy (rtb_VB_CHARGE, rtb_Sum5);
  }
} else {
  if (EMULATOR_M_DWork.DISCHARGE_M_MODE) {
    EMULATOR_M_DWork.DISCHARGE_M_MODE = FALSE;
  }
}

/* End of Outputs for SubSystem: '<S6>/DISCHARGE_M' */

/* C28x IQmath Library (stiiqmath_iqmpy) - '<S6>/IQN x IQN2' */
{
  EMULATOR_M_Y.VB_OUT_NOT_LIM = _IQ18mpy (EMULATOR_M_DWork.VB_CELL, EE_S_CELLS);
}

/* Saturate: '<S6>/Saturation1' */
if (EMULATOR_M_Y.VB_OUT_NOT_LIM >= EE_VB_PACK_MAX) {
  /* Outport: '<Root>/VB_OUT' */
  EMULATOR_M_Y.VB_OUT = EE_VB_PACK_MAX;
} else if (EMULATOR_M_Y.VB_OUT_NOT_LIM <= EE_VB_PACK_MIN) {
  /* Outport: '<Root>/VB_OUT' */
  EMULATOR_M_Y.VB_OUT = EE_VB_PACK_MIN;
} else {
  /* Outport: '<Root>/VB_OUT' */
  EMULATOR_M_Y.VB_OUT = EMULATOR_M_Y.VB_OUT_NOT_LIM;
}

/* End of Saturate: '<S6>/Saturation1' */
/* End of Outputs for SubSystem: '<S2>/04_VB_MODEL_M' */

/* Saturate: '<S2>/Saturation2' */
if (rtb_Sum1 >= EE_SOC_REL_MAX) {
  rtb_Saturation1_f = EE_SOC_REL_MAX;
} else if (rtb_Sum1 <= EE_SOC_REL_MIN) {
  rtb_Saturation1_f = EE_SOC_REL_MIN;
} else {
  rtb_Saturation1_f = rtb_Sum1;
}

/* End of Saturate: '<S2>/Saturation2' */
```

```
/* Outport: '<Root>/SOC_RELATIVE' */
EMULATOR_M_Y.SOC_RELATIVE = rtb_Saturation1_f;

/* Outputs for Atomic SubSystem: '<S2>/05_SOC_REAL' */
/* Outputs for Enabled SubSystem: '<S7>/SOC_REAL_DISCH_M' incorporates:
 *  EnablePort: '<S26>/Enable'
 */
if (EMULATOR_M_DWork.Merge_c) {
  /* C28x IQmath Library (stiiqmath_iqdiv) - '<S26>/IQN // IQN1' */
  {
    rtb_IQNIQN1 = _IQ18div (EE_K1_DISCH_REF, ((int32_T)26214400L));
  }

  /* C28x IQmath Library (stiiqmath_iqdiv) - '<S26>/IQN // IQN3' */
  {
    EMULATOR_M_DWork.Merge = _IQ18div (rtb_IQNIQN1, EMULATOR_M_Y.K1);
  }
}

/* End of Outputs for SubSystem: '<S7>/SOC_REAL_DISCH_M' */

/* Outputs for Enabled SubSystem: '<S7>/SOC_REAL_CHARGE_M' incorporates:
 *  EnablePort: '<S25>/Enable'
 */
if (rtb_RelationalOperator_o) {
  /* C28x IQmath Library (stiiqmath_iqdiv) - '<S25>/IQN // IQN4' */
  {
    rtb_IQNIQN4 = _IQ18div (EE_L1_CHARGE_REF, ((int32_T)26214400L));
  }

  /* C28x IQmath Library (stiiqmath_iqdiv) - '<S25>/IQN // IQN5' */
  {
    EMULATOR_M_DWork.Merge = _IQ18div (rtb_IQNIQN4, EMULATOR_M_Y.L1);
  }
}

/* End of Outputs for SubSystem: '<S7>/SOC_REAL_CHARGE_M' */

/* C28x IQmath Library (stiiqmath_iqmpy) - '<S7>/IQN x IQN' */
{
  rtb_IQNxIQN2_b = _IQ18mpy (EE_C_NOM, EMULATOR_M_DWork.Merge);
}

/* C28x IQmath Library (stiiqmath_iqdiv) - '<S7>/IQN // IQN2' */
{
  rtb_IQNIQN2_k = _IQ18div (rtb_SOD, rtb_IQNxIQN2_b);
}

/* C28x IQmath Library (stiiqmath_iqmpy) - '<S7>/IQN x IQN2' */
{
  rtb_IQNxIQN2_b = _IQ18mpy (rtb_IQNIQN2_k, ((int32_T)26214400L));
}

/* Sum: '<S7>/Sum2' incorporates:
 *  Constant: '<S7>/Constant5'
 */
rtb_Saturation1_f = rtb_IQNxIQN2_b + EE_SOC_INIT;

/* End of Outputs for SubSystem: '<S2>/05_SOC_REAL' */

/* Saturate: '<S2>/Saturation1' */
if (rtb_Saturation1_f >= EE_SOC_REAL_MAX) {
```

```
    rtb_Saturation1_f = EE_SOC_REAL_MAX;
  } else {
    if (rtb_Saturation1_f <= EE_SOC_REAL_MIN) {
      rtb_Saturation1_f = EE_SOC_REAL_MIN;
    }
  }

  /* End of Saturate: '<S2>/Saturation1' */

  /* Outport: '<Root>/SOC_REAL' */
  EMULATOR_M_Y.SOC_REAL = rtb_Saturation1_f;

  /* Outport: '<Root>/SOC_REL_HOLD' */
  EMULATOR_M_Y.SOC_REL_HOLD = EMULATOR_M_DWork.Merge1;

  /* Outport: '<Root>/DISCH_STATE' */
  EMULATOR_M_Y.DISCH_STATE = EMULATOR_M_DWork.Merge_c;

  /* Outport: '<Root>/ICELL_INT' */
  EMULATOR_M_Y.ICELL_INT = rtb_SOD;

  /* Outport: '<Root>/SOC_REAL_SCALE' */
  EMULATOR_M_Y.SOC_REAL_SCALE = EMULATOR_M_DWork.Merge;

  /* Outport: '<Root>/VB_CELL_OUT' */
  EMULATOR_M_Y.VB_CELL_OUT = EMULATOR_M_DWork.VB_CELL;
}

/* Model initialize function */
void EMULATOR_M_initialize(void)
{
  /* Registration code */

  /* states (dwork) */
  (void) memset((void *)&EMULATOR_M_DWork, 0,
                sizeof(D_Work_EMULATOR_M));

  /* external inputs */
  EMULATOR_M_U.ICELL = 0;

  /* external outputs */
  (void) memset((void *)&EMULATOR_M_Y, 0,
                sizeof(ExternalOutputs_EMULATOR_M));

  /* Start for Atomic SubSystem: '<S2>/04_VB_MODEL_M' */
  /* Start for Enabled SubSystem: '<S6>/CHARGE_M' */

  /* InitializeConditions for Atomic SubSystem: '<S16>/CHARGE_MATH' */
  /* InitializeConditions for DiscreteIntegrator: '<S18>/Discrete-Time Integrator' */
  EMULATOR_M_DWork.DiscreteTimeIntegrator_DSTATE_k = 0L;

  /* End of InitializeConditions for SubSystem: '<S16>/CHARGE_MATH' */
  /* End of Start for SubSystem: '<S6>/CHARGE_M' */

  /* Start for Enabled SubSystem: '<S6>/DISCHARGE_M' */

  /* InitializeConditions for Atomic SubSystem: '<S17>/DISCH_MATH' */
  /* InitializeConditions for DiscreteIntegrator: '<S21>/Discrete-Time Integrator' */
  EMULATOR_M_DWork.DiscreteTimeIntegrator_DSTATE = 0L;

  /* End of InitializeConditions for SubSystem: '<S17>/DISCH_MATH' */
  /* End of Start for SubSystem: '<S6>/DISCHARGE_M' */
```

```
}

/*
 * File trailer for generated code.
 *
 * [EOF]
 */
```

# Bibliography


[1] Experimental validation of a battery dynamic model for ev applications. *World Electric Vehicle Journal*, 3:1 – 10, 2009.

[2] SIEMENS AG. Siemens siestorage - the modular energy storage system for a reliable power supply, 2014.

[3] David Anderson. Status and trends in the hev/phev/ev battery induxtry, 2008.

[4] G. Aurilio, D. Gallo, C. Landi, M. Luiso, A. Rosano, M. Landi, and V. Paciello. A battery equivalent-circuit model and an advanced technique for parameter estimation. In *Instrumentation and Measurement Technology Conference (I2MTC), 2015 IEEE International*, pages 1705–1710, May 2015.

[5] D. Bazargan, S. Filizadeh, and G. Bistyak. Battery characterization for vehicular applications using hardware-in-loop real-time simulation. In *Electric Power and Energy Conversion Systems (EPECS), 2013 3rd International Conference on*, pages 1–6, Oct 2013.

[6] Isidor Buchmann. Bu-205: Types of lithium-ion, 2015.

[7] Isidor Buchmann. Bu-802b: Elevating self discharge, 2015.

[8] H. Budde-Meiwes, J. Drillkens, B. Lunz, J. Muennix, S. Rothgang, J. Kowal, and D. U. Sauer. A Review of Current Automotive Battery Technology and Future Prospects. 2013.

[9] Wen-Yeau Chang. The state of charge estimating methods for battery: A review. *ISRN Applied Mathematics*, 2013:7, 2013.

[10] H. Chaoui, N. Golbon, I. Hmouz, R. Souissi, and S. Tahar. Lyapunov-based adaptive state of charge and state of health estimation for lithium-ion batteries. *Industrial Electronics, IEEE Transactions on*, 62(3):1610–1618, March 2015.

[11] LG Chem. Advanced battery for energy storage system, 2015.

[12] Min Chen and G.A. Rincon-Mora. Accurate electrical battery model capable of predicting runtime and i-v performance. *Energy Conversion, IEEE Transactions on*, 21(2):504–511, June 2006.

[13] Andy Colthorpe. A123 offshoot 24m targets us$100 per kwh costs for li-ion by 2020, 2015.

[14] Thomas Fisher. What goes into a tesla model s battery–and what it may cost, 2015.

[15] Lijun Gao, Shengyi Liu, and R.A. Dougal. Dynamic lithium-ion battery model for system simulation. *Components and Packaging Technologies, IEEE Transactions on*, 25(3):495–505, Sep 2002.

[16] Bettina Kampman Max Grünig Gopalakrishnan Duleep, Huib van Essen. Assessment of electric vehicle and battery technology. Technical report, Delft, 2011.

[17] Dai Haifeng, Wei Xuezhe, and Sun Zechang. State and parameter estimation of a hev li-ion battery pack using adaptive kalman filter with a new soc-ocv concept. In *Measuring Technology and Mechatronics Automation, 2009. ICMTMA '09. International Conference on*, volume 2, pages 375–380, April 2009.

[18] Hongwen He, Rui Xiong, and Jinxin Fan. Evaluation of lithium-ion battery equivalent circuit models for state of charge estimation by an experimental approach. *Energies*, 4(4):582, 2011.

[19] A. Hentunen, T. Lehmuspelto, and J. Suomela. Time-domain parameter extraction method for thvenin-equivalent circuit battery models. *Energy Conversion, IEEE Transactions on*, 29(3):558–566, Sept 2014.

[20] Fran Hoffart. Proper care extends li-ion battery life, 2008.

[21] H.A.-H. Hussein and I. Batarseh. An overview of generic battery models. In *Power and Energy Society General Meeting, 2011 IEEE*, pages 1–6, July 2011.

[22] Tsinghua University Institute of New Energy Technology, INET. 12ah ncm batteries - test of li-ion battery for self-heating & lifetime evaluation.

[23] Sun Kai and Shu Qifang. Overview of the types of battery models. In *Control Conference (CCC), 2011 30th Chinese*, pages 3644–3648, July 2011.

[24] R.C. Kroeze and P.T. Krein. Electrical battery model for use in dynamic electric vehicle simulations. In *Power Electronics Specialists Conference, 2008. PESC 2008. IEEE*, pages 1336–1342, June 2008.

[25] M.T. Lawder, B. Suthar, P.W.C. Northrop, S. De, C.M. Hoff, O. Leitermann, M.L. Crow, S. Santhanagopalan, and V.R. Subramanian. Battery energy storage system (bess) and battery management system (bms) for grid-scale applications. *Proceedings of the IEEE*, 102(6):1014–1030, June 2014.

[26] Jason Leadbetter and Lukas G. Swan. Selection of battery technology to support grid-integrated renewable electricity. *Journal of Power Sources*, 216:376 – 386, 2012.

[27] lygte info.dk/. Nca battery - keeppower 18650 3600mah (black), 2014.

[28] MathWorks. Matlab-simulink - help, 2015.

[29] Sergei Melentjev and Deniss Lebedev. Overview of simplified mathematical models of batteries. In *13th International Symposium" Topical problems of education in the field of electrical and power engineering".–Doctoral school of energy and geotechnology: Parnu, Estonia*, pages 231–235, 2013.

[30] T. Mesbahi, N. Rizoug, P. Bartholomeus, and P. Le Moigne. Li-ion battery emulator for electric vehicle applications. In *Vehicle Power and Propulsion Conference (VPPC), 2013 IEEE*, pages 1–8, Oct 2013.

[31] P.-H. Michel and V. Heiries. An adaptive sigma point kalman filter hybridized by support vector machine algorithm for battery soc and soh estimation. In *Vehicular Technology Conference (VTC Spring), 2015 IEEE 81st*, pages 1–7, May 2015.

[32] Naoki Nitta, Feixiang Wu, Jung Tae Lee, and Gleb Yushin. Li-ion battery materials: present and future. *Materials Today*, 18(5):252 – 264, 2015.

[33] Panasonic. Storage energy system using lithium-ion batteries, 2015.

[34] POWERSIM. Psim tutorial - how to use lithium-ion battery model, 2013.

[35] H. Rahimi-Eichi, U. Ojha, F. Baronti, and M. Chow. Battery management system: An overview of its application in the smart grid and electric vehicles. *Industrial Electronics Magazine, IEEE*, 7(2):4–16, June 2013.

[36] R. Rao, S. Vrudhula, and D.N. Rakhmatov. Battery modeling for energy aware system design. *Computer*, 36(12):77–87, Dec 2003.

[37] SAFT. Lithium-ion battery life.

[38] Navigant Research Sam Jaffe. The lithium ion inflection point, 2013.

[39] Dr. John Schonberger. Modeling a lithium-ion cell using plecs. Technical report, Plexim GmbH, 2013.

[40] B. Schweighofer, K.M. Raab, and G. Brasseur. Modeling of high power automotive batteries by the use of an automated test system. *Instrumentation and Measurement, IEEE Transactions on*, 52(4):1087–1091, Aug 2003.

[41] SAMSUNG SDI. Samsung sdi - energy storage system business presentation, 2013.

[42] Samsung SDI. Samsung sdi - our next technology roadmap, 2015.

[43] C. M. Shepherd. Theoretical design of primary and secondary cells, part iii - battery descharge equation. Technical report, U. S. NAVAL RESEARCH LABORATORY, 1963.

[44] Pu Shi, Yiwen Zhao, and Pu Shi. Application of unscented kalman filter in the soc estimation of li-ion battery for autonomous mobile robot. In *Information Acquisition, 2006 IEEE International Conference on*, pages 1279–1283, Aug 2006.

[45] Chester Simpson. National instruments - characteristics of rechargeable batteries, 2011.

[46] A.R. Sparacino, G.F. Reed, R.J. Kerestes, B.M. Grainger, and Z.T. Smith. Survey of battery energy storage systems and modeling techniques. In *Power and Energy Society General Meeting, 2012 IEEE*, pages 1–8, July 2012.

[47] A.-I. Stan, M. Swierczynski, D.-I. Stroe, R. Teodorescu, and S.J. Andreasen. Lithium ion battery chemistries from renewable energy storage to automotive and back-up power applications; an overview. In *Optimization of Electrical and Electronic Equipment (OPTIM), 2014 International Conference on*, pages 713–720, May 2014.

[48] NEC Energy Systems. Nec acquires grid energy storage and commercial systems business of a123 systems from wanxiang, 2014.

[49] M. Tamaki, K. Takagi, K. Shimada, N. Kawakami, and Y. Iijima. Development of pcs for battery system installed in megawatt photovoltaic system. In *Power Electronics and Motion Control Conference (EPE/PEMC), 2012 15th International*, pages LS1a–2.1–1–LS1a–2.1–4, Sept 2012.

[50] Inc. The MathWorks. Generic simulink battery model implementation, 2015.

[51] O. Tremblay, L.-A. Dessaint, and A.-I. Dekkiche. A generic battery model for the dynamic simulation of hybrid electric vehicles. In *Vehicle Power and Propulsion Conference, 2007. VPPC 2007. IEEE*, pages 284–289, Sept 2007.

[52] MPOWER UK. Nickel metal hydride batteries, 2014.

[53] Office of Electricity Delivery U.S. Department of Energy and Energy Reliability. Electric power industry needs for grid-scale storage applications, 2010.

[54] S. Wijewardana. New dynamic battery model for hybrid vehicles. *International Journal of Emerging and Advanced Engineering*, 4(4):623 – 631, 2014.

[55] N.A. Windarko, J. Choi, and Gyo-Bum Chung. Soc estimation of lipb batteries using extended kalman filter based on high accuracy electrical model. In *Power Electronics and ECCE Asia (ICPE ECCE), 2011 IEEE 8th International Conference on*, pages 2015–2022, May 2011.

[56] Low Wen Yao, J.A. Aziz, Pui Yee Kong, and N.R.N. Idris. Modeling of lithium-ion battery using matlab/simulink. In *Industrial Electronics Society, IECON 2013 - 39th Annual Conference of the IEEE*, pages 1729–1734, Nov 2013.

[57] Cheng Zhang, Kang Li, S. McLoone, and Zhile Yang. Battery modelling methods for electric vehicles - a review. In *Control Conference (ECC), 2014 European*, pages 2673–2678, June 2014.